STUDY OF VOLTAGE STABILITY USING INTELLIGENT TECHNIQUES

A thesis submitted in partial fulfillment of the requirements for the degree of

Doctor of Philosophy
in
Electrical Engineering

By

Santi Behera

ROLL NO. 509EE810

Under the Guidance

of

Prof. J. K. Satapathy & Dr. Manish Tripathy

Department of Electrical Engineering
National Institute of Technology
Rourkela-769008 (Odisha)

Sept 2015

CERTIFICATE

This is to certify that the thesis entitled "***Study of Voltage Stability using Intelligent Techniques***", being submitted by Smt. Santi Behera, is a record of bonafide research carried out by her in the Department of Electrical Engineering, National Institute of Technology, Rourkela, under guidance and supervision of Prof J. K. Satapathy, Department of Electrical Engineering, NIT, Rourkela and Dr. M. Tripathy, Department of Electrical Engineering VSSUT, Burla. The work incorporated in this thesis has not been, to the best of our knowledge, submitted to any other university or institute for the award of any degree or diploma.

(Dr. M. Tripathy)   (Dr. J. K. Satapathy)
Associate Professor,   Professor & HOD,
Department of Elect. Engg   Department of Elect. Engg
VSSUT, Burla-768018 (Odisha)   NIT, Rourkela-769 008 (Odisha)

Acknowledgements

This thesis is a result of research work carried out at National Institute of Technology, Rourkela. During this period I faced many obstacles and hurdles but due to constant encouragement from the people close to me, this thesis finally saw the light of the day

Firstly, I wish to express my sincere gratitude to my supervisor Professor J. K. Satapathy for his enthusiasm and sincere guidance which highly motivated me to carry out this research work. My dream of completing this thesis would not have been possible without his support and inspiration.

I would like to express my heartfelt thanks to the co-supervisor Dr. M. Tripathy for his constant help and advice throughout this arduous journey of pursuing research. His path breaking ideas and suggestion during the course of this research is truly commendable and I am highly indebted to him for the same.

In fact the untiring and unflinching support I received from both my supervisors has ignited within me a source of confidence and dedication to enrich my knowledge further enabling me to march ahead to explore more on the topic I worked.

I am grateful to Prof. A. Biswas, Director, National Institute of Technology, Rourkela and Prof. Jitendriya Kumar Satapathy, Head of Electrical Engineering Department, National Institute of Technology, Rourkela, for their kind support and concern regarding my academic requirements.

I express my deep sense of gratitude to the members of Doctoral Scrutiny Committee, Prof. B. Subudhi, Prof. B. Majhi, Prof. K. K. Mohapatra, and Prof. S. Maity for their advice and care. I express my thankfulness to the faculty and staff members of the Electrical Engineering Department for their continuous encouragement and suggestions. Thanks are also due to my co-scholars at National Institute of Technology, Rourkela, for their whole hearted support and co-operation during the tenure of this research work. My parents deserve special mention for their

inseparable support and prayers. They are the persons who show me the joy of intellectual pursuit ever since I was a child. I thank them for sincerely bringing up me with care and love.

The completion of this work came at the expense of my long hours of absence from home. Words fail me to express my appreciation to my husband Er. Jyotirmaya Behera and my daughter Tanya Priyadarshini for her understanding, patience and active cooperation throughout the course of my doctoral dissertation. I thank them for being supportive and caring. Last, but not the least, I thank the one above all of us, the omnipresent God, for giving me the strength during the course of this research work.

<div align="right">

Santi Behera

Roll No. 509 EE 810

</div>

Summary

The continuous increase in the demand of active and reactive power in the power system network has limits as scope for network expansion many a times poses serious problems. The power system must be able to maintain acceptable voltage at all nodes in the system at a normal operating condition as well as post disturbance periods. Voltage instability is a serious issue in the system due to progressive and uncontrollable fall in voltage level. The research presented in this thesis is concerned with several facets of the voltage stability problem.

The focus of this thesis is to improve the voltage stability of the system. The sensitivity analysis plays an important role as it monitors the nearness of the system towards the voltage collapse situation. The conventional offline data as well as the online data are processed to determine the weak areas are determined. As the system is having nonlinearities it is governed by differential and algebraic equations which are in turn solved by nonlinear techniques.

In this work the system is analysed with steady state model. Once the system is represented in the form of differential equations and standard form is achieved advanced control techniques can be easily applied for its solution.

The main focus of this thesis is aimed at placing FACTS device known as the Static compensator (STATCOM) at weak location of the system network to address the problem of voltage instability. With its unique capability to control reactive power flow in a transmission line as well as voltage at the bus where it is connected, this device significantly contribute to improve the power system. These features turn out to be even more prominent because STATCOM can allow loading of the transmission lines close to their thermal limits, forcing the power to flow through the desired paths. This opens up new avenues for the much needed flexibility in order to satisfy the demands. The voltage instability is improved with reactive power supports of optimal values at optimal locations.

Also renewable energy sources offer better option than the conventional types and hence attempt has been made to include the wind energy for this study the wind generator is considered delivering constant output and is assumed as a substitute to the conventional power generators.

Finally the system voltage stability is studied with design of a controller based on probabilistic neural network. The developed controller has provided much better performance under wide variations in the system loads and contingencies and shown a significant improvement in the static performance of the system. The proposed controller is tested under different scenarios of line outages and the load increase and found to be more effective than the existing ones. The research has revealed a veritable cornucopia of research opportunities, some of which are discussed in the thesis.

CONTENTS

Chapter-2: On line voltage stability assessment of transmission network through ENVCI

Chapter-3: **Optimal placement and sizing of Fixed shunt reactive compensation to increase load margin with MBFO algorithm**

**Chapter-4: Load margin improvement with inclusion Of STATCOM
　　　　　　　Device in transmission System**

**Chapter-5: Voltage stability study of transmission system with penetration
　　　　　　　of wind generator**

Chapter-6: Application of probabilistic neural network for voltage stability enhancement in power based on stability index

Chapter-7: Conclusions and recommendations for future research

GLOSSARY OF ACRONYMS

ANN	Artificial Neural Network
AVRs	Automatic Voltage Regulators
CPF	Continuation Power Flow
DE	Differential Evolution
DFIG	Doubly Fed Induction Generator
ELNM	Equivalent Local Network Model
ELNM	Equivalent Local Network Model
EMS	Energy Management System
ENVCI	Equivalent Node Voltage Collapse Index
ESM	Equivalent System Model
EVPA	Extended Voltage Phasors Approach
FACTS	Flexible AC Transmission System
FFNN	Feed-Forward Artificial Neural Network
FVSI	Fast Voltage Stability Index
GA	Genetic Algorithm
GTO	Gate Turn Off
HVDC	High Voltage Direct Current
IP	Interior Point
IPFC	Interline Power Flow Controller
LI	Load increase
LM	Load multiplier
LO	Line Outage
LP	Linear Programming
MBFOA	Modified Bacteria Foraging Optimization Algorithm
MFLP	Multi-objective Fuzzy LP
MVA	Mega Volt Ampere
MVAR	Mega Volt Ampere Reactive
NGHS	Novel Global Harmony Search Algorithm
ORPD	Optimal Reactive Power Dispatch

ORPF	Optimal Reactive Power Flow
PDF	Probability Density Function
PMU	Phasor Measurement Units
PNN	Probabilistic Neural Network
PSO	Particle Swarm Optimization
RBF	Radial Basis Function
RSC	Rotor Side Converter
SA	Simulated Annealing
SFIG	Singly Fed Induction Generator
SQP	Sequential Quadratic Programming
SSSC	Static Switched Series Capacitor
SSSC	Static Synchronous Series Compensator
STATCOM	Static Synchronous Compensator
STATCOM	Static Synchronous Compensator
SVCs	Static Var Compensators
TCPST	Thyristor Controlled Phase Shifting Transformer
TCSC	Thyristor Controlled Series Capacitor
TCSR	Thyristor Control Series Reactor
ULTCs	Under-Load Tap Changers
UPFC	Unified Power Flow Controller
UVLS	Under Voltage Load Shedding
VCPI	Voltage Collapse Proximity
VSC	Voltage-Sourced Converter
VSENN	Voltage Stability Enhancing Neural Network
VSI	Voltage Stability Indices
WAM	Wide Area Measured
WASI	Weighted Average Sensitivity Index
WECS	Wind Energy Conversion System
WG	Wind Generation

LIST OF FIGURES

Figure	Title	Page

List Of Figures

List of Tables

INTRODUCTION

1.0. Introduction

With a growing world economy, there has been an ever increasing demand in generation of electrical power, facilities and interconnections to serve a widely dispersed load. Power system stability has been acknowledged as a key problem for secure system operation ever since 1926 [1]. Several numbers of blackouts affecting integrated system have resulted in large scale load loss and are difficult to restore [2-6]. The reason of unreliable power has been broadly attributed to inadequacy in reserve where as the security is affected more by insufficient as well as improper controls. Subsequently, these factors lead to instability. Moreover, as the existing corrective control mechanisms sometimes fail to the cope up with the increase in numbers of operating constraints, the system may start to operate in an insecure manner. The system security and reliability [7, 8] gets compromised in the process, and as a result problems in connection with the stability of the system arise. The operation and control of power system has become a major issue in present scenario when there is an ever increasing demand of load with restricted scope in generation and transmission system expansion. Traditionally, the stability means maintaining synchronous operation of the alternators with the system. Different types of system instability have come into view as power systems undergo changes through ongoing growth in interconnections, use of latest technologies and controls, and the enlarged operation in highly stressed circumstances [9]. As generation and transmission units need to operate at critical limits, voltage stability problems may take place in power system once there is an increase in the load in requirement of load. Sometimes due to voltage instability problems, major blackouts may arise in a considerable part of a system. In fact, out of many cases of voltage instability or voltage collapses, 12 cases of great blackouts were reported all over the world between 1977 and 2012. The most recent blackout in India affected northern states from the country's Eastern border with Myanmar to its western border with Pakistan in the year 2012 [10]. However, voltage instability initiates in a local network and gradually to the whole system which leads the system to voltage collapse. The diagnosis of the problems of stability has

originated by understanding the reasons which affect the generator power angle, its ability to maintain synchronous operation and constant voltage. The power system is a highly nonlinear system which is operating in a constantly varying environment of loads, generator outputs and key operating parameters [11]. Further, with continuing growth in power demand, it has become necessary to the use fast and efficient technologies for stable operation and better controls. Apart from more complex decentralized control, a coordinated operation of many controllers may be beneficial in enhancing the corrective capacities of the system to alleviate voltage instability [12]. It is essential to study the definition and classification of power system stability in brief for a meaningful practical analysis of power system stability problems.

1.2. Definition of Power System Stability

The power system stability can be defined as *Power system stability is the ability of an electric power system, for a given initial operating condition, to recover to a state of operating equilibrium after being subjected to a physical disturbance* [13]. The power system stability can be classified into three types as explained in the following section.

1.3. Classification of Power System Stability

Similar to the definition of stability, its classification yet again depends on type of study. However, essentially the power system stability can be classified into three main categories as mentioned below:

   i.   Rotor angle stability
  ii.   Frequency stability
 iii.   Voltage stability

This work primarily focuses on the problem of voltage stability; therefore other categories of stabilities are discussed very briefly as follows.

1.3.1. Rotor angle stability

Rotor angle stability refers to the ability of synchronous machines of an interconnected power system to remain in synchronism even after being subjected to an

interruption [12]. In steady-state conditions, there is balance between the input mechanical torque and the output electromagnetic torque of every generator, and the speed continues to be constant. If the system is perturbed, this equilibrium is disturbed, resulting in speeding up or deceleration of the rotors of the machines. This tends to decrease the speed difference and hence the angular separation. The power-angle relationship is nonlinear and the response of the system differs according to different types of disturbances. The rotor angle stability is categorized as shown below:

    i.   Small-disturbance rotor angle stability
    ii.   Large-disturbance rotor angle stability

1.3.1.1. Small disturbance rotor angle stability

The small disturbance rotor angle stability is the ability of the power system to sustain synchronism under small disturbances [14]. In modern power systems, small-disturbance rotor angle stability problem is usually related to insufficient damping of oscillations. The time frame of interest is usually within 10 to 20 seconds subsequent to a disturbance.

1.3.1.2. Large-disturbance rotor angle stability

Large disturbance rotor angle stability is mainly the ability of the power system to maintain synchronism after being subjected to a severe disturbance, like a short circuit on a transmission line [15]. The time frame of interest in transient stability studies is usually 3 to 5 seconds after the disturbance [16]. It may extend 10 to 20 seconds for very large systems with prevailing inter-area oscillations.

1.3.2. Frequency Stability

Frequency stability means the ability of a power system to maintain constant frequency subsequent to a major disturbance resulting in a considerable imbalance between load and generation [17]. Generally, frequency stability problems are associated with poor response of tools, poor management of control and protection tools, or scarce reactive power generation reserve. As identified in Figure **1.1**, frequency stability may be a short-term phenomenon or a long-term phenomenon.
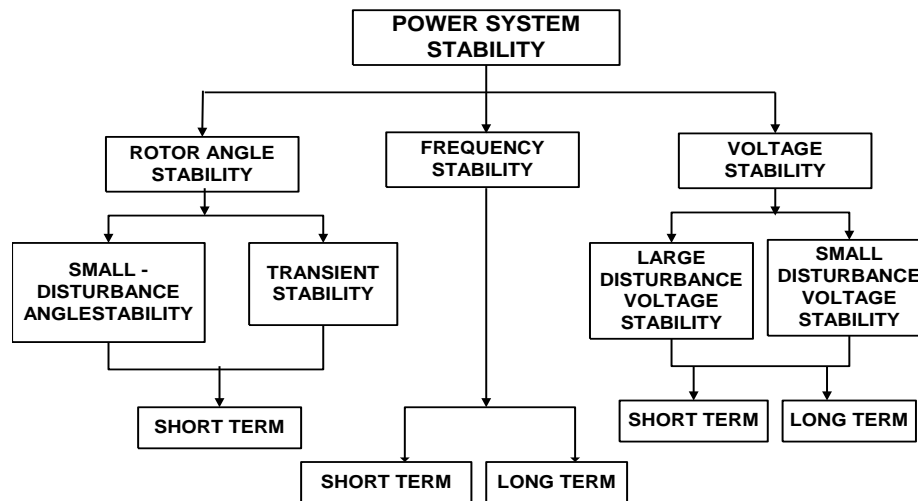
Figure 1.1. Classification of power system stability.

1.3.3. Voltage Stability

Voltage stability is the ability of a power system to maintain balanced voltages at all buses in the system even after being subjected to a disturbance from a certain initial operating condition [13]. It is the ability to maintain equilibrium between the demand and supply of both active and reactive power loads in the power system. Instability occurs in the form of a sudden fall or rise of voltages at some buses. A possible effect of voltage instability is loss of load in an area, or tripping of transmission lines leading to cascading outages. A major factor of causing voltage instability is the voltage drop due to real and reactive power flow in inductive reactance of the transmission system, which confines the capability of the transmission system for power transmission and voltage support [18]. The facilities of power transmission and voltage support are limited. The problem of voltage instability makes the system vulnerable with increase in reactive power demand and control mechanism of converter, transformer tap-changer, shunt reactors and or capacitors etc. [19]. As in the case of rotor angle stability, voltage stability can also be classified into two sub-categories as :

   i.   Large-disturbance voltage stability
   ii.   Small-disturbance voltage stability

1.3.3.1. Large-disturbance voltage stability

The large-disturbance voltage stability implies the ability of the system to maintain stable voltages even after being subjected to large disturbances like faults in the system, loss

of generation or any network contingencies. This ability is determined by load characteristics, and the relations between both continuous and separate controls and security schemes. The study period of interest may widen from a few seconds to tens of minutes.

1.3.3.2. Small-disturbance voltage stability

It indicates the ability of the system to maintain stable voltages when subjected to small changes in system load [12]. This form of stability is subjective to the characteristics of loads, continuous as well as distinct controls at a given point of time. This concept is useful in determining how the system voltages will respond to small system changes instantly. For analysis, system equations can be linearized with proper assumptions, thus allowing computation of important sensitivity information helpful in distinguishing factors which help maintaining stability. However, the linearization cannot make up nonlinear effects such as tap changer controls. Therefore, a combination of linear and nonlinear analyzes are used in a harmonizing manner [20]. As illustrated above, voltage instability problems may last for a few seconds to tens of minutes. Hence, voltage stability may be either a short-term or a long-term incident as depicted in Figure **1.1**.

Short-term voltage stability includes dynamics of fast acting load apparatus like induction motors, loads with electronic controller, and HVDC converters. The study period is of several seconds, and analysis requires solution of proper system differential equations, this is similar to analysis of rotor angle stability. Dynamic modeling of loads is often essential [21]. In contrast to angle stability, short circuits close to loads are vital in the case of voltage stability. Long-term voltage stability involves slower acting tools like-changing transformers, loads with thermostatic controller as well as generator current limiters. The study last for many minutes, and simulations required for analysis of system dynamic aspect [22].

1.4. Causes of Voltage Instability

The various causes of voltage instability [23] are studied and explained as follows:

1.4.1. Generator breakdown

Some of the bulky generating units operating close to the load centers will be out of service due to abnormal operation. As a result the reactive power supply becomes deficient and few transmission lines become heavily loaded in order to carry sufficient reactive power to critical areas of the grid.

1.4.2. Line outage

As the transmission lines are operating under heavily loaded condition for economical operation, there is a chance of loss of this transmission line due to a fault. Thus it results in further loading on the rest of the lines and the reactive power necessity in lines rises as reactive power demand increases rapidly for loads above surge impedance loading. Thus, reactive power demand boosts in the system.

1.4.3. Consumption of reactive power by the motors used in the industries

The operating voltage level at the load end decreases due to increase in reactive power demand. The added reactive power flow through transformers and transmission lines causes large voltage drop across each of these parts.

1.4.4. Transformer tap changer

The voltage decline in transmission system affects the distribution system. Substation transformers can bring back stable operating voltages by changing the transformer taps in a few minutes following up the time delay of tap changer. When transmission lines are loaded above surge impedance loading for each MVA increase, causes great amount of reactive power requirement in systems. As a result of tap changing operations, the reactive power output of generators increase which is another cause of voltage instability.

1.4.5. Location of generators

The generating stations are located at remote places according to the availability of the raw materials as well as land. Because of which the plants are at far distance from the load centers. The long transmission line results in voltage drop occurs while transmitting the power can also lead to voltage drop at the load end.

1.4.6. Location and coordination of FACTS devices

FACTS devices are used at various locations to provide the reactive power support. When FACTS devices are placed at unsuitable locations and there is a chance of poor co-

ordination between the multiple devices. Due to disoperation of FACTS devices, the reactive power cannot be not supplied, thus the operating voltage will fall down. Ramirez *et al*. [24] proposed a method to co-ordinate stabilizers like a thyristor controlled series capacitor (TCSC) and a unified power flow controller (UPFC) taking into account the several operating conditions to enhance the dynamic stability margin of the power system.

1.5. Analysis Methods for Study of Voltage Stability

The power systems are forced to operate at stressed condition due to the continuous increase in the load demand and limited scope for the expansion of the existing network. At this operating condition the system voltage drops and any sudden disturbance to the system (*i.e.* line outage; generation loss; or any fault) will cause the system to face voltage instability leading to voltage collapse. This situation can be avoided by analyzing the voltage stability studies and bringing remedial measures to address the issue. Various methods are employed to analyze the problem as mentioned hereafter.

1.5.1. Static analysis

Static analysis or steady-state analysis discloses equilibrium points of a system under study. The power flow equations utilized in static analysis consider constant frequency of the system. Voltage stability studies are regularly carried out using static analysis. The use of static analysis is the development of P-V curves as well as Q-V curves. The P-V curves are the most established technique for prediction of voltage instability [25]. The main reason for voltage instability is the lack of sufficient reactive power in a system. Generator reactive power limits and reactive power requirements in transmission lines are the main causes of insufficient reactive power. Synchronous generators are the main devices for voltage control and reactive power control in power systems. In voltage stability analysis active and reactive power capabilities of generators play an important role. The active power limits are due to the design of the turbine and the boiler. Therefore, active power limits are constant. Reactive power limits of generators are more complicated than active power limits. There are three different causes of reactive power limits that are stator current, over-excitation current and under-excitation limits. The generator field current is limited by over-excitation limiter in order to avoid damage in field winding. In fact, reactive power limits are voltage dependent. However, in load flow programs they are taken to be constant in order to simplify analysis. Transfer of active and reactive power is provided by transmission lines. Since transmission

lines are generally long, transfer of reactive power over these lines is very difficult due to significant amount of reactive power requirement. The power system load is gradually increased and at each increment, it is necessary to re-compute the power flows till it reached the nose of PV curve (see Figure **1.2.**). The margin between the voltage collapse point and the current operating point is used as voltage stability criterion.
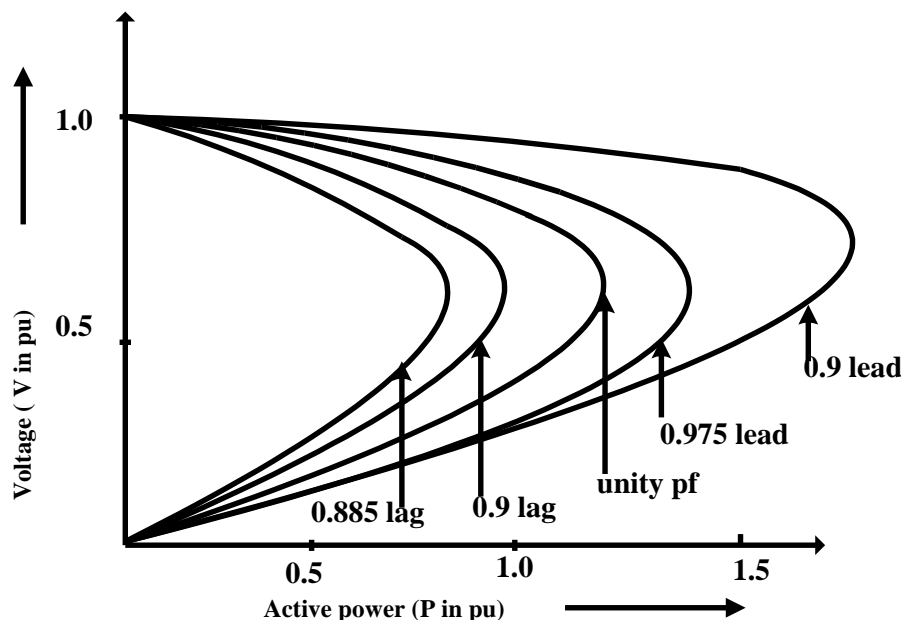
Figure 1.2. P-V curve.

With the probable Q-V curve, the maximum reactive power can be determined and added to the weakest bus before reaching minimum voltage limit. The reactive power margin is the MVAR distance from the operating point to the bottom of the Q-V curve. The Q-V curve can be used as an index for voltage instability. The point at which dQ/dV becomes zero is the point of voltage stability limit [26]. The graph is obtained from power-flow simulation by monitoring a voltage at a required bus and varying the power in small increments until power-flow divergence is met. Each equilibrium point indicates a steady-state operating condition.

1.5.2. Dynamic analysis

Dynamic analysis is commonly applied in the study of power system stability to study system behaviour after a disturbance [27-28]. In comparison to static analysis in which equilibria points of a P-V curve are independent of time, dynamic analysis method tells the transient and/or the long-term stability of a power system.

1.5.3. CPF analysis: The method of continuation power flow

The common theory behind the continuation power flow (CPF) is simple utilizing a predictor-corrector scheme so as to find a solution [29]. From a known base solution, a tangent predictor is utilized to estimate next solution for a particular pattern of load increase. The corrector step then gets the accurate solution using a conventional power flow. Thereafter a new prediction is assumed for a precise increase in load based upon the new tangent vector and a corrector step is applied. This process continues till critical point is reached. The critical point is the point at which the tangent vector is zero.

1.5.4. Index analysis

A number of sensitivity based analysis are carried out to determine the vulnerable buses where the voltage instability problem may be initiated much earlier than other parts of the system in the event of load increase. The condition of voltage stability in a power system can be known using Voltage Stability Indices (VSI). Since, the present work is based on the evaluation of one of similar VSI for its analysis, a preliminary understanding of some the methods reported by earlier research needs to be discussed here.

There are many indices used to find the voltage stability limit of power system. Kessel and Glavitsch [30] have developed a voltage stability index L-index derived from the solution of the power flow equations. Gao *et al*. [31] proposed a method which determines the smallest eigen value and related eigen vectors of the reduced Jacobian matrix of the power system. The magnitude of each lowest eigen value gives a measure to know how near the system is to voltage collapse condition. The voltage collapse proximity indices (VCPI) addressed by Moghavvemi and Faruque [32] looked into the stability of every line of the system which are based on the concept of maximum power transferred in a line. The VCPI index varies from 0 stable to 1 unstable condition. Moghavemmi and Omar [33] derived a line stability index in single transmission line. The fast voltage stability index (FVSI) proposed by Musirin and Rahman [34] is derived utilizing a concept of power flow in a lone line. Aghamohmmadi *et al*. [35] introduced a new index based on the correlation characteristic of system voltage profile applicable to online voltage security evaluation. Rabiee *et al*. [36] reintroduced a new voltage stability index using scalar local measurements

to estimate closeness of the operating point to the nose points of P-V curves. Smon *et al*. [37] applied the Tellegen's theorem and ad-joint networks to derive a new, local voltage-stability index. Gubina and Strmenik [38] introduced an analytical approach to determine index in radial network. Veraviah and Abidin [39] have approached a technique to investigate each line of the system through calculating an indicator that varies from zero (no load condition) to unity (maximum permissible loading condition). They have utilized the basic concepts of maximum power transfer through each line. Young *et al*. [40] have proposed an algorithm to calculate the smallest singular value of a Jacobian matrix used in the load flow equations through an incremental condition estimation method. Wang *et al*. [41] proposed a voltage stability index called the equivalent node voltage collapse index (ENVCI) based on equivalent system model that includes the effects of system outside the local network as well as the local network and uses only local voltage phasors. The ENVCI can identify weakest bus causing system instability. The power system voltage stability analysis based on the various methods indicates whether the system is stable or not. When the system voltage unstable, it will lead to major voltage collapse with any disturbance. This issue of voltage instability needs attention in order to prevent / or correct the voltage instability which may cause the voltage collapse subsequently. The prevention of voltage instability can be addressed in the following section.

1.6. Prevention of Voltage Instability

There are some measures that can be taken to counter voltage instability. Automatic voltage regulators (AVRs), under-load tap changers (ULTCs) and compensation devices are common means to keep bus voltage magnitude in acceptable ranges.

1.6.1 Automatic voltage regulator (AVR) of a generator

Generator AVRs are the main significant means of voltage control in a power system [12]. The terminal voltages of generators are retained constant under normal as well abnormal conditions. When the voltage stability problem arises because of reactive power demand, generators are able to supply more power to network considering field current limits. The AVRs take action on the exciter side of alternators. It can regulate the bus voltage within the availability limits of the generator.

1.6.2. Under-load tap changers

Transformers allow various operating voltage levels in the power system [12]. Besides voltage transformation and transformers are used for reactive power flow and control of voltage respectively. Thus basically all transformers are used for large power transfer and some distribution transformers are offered with taps in the windings. Under-load tap changing (ULTC) is used when repeated turns ratio has to be changed due to coincident changes in load like daily load variations. Thus, in order to maintain voltage stability ULTCs are often used. Similar research has been carried out by Kim and Lee [42] to develop a control technique in minimizing the ULTC and STATCOM output and maintaining the stable operating substation bus voltage magnitude at a stable operating condition.

1.6.3. Compensation devices

The reactive compensation devices are mainly incorporated to draw or supply reactive power and hence control the reactive power balance in a required manner [12]. Series capacitors, shunt capacitors, series reactors, shunt reactors, synchronous condensers and static VAR compensators are used for these purposes.

1.6.3.1. Shunt capacitors

The shunt capacitors are applied to compensate the reactive power needed to ensure acceptable voltage levels when the system is heavily loaded. Capacitor banks of suitable sizes are connected directly to bus or to the tertiary winding of the transformer. Switched capacitor banks provide a convenient way of maintaining bus voltages. They are normally distributed all over the system so as to reduce losses and voltage drops. Mesut *et al.* [43] proposed a solution technique which transforms the problem into a master-slave problem. The master problem is used to resolve the location of the capacitors and the slave problem is used by the master problem to determine the type and size of the capacitors placed on the system.

1.6.3.2. Series capacitors

The capacitors connected in series with the transmission line help reduce the net reactance of the transmission line [12]. Therefore, the maximum power is transferred and it reduces the reactive power requirement of the line. As series capacitors allow economical

loading of long transmission lines they are used in power systems. However, problems related to Sub Synchronous Resonance (SSR) associated with the use of series capacitor have restricted their use [50].

1.6.3.3. Shunt reactors

The shunt reactors are used to balance the effects of line capacitance [12]. In case of undesirable voltage rises they are activated in order to check voltage rise. In fact, it is not a counter action taken to mitigate voltage collapse. Especially under light loading conditions, they are used so as to prevent over-voltages as power lines produce reactive power. During heavy loading conditions, they may have to be removed.

1.6.3.4. Synchronous condensers

The synchronous condenser is a synchronous machine operating with controlled excitation of field [12] so as to enable the machine to either generate or absorb reactive power. They can automatically adjust the reactive power output to maintain constant terminal voltage with a voltage regulator. They are mostly connected to tertiary windings of transformers. Nevertheless, they are not chosen frequently due to high installation and operating costs.

1.6.3.5. Static var systems

The static var compensators are connected in shunt with the bus to control individual phase voltages of the bus. A static var system is ideally suited for applications for direct and quick control of voltage. This is reported by Minguez *et al*. [44] that the static var compensators (SVCs) are placed optimally in a transmission network so as to maximize the loading margin.

1.6.3.6. Load shedding

The load shedding is another method to maintain power system voltage stability. In many cases, the last line of defense is to initiate load shedding. Wiszniewski [45] has proposed a method to avoid voltage instability by using devices which can process local signals, sense the decreased margin, and start the load shedding. Capitanescu *et al*. [46] have

used load shedding scheme to solve voltage instability. The decision by a controller to shed load is based on the comparison of voltage with a threshold value.

1.6.3.7. Generator rescheduling

Another way to keep system voltage stable is the activation of new generators. They can be activated in a few minutes to face the stability problems in short time interval. In order to solve this, spinning reactive power reserves have to be guaranteed by generators under operation. Raoufi and Mohsenar [47] have focused on the generator reactive power rescheduling for voltage stability enhancement.

1.6.3.8. Power loss reduction

Qiu and Shahidehpour [48] have emphasized on transmission line power loss reduction which also leads to voltage profile improvement and increase in the maximum transmitted power in cables and transformers by controlling the variables like transformer tap position and reactive power injection of the var resources.

1.6.3.9. FACTS devices

The flexible AC transmission systems (FACTS) devices are the examples of switched capacitors [49]. The FACTS devices help supplying and controlling the power flow in the transmission lines as well as increasing the usable transmission capacity. Hingorani and Gyugyi [50] have described the concept of FACTS and terms and definitions for different FACTS controllers. As FACTS devices are made-up using solid state controllers, their response is fast and accurate. Hence these devices can be utilized to enhance the voltage profile of the system using coordinated FACTS controllers in power systems.

1.6.3.9.1. Generation of FACTS controllers

Due to the development of the FACTS devices the voltage instability issues have been alleviated and have gained lots of interest in recent years. There are two generations of power electronics based FACTS controllers. The first generation uses conventional thyristor switched capacitor and reactors. The FACTS controllers such as thyristor controlled series capacitor (TCSC), static var compensator (SVC), and thyristor controlled phase shifting

transformer (TCPST) are developed in the first generation of FACTS controllers. The second generation of FACTS controllers employs gate turn off (GTO) thyristor switched convertors. The FACTS controllers such as static synchronous series compensator (SSSC), unified power flow controller (UPFC), static synchronous compensator (STATCOM), and interline power flow controller (IPFC) are developed in the second generation of FACTS controllers. Past research works have explored into the use of almost all of these categories of controllers to improve the system performance within several domains of interest both in the fields of static as well as dynamic analysis of power system. Due to their several advantages, some reported literatures have utilized one or more of the either generation devices and their related controllers in different types of systems ranging from benchmarked test systems to the actual ones. Therefore, they need to be reviewed here in some detail.

Sharma *et al*. [51] have also proposed a new method known as the extended voltage phasors approach (EVPA) for installation of FACTS (TCSC) controllers in power systems. Yorino *et al*. [52] proposed a new formula for reactive power (VAR) planning problem to allocate flexible ac transmission systems (FACTS) devices. The problem is formulated as a mixed integer nonlinear programming problem of a large dimension. Orfanogianni and Bacher [53] both presented an optimization-based methodology to identify key locations in the ac network where placement of a series-connected FACTS device increases the maximum megawatt power transfer. Minguez *et al*. [54] also addressed the issue of the optimal placement of static var compensators (SVCs) in a transmission network in such a manner that its loading margin is maximized. In another work of similar field, Farsangi and Mezamabadi-pour [55] proposed placement of SVCs and selection of stabilizing signals in power systems [54]. Among more advanced categories of FACTs Kannan *et al*. [56] proposed a new real and reactive power coordination controller for a unified power flow controller (UPFC). Similarly Alamelu and Devi [57] explained the method of placement of UPFC based on sensitivity analysis and evolutionary programming. In the domain of optimization, the problem was solved using the method of evolutionary programming. Donapati and Verma [58] approached for optimal placement of UPFC to enhance voltage stability margin under contingencies. In a problem of voltage stability, Singh and Erlich [59] suggested the location of the UPFC for enhancing power system loadability of the system. Some of the works have reported effective modeling of these devices for a particular application. In one such work, Niaki *et. al*. [60] did the steady state analysis of a novel hybrid flow controller. In another similar work, Bhowmick *et. al*. [61] reutilized the Newton power flow codes for an advanced IPFC power flow model. Zhang and Chen [62] suggested a power insertion model of IPFC for power flow

analysis inclusive of practical constraints. Verma and Srivastava [63] analyzed optimal placement of SVC for static and dynamic voltage stability. Sen [64] applied the theory and modeling of STATCOM applications.

An extensive discussion of many other literatures in the same field is out of scope of this present work and therefore it is limited to the extent of highlighting its importance in power system. Even though there are different approaches involving methods to formulate and solve the problem of voltage stability, the present work mostly is focused on the domain of optimization and application of heuristic optimization technique in solving the problem. Therefore, a review of similar earlier reported works need to be discussed here.

1.7. Methods and Techniques for Voltage Stability Analysis

A variety of optimization methods are used to optimize the allocation of reactive power compensating devices in power systems. Presently the shunt var compensator allocation problem is generally solved using evolutionary programming techniques. Numerous techniques for solving the optimal capacitor location problem in power systems have been reported in literatures. These techniques are classified into the different categories which are explained in the following paragraph.

1.7.1. Classical / analytical techniques

The classical optimization techniques are useful in finding the best possible solution or unconstrained maxima or minima of functions which are continuous and differentiable. These are analytical methods and apply differential calculus in locating the optimum solution. These classical techniques of optimization figure out a foundation to develop most of the numerical techniques that have grown into advanced techniques more suitable to modern problems. Various methods are adopted for the analysis of voltage stability and optimization techniques are used to find the solution for the problem of voltage stability. In [65], Yang *et al*. attempted to determine the optimal locations of thyristor-controlled series capacitor (TCSC) and their initial compensation levels using mixed-integer programming. Granville *et al*. [66] described an application of an optimal power flow, solved by a direct interior point (IP) method, to restore system solvability. A sequential quadratic programming algorithm for optimization power system is introduced by Fletcher [67]. Then Yan *et al*. [68] proposed a

new optimal reactive power flow (ORPF) model in rectangular form. In this work, prime dual interior point method used for solving the problem of voltage stability.

1.7.2. Heuristic techniques

The heuristic-based techniques have been widely applied in solving the optimal capacitor placement problem. In [69], Devaraj and Roselyn presented an improved genetic algorithm (GA) approach for voltage stability improvement. Paterni *et al*. [70] have used series FACTS as phase shifters, where the best location for a set of phase shifters is found by a genetic algorithm. Sirjani *et al*. [71] have addressed a novel global harmony search algorithm (NGHS) to determine the optimal location and size of shunt reactive power compensators such as static synchronous compensators (STATCOMs), shunt capacitors and static var compensators (SVCs) in a transmission network. Xu *et al*. [72] have studied a systematic method for optimal placement of dynamic VAR support using STATCOM against short-term voltage instability for a multi-objective optimization model. Mozafari *et al*. [73] have suggested under voltage load shedding (UVLS) to sustain voltage stability for contingencies in power systems. Huang and Huang [74] have also proposed a hybrid approach to solve the optimal reactive power dispatch (ORPD) problem based on the original differential evolution (DE) algorithm. Gerbex *et al*. [75] presents a genetic algorithm to seek the optimal location of multi-type FACTS devices in a power system.

1.7.3. Artificial intelligence based techniques

This section reviews the coordinated control of FACTS controllers based on various artificial intelligence based techniques like expert system (ES), genetic algorithm (GA), and artificial neural network (ANN). A new formulation of multi-objective reactive power and voltage control for power system is proposed by Zhang and Yutian [76]. The multi-objective formulation requires a global performance index of the problem. A pseudo goal function derived on the basis of the fuzzy sets theory gives an unique expression for the global objective function, eliminating the use of weighing coefficients or penalty terms. A fuzzy adaptive particle swarm optimization (FAPSO) is proposed to adaptively adjust the parameters of particle swarm optimization (PSO), such as the inertia weight and learning factors, during the evolutionary process. Wang *et al*. [77] proposed a new approach for modeling and solving var planning problem using an enhanced simulated annealing (SA) algorithm taking advantage of the modified gray code. Phadke *et al*. [78] have suggested a

strategy for placement and sizing of shunt FACTS controller using fuzzy logic and real coded genetic algorithm. Venkatesh *et al.* [79] suggested a multi-objective fuzzy linear programming (MFLP) method for optimal reactive power scheduling. In [80], Verma and Niazi proposed a supervised learning approach for fast and accurate power system security assessment and contingency analysis. Feed-forward artificial neural network (FFNN) is employed that uses pattern recognition methodology for security assessment and contingency analysis.

1.8. Motivation of the Research

The study of literature review has motivated further for analyzing the issue of voltage instability by modeling power system in contingent condition or increased load condition with consideration of security constraints. The study primarily limits its field of interest in determining the system stability with a faster technique of stability index that is within the realms of static analysis of the system. In recent years classical/analytical, heuristic, artificial intelligence based techniques have emerged as powerful tools capable of finding the optimum solution of a voltage stability problem. For improving the performance in different critical conditions, a number of modifications of these techniques or methodologies have been suggested in different literatures. Some methodologies are more complex than others and algorithms used are also not very accurate, reliable and flexible with respect to the sensitivity analysis in transmission network.

In the literatures, researchers have attempted to develop efficient techniques and tools for sensitivity analysis under practical constraints for determining the weak buses susceptible to the voltage instability. Various techniques of calculating performance indices are although surveyed in the literatures, the index calculations are basically based on the off line data, and local online data. The index value usually uses the parameters of the concerned network only and do not take into account the effects of the network outside or neighboring the (voltage unstable affected) network which is the point of interest to be investigated. The inclusion of the effect of the network outside the local network can lead to an accurate assessment of the system behaviour towards the voltage stability issue. Thus, the concept of including the outside network in the local network to get a strong indication about the system's weakest bus has motivated the research work to carry out with an index named as equivalent node voltage collapse index (ENVCI). Further, the work is extended to find an optimal solution for compensation in the system to prevent voltage instability as well as to increase the load

margin of the whole network. Unlike other techniques, bacteria foraging optimization algorithm (BFOA) has attracted the attention in the field of optimization techniques when the number of parameters to be optimized is very much large [90]. Although GA as reported in literature to exhibit degraded efficiency but still it has ability to arrive at the global solution point swiftly. In this research, the new Modified BFOA (MBFOA) is proposed being inspired by the natural genetic process as some of its adaptive features lead to faster convergence. The results would be compared with corresponding performances in GA. The objective of research work is described in the following.

1.8.1. Objectives of the Thesis

Based on the above motivation, the primary objectives of the research work are mentioned as follows.

- To apply the voltage stability index ENVCI as the criterion for detecting voltage instability and use the same in formulating an optimization problem. To determine the relative weaknesses of system buses in terms of voltage instability, utilizing ENVCI.
- To explore the benefits of using a suitably located STATCOM in a test benchmark system for improving voltage instability.
- To understand the problem of voltage instability in a system augmented by renewable energy generation system based on wind energy that drives doubly fed induction generators (DFIGs) for wind power. To study the effects of operating constraints of wind energy conversion systems (WECS) based on DFIGs along with a STATCOM in the system, on the problem of voltage stability.
- To formulate all the problems within the framework of optimization and to solve them with the help of MBFOA, and test its efficiency.
- Finally to develop a centralized corrective controller using a class of ANN, within the frame work of classification, that aims to predict the most sensitive control action selecting from a numbers of available reactive power resources.

1.9. Organization of Thesis

The thesis consists of seven chapters that are organized as follows.

In Chapter-1, literature reviews on different voltage stability studies are presented. The techniques used to assess the system behavior under contingencies are also discussed. The sensitivity analysis methods also reviewed.

In Chapter-2, 39 Bus-New England Test System is considered for the study. By using offline method of index calculation, three different indices namely; Q-loss index, Q-V sensitivity index, and L-index are determined for load increased scenario. The three indices are combined with proper weighing to each index and a weighted average sensitivity index (WASI) found out. Although, the WASI value determines the weak bus but the online application of the stability index calculation is focused. Literature survey demonstrates ENVCI is an online stability index which gives more accurate information about the system's weakness condition as it includes the effect of the rest of the system outside the local network where the load is increased to operate in stressed condition. The index calculation gives a clear picture about the healthiness of the system. It becomes very much approximate / concrete as it is compared with the established offline stability index (WASI). The study is made with same 39- bus New England test system. The ENVCI value becomes 1 means the system is healthy/ strong. The concept, modeling and equations involved in deriving the index are expressed in this chapter. The ENVCI is used for determining the maximum loading of each bus and rank the buses in the decreasing order of weakness.

In Chapter-3, top five weak buses listed from the result obtained in Chapter -2, considered for the optimization and only two candidate buses are used for optimal location and size of the static VAR compensation. Four optimization techniques namely MBFOA, DE, PSO and GA are used. The comparisons between the techniques are studied.

In Chapter-4, the system model is modified with inclusion of STATCOM in the weakest bus (bus no 20 from ENVCI calculation with load increase). The maximum loadability of the buses without STATCOM are found out. The bus with minimum value of maximum loading limit among all the buses is tagged as the weakest bus. The STATCOM is placed in the weakest bus. With the load increase in the weakest bus, it requires optimal value of VAR in addition to the STATCOM already installed. The objective is to increase the load margin and maintain the operating voltage level.

In **Chapter-5,** a generator is replaced by an equivalent wind farm in addition to the modified model as considered in Chapter-4 (STATCOM at bus no 20 in the IEEE-39 bus system). The objective function is formulated with three constraints. These are load margin, voltage deviation and power loss respectively. Here, the main aim is to increase the load margin and to improve the voltage profile for optimal location as well as size of VAR. The optimization is employed the MBFOA technique. The modified Y bus matrix of the system is found out. With the system structure, the loading margin is enhanced keeping the operating voltage at stable condition with the system being subjected to further load increase in the weak bus only as there may be demand of load increase. The optimal value of the STATCOM is obtained from the MBFOA technique.

In **Chapter-6,** the New England 39 Bus system is loaded with step load increase and made to behave as a stressed operating system. In the stressed system the contingency case is studied. Some contingencies were taken up for studying voltage instability. Different control parameters which help improving the voltage stability are considered for this study. The parameters are the transformer taps, AVR setting of generators, real and reactive power rescheduling of generators, shunt static capacitive compensation, and selective minimum load shedding. For a single line outage contingency case the appropriate control action is determined. Similarly this process is repeated for many cases of line outages. The data are now trained with inputs as the line flows as well as voltage of buses. The output of the training set is a single output which is a control action with help of a controller. Data collected are fed to the artificial neural network for training. A PNN controller is designed to control the voltage instability. The sensitivity analysis is also carried out using ENVCI.

Chapte-7 includes the conclusions and scope for future work.

ON LINE VOLTAGE STABILITY ASSESSMENT OF TRANSMISSION NETWORK THROUGH ENVCI

2.1. Introduction

The steady state static analysis of voltage instability in a large interconnected power system gives considerable idea about the vulnerability of the system. The steady state stability analysis is made because of the followings:

a. Dynamic stability studies require dynamics of the components of a large network which can have a large number of equations containing nonlinearities. The dynamic study is time dependent. Thus the system models used in such studies are extensive because of the system are large, complex in interconnection with many machines.

b. These machines have excitation systems and turbine governing system controls on the whole cannot be modeled in ordered to reveal accurately correct dynamic performance of the system. The nonlinear differential equations are formed and this has to be solved.

c. Dynamic stability involves the study of a large network where the disturbance to the system is quite large *i.e* large fault for long time, loss of generators, sudden load changes and line switching .in dynamic stability the linearization of the system equations are not allowed.

d. Steady state analysis is the linear version of dynamic stability. The nonlinear differential and algebraic equations of the system are replaced by a set of linear equations which can be solved.

The researchers in this field have tried to find out an effective voltage stability index, which should be able to forecast the voltage stability condition of the system in an accurate and fast manner [82-85] As discussed in the previous chapter, the vulnerable or weak areas (buses) of the system is usually judged by the sensitivity of any index with respect to load

Chapter 2

increase in a particular bus. However, the results obtained with different indices are different and gives different indication about the ranking of weak buses in the system. Without accurate information about the relative weakness of all the system buses, it is not possible to do any further analysis. Therefore, to avoid the situation, a weighted index known as weighted average sensitivity index (WASI) is proposed and formulated in this work. Some other important issues also decide the accuracy of an index. One of them is that most of the index calculations generally neglect the effects of network portions which are distant to the locality (area of operation under study), but, those areas may have become more vulnerable to instability. Similarly, many of the indices are evaluated in an off line manner, which make them unfit for their application in designing online index based controllers. Therefore, this work selects a more recently proposed index ENVCI [41], which can also be evaluated from bus voltage phasor data obtained by phasor measuring units (PMUs). Since this work is limited to simulation and analysis only, it has utilized the power flow algorithm for its calculation. The index is compared for its accuracy with other indices including a relatively more accurate index WASI. The value obtained being very close to the respective WASI value, the ease of computation of this index has encouraged this work to consider it for formulating the same in subsequent problems.

2.2. Steady State Voltage Stability Indices

Besides P-V and Q-V curves discussed in the previous chapter, there are several other steady state voltage stability indices (VSIs) playing important role for assessing the state of system quickly as there may be a continuous load increase or occurrence of any contingency. The voltage stability index (VSI), can be utilized to estimate the vulnerable condition of the line, *i.e.* the proximity of the line towards voltage collapse. A brief overview gives insight into some of these indices with their relative merits and demerits for suitability towards their use described in the following section.

2.2.1.   Line stability index

The line stability index is obtained [33] with the value of active power, reactive power, voltage and reactance. The index value can be calculated by using the following formula as given in the equation

$$LQP = 4\left(\frac{X}{V_m}\right)\left(\frac{X}{V_m}P_m^2 + Q_n^2\right) \qquad (2.1)$$

Where, X is the line reactance,

Q_n is the reactive power flow at the receiving bus,

V_m and P_m are the voltage and active power at the sending bus respectively.

To maintain a stable operating condition, the value of index should be maintained less than 1.

2.2.2. V/V$_0$ index

A very elementary knowledge about the system bus voltage conditions under a particular operating condition can be obtained with this index. The bus voltage values are determined for the two different operating cases. The bus voltage (V) values are normally very close to 1 at base case loading and the voltage (V_0) are attained which are very less than 1 at critical loading case. The ratio V/V$_0$ at each node yield a voltage stability record of the system, allowing for immediate detection of weak buses of the system for effective countermeasure [27].

2.2.3. Line stability index

In [33], Moghavemmi *et al.* have derived a line stability index based on the power transmission concept in a single line as shown in Figure 2.1.
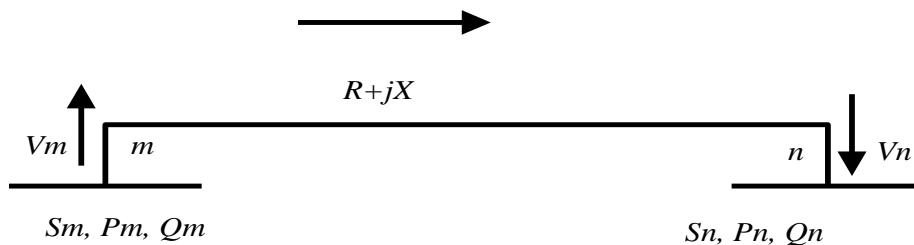
Figure 2.1. A single line of an interconnected network.

It illustrates a single line of an interconnected network where, R is resistance of the transmission line, X is reactance of the transmission line, P_m and P_n are the real power at m[th] and n[th] nodes respectively, Q_m and Q_n are reactive power at m[th] and n[th] nodes respectively, S_m

and S_n are conjugate power at m^{th} and n^{th} nodes respectively, θ is the line impedance angle and δ is the angle difference between the supply voltage and the receiving end voltage.

The line stability index for this model can be expressed as

$$L_{mn} = \frac{4XQ_n}{[V_m \sin(\theta - \delta)]^2}$$

(2.2)

Lines that represent values of L_{mn} close to 1, indicates that those lines are closer to their stability limit. To maintain a secure condition, the L_{mn} index should be less than 1. The discriminant of the voltage quadratic equation is set to be greater or equal than zero to achieve stability. If the discriminant is smaller than zero, then the roots will be imaginary, which indicates an unstable condition in the system.

2.2.4. Fast voltage stability index (FVSI)

The line stability index fast voltage stability index (FVSI) proposed by Musirin *et al.* [35] is based on a concept of power flow through a single line. For a typical transmission line, the stability index is calculated by:

$$FVSI_{ij} = \frac{4Z^2 Q_j}{V_i^2 X}$$

(2.3)

where, Z is the line impedance, X is the line reactance, Q_j is the reactive power flow at the receiving end and V_i is the sending end voltage.

The line that gives index value closest to 1 will be the most critical line of the bus and may lead to the whole system instability. The calculated FVSI can also be used to determine the weakest bus on the system. The determination of the weakest bus is based on the maximum load allowed on a load bus. The most vulnerable bus in the system corresponds to the bus with the smallest maximum permissible load.

2.2.5 Q-loss sensitivity index

The basic equations used for N-R power flow method are expressed [81] in following equation

$$\begin{bmatrix} \Delta P \\ \Delta Q \end{bmatrix} = \begin{bmatrix} \dfrac{\partial P}{\partial \delta} & |V|\dfrac{\partial P}{\partial |V|} \\ \dfrac{\partial Q}{\partial \delta} & |V|\dfrac{\partial Q}{\partial |V|} \end{bmatrix} \begin{bmatrix} \Delta \delta \\ \dfrac{\Delta |V|}{|V|} \end{bmatrix} \tag{2.4}$$

Or, $$\begin{bmatrix} \Delta P \\ \Delta Q \end{bmatrix} = \begin{bmatrix} J_{11} & J_{12} \\ J_{21} & J_{22} \end{bmatrix} \begin{bmatrix} \Delta \delta \\ \dfrac{\Delta |V|}{|V|} \end{bmatrix} \tag{2.5}$$

From the above equation the reactive power sensitivity for the ith bus is formed and expressed as in the following equation. Hence the equation can be termed as the Q-loss sensitivity, denoted by SI_1 in the following equation.

$$SI_1 = \frac{\partial Q_i}{\partial |V_i|} = \left[J_{22_{ii}} \right] \div |V_i| \tag{2.6}$$

For SI_1 having higher value the degree of weakness is less for a bus.

2.2.6. L-index

L-Index is evaluated here for any j^{th} non-generator bus in a N-Bus system having g numbers of generators *i.e.*, 1…g, and (g+1)…..N, (N-g) numbers of load buses. It can be evaluated by the following equation [30].

$$SI_2 = L_j = \left| 1 - \sum_{i=1}^{i=j} F_{ji} \left(\frac{V_i}{V_j} \right) \right| \tag{2.7}$$

where, V_i, V_j are the complex voltages of the generator buses and load buses respectively. The elements F_{ji} can be evaluated from the Y-bus matrix of the system as depicted below by equation,

$$\begin{bmatrix} I_G \\ I_L \end{bmatrix} = \begin{bmatrix} Y_{GG} & Y_{GL} \\ Y_{LG} & Y_{LL} \end{bmatrix} \begin{bmatrix} V_G \\ V_L \end{bmatrix} \tag{2.8}$$

where, I_G, I_L, V_G, V_L are the complex currents and voltages of the generator bus and load buses respectively. $[Y_{GG}], [Y_{GL}], [Y_{LG}], [Y_{GG}]$ are corresponding partitioned portions of the network Y-bus matrix, the equation can be rewritten by rearranging in the following way

$$\begin{bmatrix} V_L \\ V_G \end{bmatrix} = \begin{bmatrix} Z_{LL} & F_{LG} \\ K_{GL} & Y_{GG} \end{bmatrix} \begin{bmatrix} I_L \\ V_G \end{bmatrix}$$

(2.9)

where, $\qquad F_{LG} = -\left[Y_{LL} \right]^{-1} \left[Y_{LG} \right]$ (2.10)

The L_{index} of the system or at a particular bus, varies in a range between 0 (no load) and 1 (voltage collapse). For L_j , the threshold value is supposed to be 1.0.

2.2.7. V-Q sensitivity index

The jacobian matrix employed to compute bus voltages in Newton-Raphson load flow (NRLF) method is given by

$$\begin{bmatrix} \Delta P \\ \Delta Q \end{bmatrix} = \begin{bmatrix} J_{11} & J_{12} \\ J_{21} & J_{22} \end{bmatrix} \begin{bmatrix} \Delta \delta \\ \Delta |V| \end{bmatrix}$$

(2.11)

The ith diagonal element of the matrix $[J_{22}]$ of Equation 2.4 is the V-Q sensitivity of the ith load bus use

$$\frac{dQ_i}{dV_i} = [J_{22}]_{ii}$$

(2.12)

$$[\Delta |V|] = [J_R]^{-1}[\Delta Q]$$

(2.13)

or, $\qquad [\Delta Q] = [J_R][\Delta |V|]$ (2.14)

where, $\qquad [J_R] = [J_{22}] - [J_{21}][J_{11}]^{-1}[J_{12}]$ (2.15)

The ith diagonal element of $[J_R]^{-1}$ also indicates the V-Q sensitivity of the load bus-i,

when $\qquad \dfrac{d|V_i|}{dQ_i} = [J_R]_{ii}^{-1}$ (2.16)

The slope of V-Q curve is the V-Q sensitivity of the bus. A positive V-Q sensitivity is an indicator of stable operation, the smaller the sensitivity the more the stable operation as the value increases, the system becomes vulnerable to voltage stability. A set of eigen values are

computed to assess the voltage stability characteristic. The reduced Jacobian matrix $[J_R]$, given by the following equation is [81]

$$[J_R] = [\xi][\lambda][\eta] \tag{2.17}$$

where, ξ_b = right eigenvector, η = left eigenvector matrix of J_R and λ = eigen value

Combining Equation 2.13 and 2.17 the following equation is developed

$$[\Delta V] = [\xi][\lambda]^{-1}[\eta][\Delta Q] \tag{2.18}$$

$$[\Delta V] = \left[\sum_i \frac{\xi_i \eta_i}{\lambda_i} \Delta Q \right] \tag{2.19}$$

Thus, from the above equation the V-Q sensitivity index at k^{th} bus can be written as

$$\frac{\partial V_k}{\Delta Q_k} = \sum_i \frac{\xi_{ki} \eta_{ik}}{\lambda_i} \tag{2.20}$$

$$SI_3 = \frac{\partial V_k}{\partial Q_k} = \sum_i \frac{\xi_{ki} \eta_{ik}}{\lambda_i} \tag{2.21}$$

where, $\xi_i = i^{th}$ column right eigenvector, $\eta_i = i^{th}$ row left eigenvector matrix of J_R and λ_i = eigen value of i -bus

Even though, a comprehensive study of different VSIs are not elaborated, but most widely used ones also possess some drawbacks, particularly when their status needs to be known quickly in an online manner. A fast online evaluation of the VSI is necessary so that a quick decision of any possible corrective action can be chosen. The limitation and drawbacks are elaborated below.

2.2.8. Drawbacks of different VSIs

The voltage stability indices possess some demerits. The major drawbacks of the existing indices are given below. A common demerit of the existing line-based indices is the fact that impacts of the rest of system outside the line have been ignored and this will lead to inaccurate or even incorrect results in some cases. In these indices effect of outside line cannot be ignored.

i. The existing indices may become unstable in its numerical determination near the Notch point of the P-V curve (the limiting point), when the loads at some buses in an area are gradually increased and the steady state load flow is carried out in offline mode taking the system voltage stability into account.

ii. Even for an online application when a corrective action needs to be taken based on estimated bus voltage or Wide Area Measured (WAM) data, the speed and accuracy of the line based indices may deteriorate near the limiting loading condition.

iii. The most commonly used index is the *L*-index. Generally, the point of voltage instability is reached when the value exceeds 0.9. However, in many cases it has been reported [30] that, the voltage collapse does not occur even when *L-index* is 1.7 and sometimes voltage collapse occurs even before when *L-index* < 0.9.

Due to the inefficiencies of each index the formulation of another common index is made which is explained in the next section.

2.3. Weighted Average Sensitivity Index (WASI)

A weighted index termed as weighted average sensitivity index(WASI) comprising the effects of all the above mentioned indices is formulated, based on whose value a weak bus ranking could be done. This approach helps to determine a worse case loading scenario in the system. The WASI is defined as follows

$$WASI = (SI_1 \times w_1 + SI_2 \times w_2 + SI_3 \times w_3 + \ldots SI_n \times w_n)/(w_1 + w_2 + \ldots + w_n) \qquad (2.22)$$

where, w_1, w_2, w_3, w_n are the weighing factor. Though any value may be chosen, in this work it is taken between 0.1-0.9. $SI_1, SI_2, SI_{3\ldots} SI_n$ are the indices, considered for its evaluation. The problems of considering only the local network can be solved by using a comparatively more recently proposed voltage stability index, called ENVCI. It is discussed in the next subsection.

2.4. Equivalent Node Voltage Collapse Index (ENVCI) [41]

In this index, the effect of outside the local network is considered. This is the unique characteristic of this index. In the simulations, loads at the weaker nodes are gradually and proportionally increased to stress the system with multiplying a load parameter (LP) 'λ'. This work uses a voltage stability index, which is called as ENVCI [41]. It has the following features:

- Compared to the existing line-based voltage indices, the effect of the rest of a system outside the local network is included through an equivalent model of the system. This assures accuracy of the index in modeling.

- Compared to the internal and external impedance method, the equivalent system impedance that needs to be estimated using two system states is only a small part of the total impedance whereas the impedances of local network (branches that are directly connected to the considered node) are known and need not be estimated using two system states.

- Unlike the conventional method based on continuation power flows, and calculation of other indices based on conventional power flow, the computation of ENVCI is much faster since it is associated with very simple calculations and no system-wide power flow evaluation.

- The calculation of ENVCI only requires the information of local voltage phasors, which can either be obtained via synchronized phasor measurement units (PMU) or through the state estimation of energy management system (EMS) at control centers of utilities. This enables ENVCI to be easily applied in on-line (EMS) or real time (PMU) environment.

- The presented method can identify the weak nodes of the system taking into account the ENVCI values of all observed nodes. The ENVCI at the weakest node will be very much near zero when the system approaches its voltage breakdown point. Therefore, an entry of ENVCI can be easily set up to cause an emergency remedial scheme to avoid the system from voltage collapse.

The formulation of ENVCI at the outset, involves the reduction of the external part of the entire network in terms of an equivalent local network model. The equivalent system

model (ESM), then includes the local network into the equivalent local network model. For the sake of clarity, the equivalent models are explained as follows.

2.4.1. Equivalent local network model (ELNM) [41]

A local network in the transmission system having N nodes is considered. The local network is divided into two portions. The first portion is represented by an equivalent outgoing power flow $P_{on}+jQ_{on}$ as shown below in the Figure **2.2**. The total power flowing out of the Nth node is the sum of line power flows on all the lines with outgoing flows, plus the load, generator power and compensated reactive power at the node N as shown in the Figure **2.2**. The second portion comprises all the lines with power flows entering the node N, each of which is expressed by a Π circuit at its left side. The P_n+jQ_n in Figure **2.2** is $P_{on}+jQ_{on}$ plus the reactive charging powers at the receiving end of all the lines in the second portion. It is obvious that the outgoing current at the node N can be expressed as

$$\vec{I}_n = {S_n^*}\Big/{V_n^*} = \sum_{i=1}^{M} Y_{ni}\left(\vec{V}_i - \vec{V}_n\right) \tag{2.23}$$

$$\text{or,} \quad = \sum_{i=1}^{M} Y_{ni}\vec{V}_i - \sum_{i=1}^{M} Y_{ni}\vec{V}_n$$
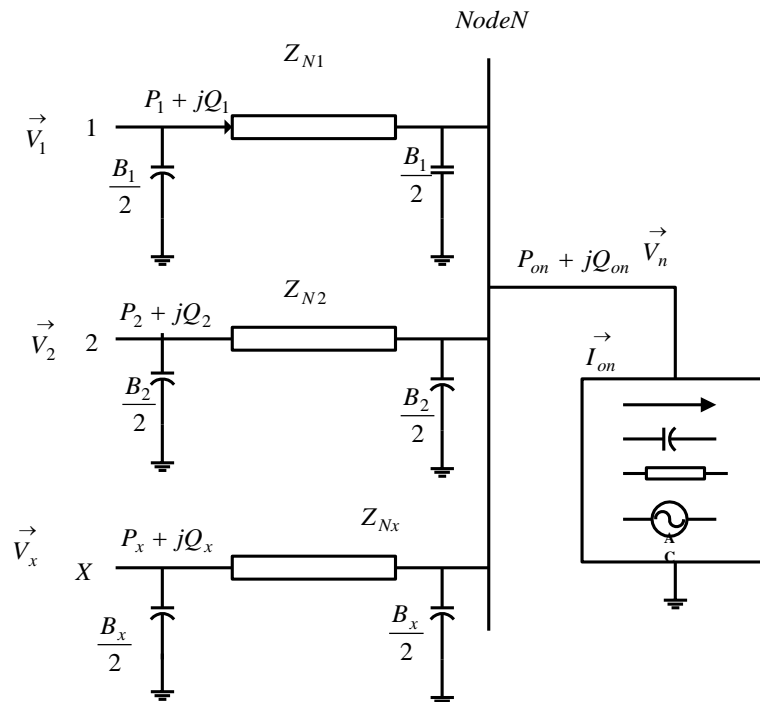
Figure 2.2. Original local network model. **[41]**

$$or, \vec{I}_n = \sum_{i=1}^{M} Y_{ni} V_i - Y_{eq} \vec{V}_n \tag{2.24}$$

where,

$$Y_{ni} = \frac{1}{Z_{ni}} \quad and \quad Y_{eq} = \sum_{i=1}^{M} Y_{ni} \tag{2.25}$$

Y_{ni} and Z_{ni} are the admittance and impedance of lines between the ith and nth nodes respectively; $\vec{V}_i$ and $\vec{V}_n$ are the voltage phasors at the ith and nth nodes; The superscript * represents conjugate in the work and thus $\overrightarrow{V_n^*}$ is the conjugate phasor of $\vec{V}_n$ and M is the number of lines with power flows entering the node N. Multiplying $\overrightarrow{V_n^*}$ at the both sides of Equation 2.23 yields

$$S_n^* = \vec{V}_n^* \vec{I}_n = \vec{V}_n^* \sum_{i=1}^{M} Y_{ni} \vec{V}_i - \vec{V}_n^* Y_{eq} \vec{V}_n \tag{2.26)}$$

$$let, \quad \vec{V}_{eq} = V_{eq} \angle \theta_{eq} = \sum_{i=1}^{M} Y_{ni} \vec{V}_i \Big/ Y_{eq} \tag{2.27}$$

Assuming $\vec{V}_n = V_n \angle \theta_n$ and substituting these values into Equation 2.26, the following equation is obtained.

$$S_n^* = (\vec{V}_n^* \vec{V}_{eq} - \vec{V}_n^* \vec{V}_n) Y_{eq} \tag{2.28}$$

$$S_n^* = \vec{V}_n^* (\vec{V}_{eq} - \vec{V}_n) Y_{eq} \tag{2.29}$$

Thus from the above equation, it is found

$$\vec{I}_n = \left(\vec{V}_{eq} - \vec{V}_n \right) Y_{eq} \tag{2.30}$$

From Equations 2.29 and 2.30, a single line model (*i.e.,* ELNM) which is equivalent to the second portion of the local network containing the lines with power flows entering the node N is obtained and shown in Figure **2.3.**
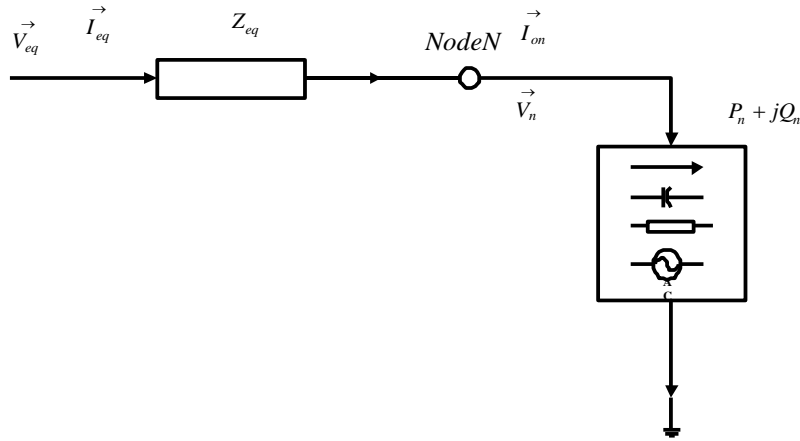
Figure 2.3. Equivalent local network model (ENLM). **[41]**

2.4.2. Equivalent system model (ESM) [41]

A replica voltage source E_k with impedance Z_{km} is added to the ELNM to include the effect of the system external of the local network, as shown in Figure **2.4.**
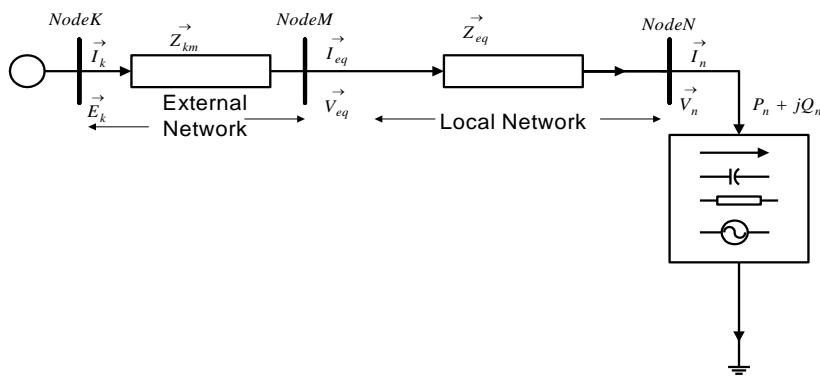
Figure 2.4. Equivalent system model. [41]

All the grounding branches representing reactive charging powers at the source end of the lines with power flows entering the node N have been assumed to be part of Z_{km}, which can be estimated later. The $\vec{E}_k$ and Z_{km} will have the exactly same effect as the whole system outside the local network as long as they can guarantee the identical voltage phasors and power flows for the equivalent line. These two are added to the ELNM to satisfy the following equation

$$\left(P_{km} + jQ_{km}\right)^* = \vec{V}_{eq}^* \cdot \frac{\vec{E}_k - \vec{V}_{eq}}{Z_{km}} = \vec{V}_{eq}^* \cdot \frac{\vec{V}_{eq} - \vec{V}_n}{Z_{eq}} \qquad (2.31)$$

where, P_{km} and Q_{km} are the real and reactive powers flowing into the local network, which corresponds to $\sum_{i=1}^{M} P_i + jQ_i$

The Z_{km} represents the equivalent system impedance that the power flow encountered in the system before it reaches the local network. From Equation 2.31, the following equations can be derived:

$$V_{eq}\angle -\theta_{eq} \cdot \frac{E_k \angle \theta_k - V_{eq}\angle \theta_{eq}}{Z_{km}} = V_{eq}\angle -\theta_{eq} \cdot \frac{V_{eq}\angle \theta_{eq} - V_n \angle \theta_n}{Z_{eq}} \qquad (2.32)$$

$$or, \quad \frac{E_k V_{eq}\angle(\theta_k - \theta_{eq}) - V^2_{eq}}{Z_{km}} = \frac{V_{eq}^2 - V_n V_{eq}\angle(\theta_n - \theta_{eq})}{Z_{eq}} \qquad (2.33)$$

$$or, \frac{Z_{km}}{Z_{eq}} = \frac{E_k V_{eq}\angle(\theta_k - \theta_{eq}) - V^2_{eq}}{V_{eq}^2 - V_n V_{eq}\angle(\theta_n - \theta_{eq})} \qquad (2.34)$$

Assuming $Z_{kn} = Z_{km} + Z_{eq}$ as well as a complex coefficient K yields

$$K = \frac{Z_{km} + Z_{eq}}{Z_{eq}} = \frac{Z_{kn}}{Z_{eq}} = \frac{E_k \angle(\theta_k - \theta_{eq}) - V_n \angle(\theta_n - \theta_{eq})}{V_{eq} - V_n \angle(\theta_n - \theta_{eq})} \qquad (2.35)$$

Letting

$$\vec{E}'_k = E'_k \angle \theta'_k = E_k V_{eq}\angle(\theta_k - \theta_{eq}), \vec{V}'_n = V'_n \angle \theta'_n = V_n V_{eq}\angle(\theta_n - \theta_{eq})$$
$$and \ \vec{V}'_{eq} = V_{eq}\angle 0 = V'_{eq}$$

And let E_k and impedance Z_{km} are constant. Thus putting these values in Equation 2.35, we have the following expression:

$$or, \quad K = \frac{\vec{E}'_k - \vec{V}'_n}{V_{eq} - \vec{V}'_n}$$

or, simplifying the above equation it becomes $\quad K(V_{eq} - \vec{V}'_n) = \vec{E}'_k - \vec{V}'_n$

And further simplification results $\quad \vec{E}'_k = K \times V'_{eq} + (1-K)\vec{V}'_n$

Finally it becomes $\quad \vec{E}'_k = K(V'_{eq} - \vec{V}'_n) + \vec{V}'_n \qquad (2.36)$

It is assumed that the equivalent voltage source E_k and impedance Z_{km} are constant between two adjacent system equilibrium states. It follows from Equation 2.36 that

$$\vec{E}'_k = K \times V'_{eq1} + (1-K)\vec{V}'_{n1} \tag{2.37}$$

$$\vec{E}'_k = K \times V'_{eq2} + (1-K)\vec{V}'_{n2} \tag{2.38}$$

Here, subscripts 1 and 2 represent the system states 1 and 2. Solving above two Equations 2.37 and 2.38 yields:

$$K \times V'_{eq1} + (1-K)\vec{V}'_{n1} = K \times V'_{eq2} + (1-K)\vec{V}'_{n2}$$

$$\text{or,} \quad K \times (V'_{eq1} - V'_{eq2}) = (1-K) \times \vec{V}'_{n2} - (1-K) \times \vec{V}'_{n1}$$

$$\text{or,} \quad K \times (V'_{eq1} - V'_{eq2}) - K \times (\vec{V}'_{n1} - \vec{V}'_{n2}) = \vec{V}'_{n2} - \vec{V}'_{n1}$$

$$\text{or,} \quad K \times (V'_{eq1} - V'_{eq2}) - K \times (\vec{V}'_{n1} - \vec{V}'_{n2}) = \vec{V}'_{n2} - \vec{V}'_{n1}$$

$$\text{or,} \quad K \times \{(\vec{V}'_{n1} - \vec{V}'_{n2}) - (V'_{eq1} - V'_{eq2})\} = (\vec{V}'_{n1} - \vec{V}'_{n2})$$

$$\text{or,} \quad K = \frac{(\vec{V}'_{n1} - \vec{V}'_{n2})}{(\vec{V}'_{n1} - \vec{V}'_{n2}) - (V'_{eq1} - V'_{eq2})}$$

$$\text{or,} \quad K = \frac{1}{1 - \dfrac{(V'_{eq1} - V'_{eq2})}{(\vec{V}'_{n1} - \vec{V}'_{n2})}}$$

$$K = \frac{1}{1 - (V'_{eq1} - V'_{eq2})/(\vec{V}'_{n1} - \vec{V}'_{n2})} \tag{2.39}$$

By substituting K into Equation 2.35, $\overrightarrow{E'_k}$ can be obtained and then $E_k \angle (\theta_k)$ can be calculated. With K, it is easy to calculate Z_{kn} from Equation 2.35

$$Z_{kn} = K.Z_{eq} \tag{2.40}$$

A single line ESM is obtained with the above derivation method, which takes into account both the local network and the system outside the local network. By using this model, the two key quantities that are essential to calculate the new ENVCI, which is derived in the next subsection, can be considered from the node voltage phasors at two line ends in the second portion of the local set-up. In fact, the voltage phasor $V_n \angle \theta_n$ at the nth node can be directly measured but the equivalent source voltage $E_k \angle \theta_k$ can be estimated from the voltage phasors and line parameters through intermediate equivalent voltage phasor $V_{eq} \angle \theta_{eq}$ and equivalent admittance Y_{eq}. It should be highlighted that the ESM derived here is an equivalence indicating the effects of the whole system on a single node (bus) in a specific system state. In other words, each node in a system state refers to a different ESM. These ESMs of individual nodes are used to compute their ENVCIs.

2.4.3. Formulation of ENVCI[41]

In the single line equivalent system model for the nth node shown in Figure **2.4**, the outgoing power at this node must satisfy the following power flow equations given by

$$P_n + jQ_n = \vec{V}_n \cdot \frac{\left(\vec{E}_k - \vec{V}_n \right)^*}{Z_{kn}} \tag{2.41}$$

Let the voltage phasors at the two nodes of an equivalent single line model are expressed in the rectangular coordinates, *i.e.*, $\vec{E}_k = e_k + jf_k$, $\vec{V}_n = e_n + jf_n$, and the line impedance is expressed by $\vec{Z}_{kn} = R_{kn} + jX_{ki}$. Equation 2.41 can be separated into a real part and an imaginary part and expressed in the following equations respectively,

$$P_n R_{kn} + Q_n X_{kn} = e_n \left(e_k - e_n \right) + f_n \left(f_k - f_n \right) \tag{2.42}$$

$$P_n X_{kn} - Q_n R_{kn} = f_n e_n - e_k f_n \tag{2.43}$$

Equations 2.42 and 2.43 are mainly the power flow equation for solving the voltage phasor at n^{th} node of the equivalent line that is corresponding to the effect of both local network and system outside the local network. If each ESM for all equivalent lines in a network state finds a mathematical solution for its receiving node, it indicates that voltages at all nodes in the network state are present, then the system must have an overall power flow solution and the network voltage stability survives. On the contrary, if an ESM for at least one node does not

find a mathematical solution, it indicates that the operational voltage at the node does not exist and the system cannot result a system-wide load flow solution, and finally the system loses voltage stability. In other words, the system stability relies on the solvability of above two Equations 2.42 and 2.43 for all nodes in the system. The solvability of the equations can be judged by singularity of its Jacobian matrix, expressed by the following equation.

$$J = \begin{bmatrix} e_k - 2e_n & f_k - 2f_n \\ f_k & -e_k \end{bmatrix}$$
(2. 44)

$$Det(J) = 2\left(e_k e_n + f_k f_n\right) - \left(e^2_k + f_k^2\right) = 0$$
(2.45)

Where the symbol *Det* denotes the determinant of the Jacobian matrix, *J*. Equation 2.46 provides a new voltage stability index, which is called the equivalent node voltage collapse index (ENVCI):

$$ENVCI = 2\left(e_k e_n + f_k f_n\right) - \left(e^2_k + f_k^2\right)$$
(2.46)

Also, it is easy to derive the expression of ENVCI in the polar coordinates, which is given by

$$ENVCI = 2E_k V_n \cos\theta_{kn} - E_k^2$$
(2.47)

where, $\theta_{kn} = \theta_k - \theta_n$. It can be noticed that the calculation of ENVCI only desires voltage phasors at the two ends of the ESM. Each node has an ESM. When the ENVCI of at least one node is close to zero in a network state, the network comes near the voltage collapse point and the subsequent node is the weakest node that leads to system instability. The ENVCI can be easily applied in a real time or on-line environment since it can be estimated very fast with the use of the voltage phasors obtained from either the state estimator of EMS or PMU measurements.

2.4.4. Algorithm steps for evaluation of ENVCI

*Step*1. Initialization
> (a) Bus data (b) Line data (c) Loading parameter(LP)= λ (d) Load voltage (e) Bus voltage are initialized.

*Step*2. Iterative Algorithm

NRLF method performs for load flow. Output of NRLF used as input for ENVCI calculation. At load buses, LP increases in stepwise manner and corresponding ENVCI value is calculated. Steps are

1. Performance of NRLF method

2. Load bus identification (node): Total no of load buses are identified varying number $n_i = [1, 2.....17]$

3. Y-equivalent calculation from y-sparse

Step 3: Iteration

1. Begin: For load bus $n_i = 1$

2. Increment of LP (λ) by 0.01

For ii=1:s

$\lambda = 1 + (ii - 1) \times stepvalue$

3. Perform load flow.

4. Compute equivalent voltage, equivalent impedance and equivalent admittance as per the Chapter 2, subsection 2.2.

5. Again (λ) increment

(λ new) = λ + *step value*

6. Go to step 4

7. Source voltage (external source, E_K) and its impedance calculation.

8. Calculate ENVCI.

9. Go to step3.2 and Repeat till (ii <= s).

10. Save ENVCI Values in a proper format.

11. Go to the beginning of Step 3

12. End

Step 4: Identification of buses with lower ENVCI value (*i.e.* near to zero). Refer these buses as weak buses. Evaluate the voltage stability limit by plotting different graphs between 'λ' versus 'ENVCI'.

It can be recalled here that, the step of NRLF method may not be used for the calculation of ENVCI and the PMU bus voltage phasor data can be utilized after proper estimation. However, since this work is limited to simulation and analysis, therefore in the first step a load flow solution is necessary for the evaluation. A brief description of NRLF method is reviewed below.

2.5. Newton-Raphson Load Flow (NRLF)

NRLF method is applied to the problems of load flow in the network. It is found to be more efficient and practical and the number of iterations necessary to obtain the solutions is independent of the system size, but more functional evaluations are required for each iteration. Since in the power flow problem, real and voltage magnitude are specified for voltage control buses, the power flow equations are formulated in polar form. The active and reactive powers at each bus are functions of magnitudes and phase angles of bus voltages. Thus,

$$P_i = f_1(\delta,|V|) \tag{2.48}$$

$$Q_i = f_2(\delta,|V|) \tag{2.49}$$

For a system having n buses and bus no 1 designated as slack bus, the equations which relate the changes in active and reactive power to changes in bus voltage magnitude and angles take the form.

$$\left. \begin{aligned} \Delta P_i &= \sum_{p=2}^{n} \frac{\partial P_i}{\partial \delta_p} \Delta\delta_p + \sum_{p=2}^{n} \frac{\partial P_i}{\partial |V_p|} \Delta|V_p| \\ \Delta Q_i &= \sum_{p=2}^{n} \frac{\partial Q_i}{\partial \delta_p} \Delta\delta_p + \sum_{p=2}^{n} \frac{\partial Q_i}{\partial |V_p|} \Delta|V_p| \end{aligned} \right\} \tag{2.50}$$

ΔP_i and ΔQ_i represent the differences between the specified and the calculated values of P_i and Q_i. Equations 2.48 and 2.49 can be used to resolve the bus voltage magnitudes and angles from a random set of values through an iterative procedure. For each load bus both P and Q are specified and therefore Equation 2.48 exists. However, for a PV bus, Q is not specified and therefore, there is no equation corresponding to Equation 2.48 for PV bus. For an n bus system having 1 slack bus and g voltage controlled (PV) buses, the total number of equations is (2n-2g). Thus, the use of polar form results in lesser number of equations and size of Jacobian is smaller as compared to the rectangular form. This is a definite advantage of polar form over the rectangular form and, therefore, only polar form is used. Rectangular form is also used in some cases although. It has been found convenient to put

$\Delta|V_p| = |V_p| \dfrac{\Delta|V_p|}{|V_p|}$ in Equations 2.48 and 2.49, thus it become

$$\Delta P_i = \sum_{p=2}^{n} \frac{\partial P_i}{\partial \delta_p} \Delta \delta_p + \sum_{p=2}^{n} \frac{\partial P_i}{\partial |V_p|} |V_p| \frac{\Delta |V_p|}{|V_p|}$$

$$\Delta Q_i = \sum_{p=2}^{n} \frac{\partial Q_i}{\partial \delta_p} \Delta \delta_p + \sum_{p=2}^{n} \frac{\partial Q_i}{\partial |V_p|} |V_p| \frac{\Delta |V_p|}{|V_p|}$$

(2.51)

The set of Equation 2.51 for all the n − 1 bus can be written in the following matrix form

$$\begin{bmatrix} \Delta P_i \\ \Delta Q_i \end{bmatrix} = \begin{bmatrix} H_{ip} & N_{ip} \\ J_{ip} & L_{ip} \end{bmatrix} \begin{bmatrix} \Delta \delta_p \\ \frac{\Delta |V_p|}{|V_p|} \end{bmatrix}$$

(2.52)

Where

$$H_{ip} = \frac{\partial P_i}{\partial \delta_p}, \quad N_{ip} = \frac{\partial P_i}{\partial |V_p|} |V_p|, \text{ and } \quad J_{ip} = \frac{\partial Q_i}{\partial \delta_p}, L_{ip} = \frac{\partial Q_i}{\partial |V_p|} |V_p|$$

The partial derivatives H_{ip}, N_{ip}, J_{ip}, L_{ip} are real functions of admittance matrix and the bus voltages. It has been found that computer computations are faster if rectangular complex arithmetic is used. Therefore, the partial derivatives are computed by rectangular complex arithmetic.

2.6. Test System

IEEE-39 bus test system consisting 10 generators, 46 transmission lines and 12 transformers [83]. The structure of the system in single line diagram is presented in Figure **2.5.** The system has 29 load buses and 10 generator buses (including one slack bus). Of the 29 buses, 17 buses are carrying load. They are *i.e.* **3, 4, 7, 8, 12, 15, 16, 18, 20, 21, 23, 24, 25, 26, 27, 28, and 29** (see Appendix-A).
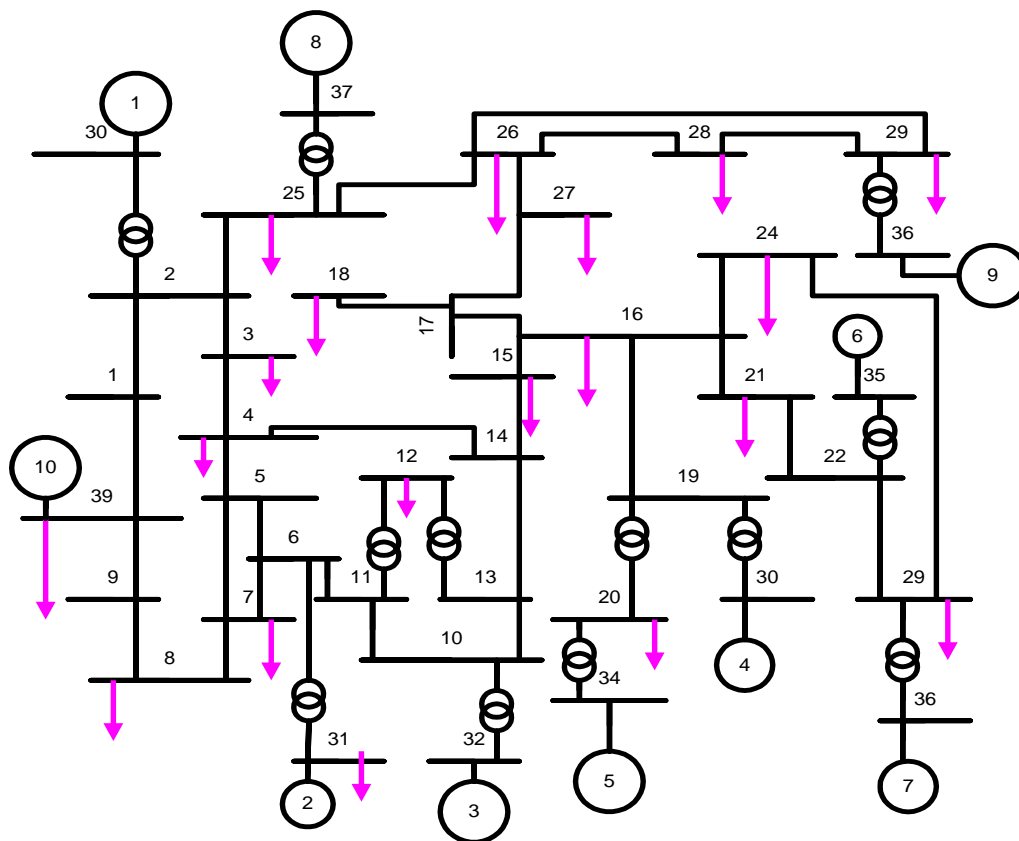
Figure 2.5. IEEE -39 Bus Test System.

2.7. Simulation Results and Discussions

Simulations were executed on a PC with Intel core DUO processor 2.2 GHz, and 4GB RAM with Matlab® code. In the simulations selected node loads are gradually increased in steps of 2% more than the nominal .here nominal means the value of line and data bus in the system before any study. The selected buses are loaded so as to stress the system (this is achieved by multiplying the nominal loads with a factor defined as loading parameter (LP)and denoted as 'λ' by assuming a constant power factor). The details of evaluation procedure are described below. It is to be noted here that a loadability limit for any bus depicted as λ in the result, implies that the corresponding bus has reached its VSL when the load at that bus is increased by λ times more than its nominal value, keeping the loads at other buses constant. To avoid repetition this fact is not repeated every time. Moreover, loads are increased at a particular bus keeping the power factor constant.

Considering these indices to be the voltage stability criteria, the voltage stability limit (VSL) or loadability limit of the system are evaluated when the loads are gradually increased in all these buses one by one. The ENVCI values obtained are recorded in the same Table **2.2.** The P-V curves and the ENVCI-Lambda (λ) curves are obtained from the simulation as shown in Figure **2.6**, and Figure **2.7.**
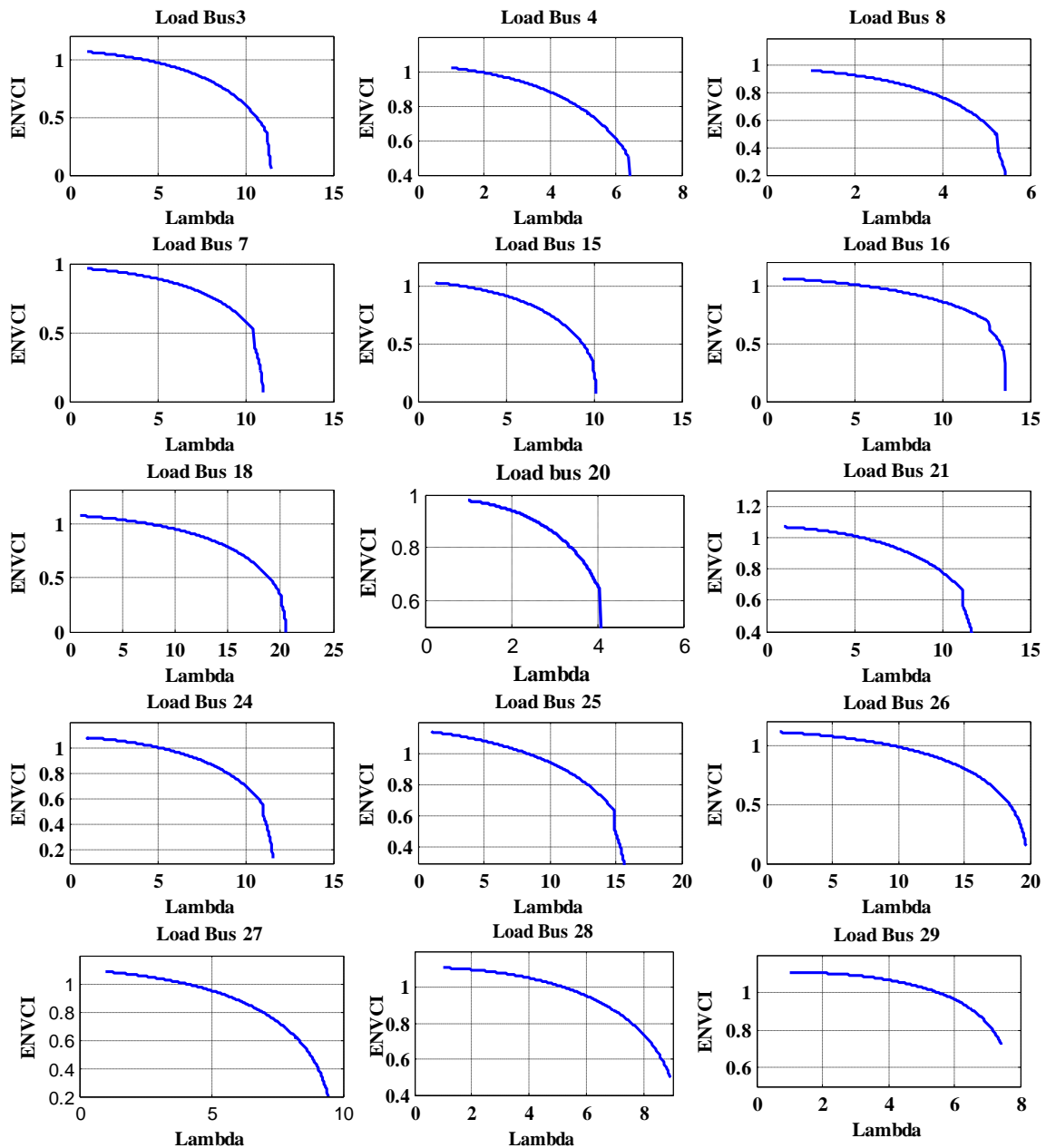
Figure 2.6. ENVCI versus lambda (λ) curve of load buses.
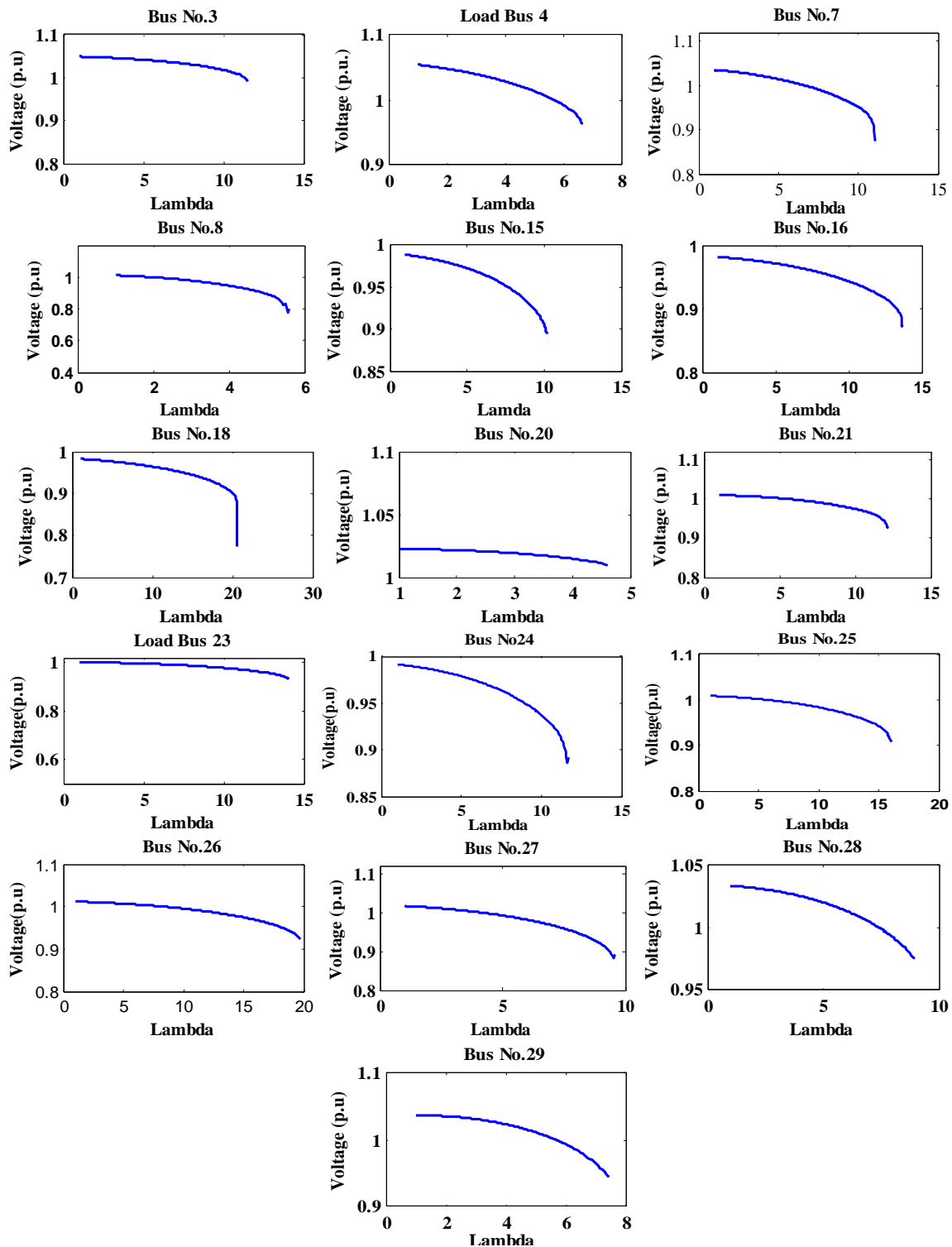
Figure 2.7. Voltage curve of load buses with λ=lambda

To examine the accuracy of VSL prediction from different perspective of indices, the following simulations were carried out separately for each of the indices. The four numbers

of indices namely; P-loss sensitivity index, V-Q sensitivity index, L-index and WASI were selected to be evaluated out of all the voltage stability indices discussed in section **2.2**. These three indices i.e. P-loss sensitivity index, V-Q sensitivity index, and L-index are generally widely used at different levels. Table **2.1** shows the Ranking of the buses with three indices when the system is not disturbed.

Table 2.1. Ranking of load buses with indices

Eigen value Sensitivity	Bus No.	Q-loss Sensitivity	Bus No.	L Index	Bus No.	WASI	Bus No.
0.0075	2	0.0054	1	0.0085	**23**	0.0136	**20**
0.0084	19	0.0001	2	0.0093	**20**	0.0146	**8**
0.009	**25**	0.007	9	0.0104	**7**	0.0186	**29**
0.0097	22	0.0116	**25**	0.0109	**8**	0.0187	**27**
0.0106	6	0.016	**29**	0.015	6	0.0192	**28**
0.0107	10	0.0173	**28**	0.0188	22	0.0197	22
0.0107	**20**	0.0187	22	0.021	9	0.0239	9
0.011	**23**	0.0219	**20**	0.022	5	0.0245	5
0.0114	**16**	0.0221	**26**	0.026	**21**	0.0294	1
0.0116	5	0.0252	10	0.0287	12	0.0304	11
0.0117	11	0.0259	19	0.0303	15	0.0333	4
0.0119	**3**	0.0276	3	0.0307	24	0.0348	24
0.0125	13	0.0319	13	0.0307	1	0.035	15
0.0127	29	0.0325	11	0.0308	11	0.0351	2
0.0129	17	0.0387	5	0.0329	4	0.0358	14
0.0132	4	0.04	23	0.0361	14	0.0359	13
0.0133	14	0.0409	4	0.0367	16	0.0359	10
0.0147	18	0.0409	27	0.0379	13	0.037	16
0.0148	24	0.0413	6	0.0398	10	0.0374	21
0.015	8	0.0419	18	0.042	3	0.0382	3
0.0154	7	0.042	14	0.0428	18	0.0404	12
0.016	15	0.0424	12	0.0437	2	0.0413	18
0.016	26	0.0458	8	0.0438	17	0.0417	17
0.0162	1	0.0474	7	0.0508	29	0.044	7
0.0172	9	0.0493	17	0.0529	27	0.0448	25
0.0185	27	0.0632	16	0.0548	25	0.0503	23
0.0217	28	0.0682	15	0.0583	28	0.0538	6
0.026	21	0.0693	24	0.0653	26	0.0562	19
0.0342	12	0.0765	21	0.0693	19	0.0566	26

2.7.1 Eigen value sensitivity

Discrepancy of result is first observed in bus number 8, where the VSL (i.e the maximum loading parameter,λ) was found to be 5.38 as shown in Table **2.2**. However, from the results of NRLF obtained at a loading of 5.36 it is seen from Figure **2.8** that, most of the bus voltages have reached very close to their upper limits means violations of operating limit on higher side.
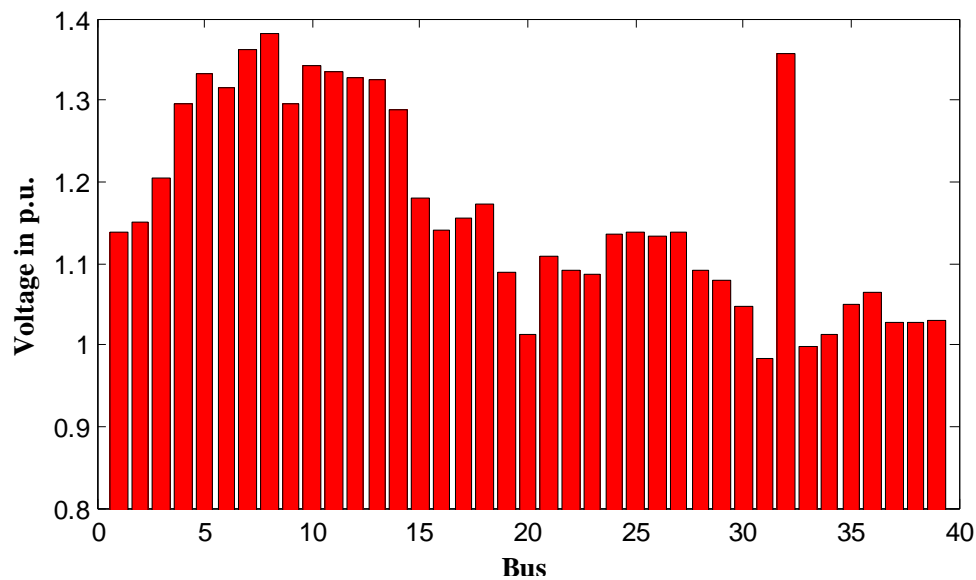
Figure 2.8. The voltage profile of the system at 5.36 times the nominal loading in bus 8.

2.7.2 Q-loss Sensitivity

In another case of loading at the bus number **25** when the load is increased to **15.88** the results of NRLF has shown voltages reaching lower limits although it is not practically feasible loading as only bus 25 among all the load buses has reactive power generated value 1.0 p.u . so it can supply reactive power thus loading can be increased as active and reactive power load is not so high. So this bus can be further loaded) ,even though the index had predicted a VSL of higher magnitude of **15.89** .(from the comparison between Figure **2.9** and the Q-loss sensitivity index for bus number **25** , in Table. **2.2**)
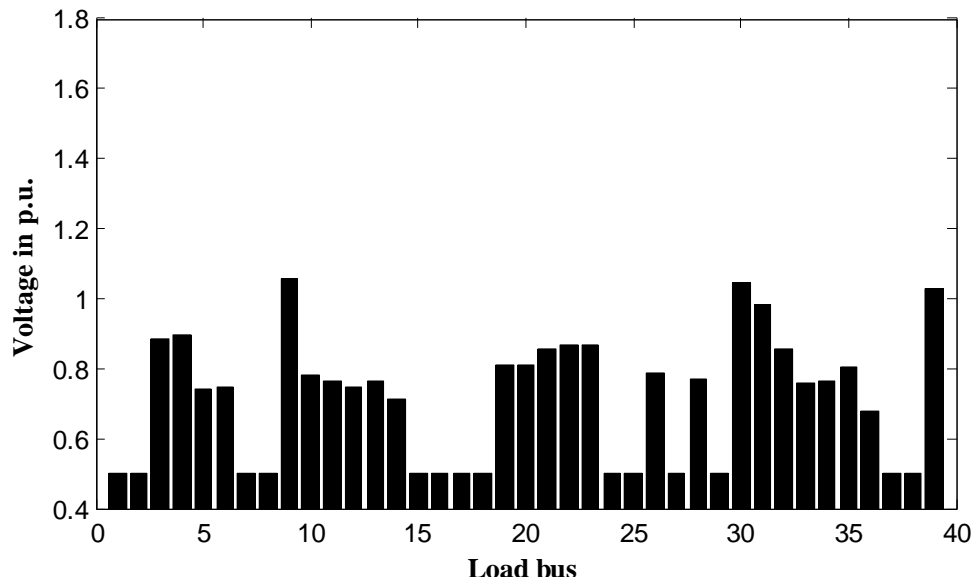
Figure 2.9. The system voltage profile at 15.88 times the nominal loading of bus 25.

2.7.3 L-index

The L-index calculation indicates the VSL for load bus number **20** is **4.2** referring to Table **2.2** where as for the same bus the NRLF study reveals the VSL **4.1**as shown in Figure **2.10**. It is to be noted that the loading parameter depends upon the nominal loading of the system.the higher the nominal loading the loading capacity of the bus will be less.
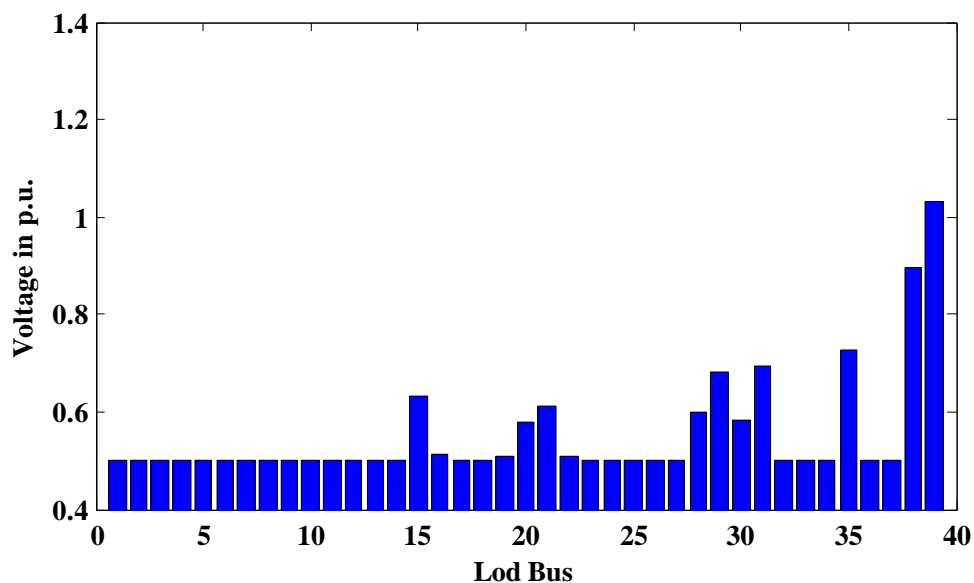
Figure 2.10. The system voltage profile at 4.1 times the nominal loading of bus 20.

2.7.4 WASI

In bus 28 reactive power load is very less. There is a chance of over voltage as only active power is increased and due to the transformer tap setting not taken into account. This is treated as close to the upper limit of voltage(i.e 1.5) assumed.Referring to Figure **2.11** the VSL for bus number 28 is **9.2**, whereas with NRLF study the same is found to be **9.21** from Table **2.2.**
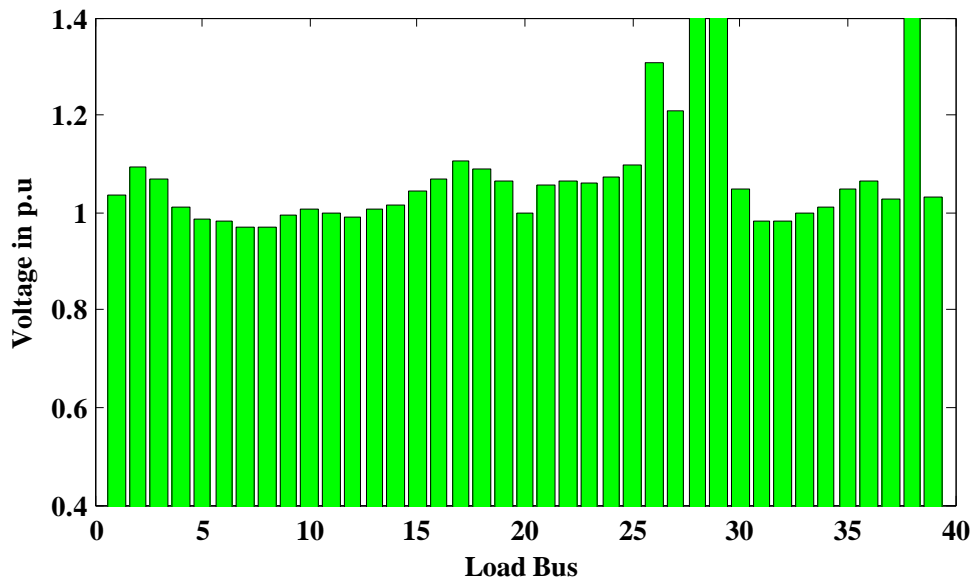
Figure 2.11. The system voltage profile at 9.2 times the nominal loading of bus 28.

Table 2.2. Weak bus ranking in IEEE-39 Bus Test System.

Rank	Weak bus ranking in descending order from different indices perspectives									
	V-Q sensitivity Index		Q-loss sensitivity Index		L-index		WASI		ENVCI	
	Bus No.	VSL (No. of times nominal)	Bus No.	VSL (No. of times nominal)	Bus No.	VSL (No. of times nominal)	Bus No.	VSL (No. of times nominal)	Bus No.	VSL (No of times nominal)
1	**8**	**5.38**	**25**	**15.89**	23	6.7	20	4.2	20	4.5
2	25	15.89	29	7.42	**20**	**4.2**	8	5.3	8	5.4
3	20	4.56	28	8.91	7	7.9	29	7.3	29	8.4
4	16	13.46	20	4.56	8	5.6	**27**	**9.21**	28	8.8
5	3	11.27	26	19.58	21	6.7	28	9.4	27	9.4

2.7.5. ENVCI

Observing all the above discrepancies in prediction of VSL by the four indices, their consideration for the criterion of detecting voltage stability may be uncertain. On the contrary, the P-V curve analysis both by ENVCI and NRLF approaches are in accordance with each other as shown in Table **2.2** (*i.e.* ENVCI column).and Figure **2.6** and Figure **2.7** respectively. The comparison between the three indices showing the weakness of the system load buses are shown in Figure **2.12.**
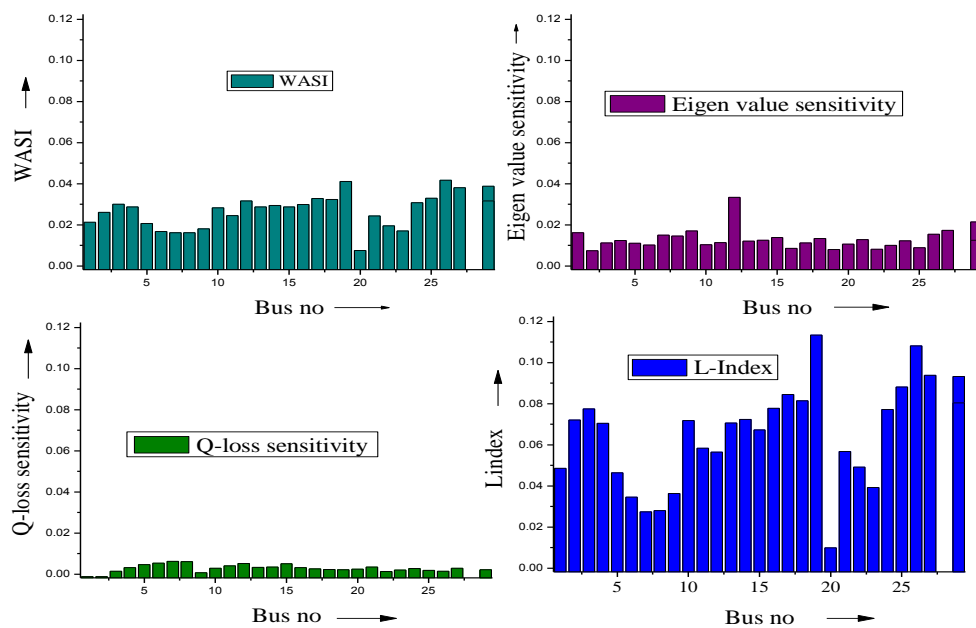
Figure 2.12. The comparison of the indices nominal case.

The maximum loading of each load bus is determined from the ENVCI calculation. The maximum loading parameter corresponds to the zero value of ENVCI. When LP is less the ENVCI is 1 approximately. With the increase in LP the ENVCI becomes less than one. With gradual increase of LP, ENVCI becomes gradually less and finally becomes close to zero. Thus LP for each load bus is found out. The maximum loading limit of each load bus for selected 13 load buses numbered as **3, 8, 15, 16, 18, 20, 21, 23, 24, 25, 26, 27, 28, and 29** . are shown in Figure **2.13.**
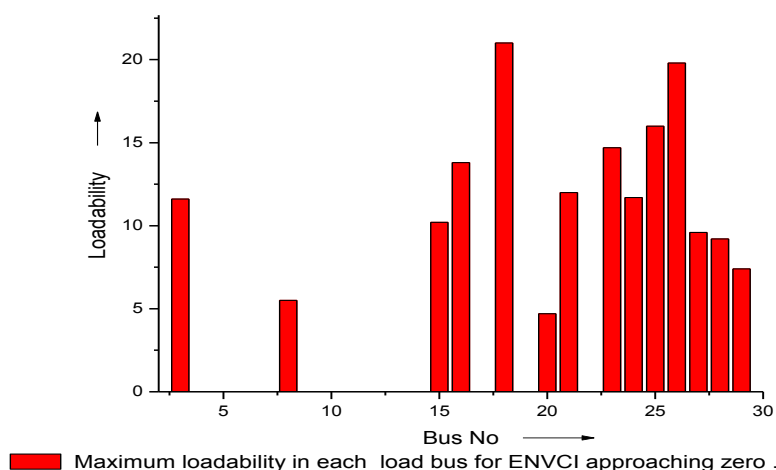
Figure 2.13. Maximum loading in the load buses with ENVCI.

2.8. Conclusions

The main objective of the work carried out in this chapter, is to determine the values of different indices and examine their accuracy in predicting the limits of voltage stability, when it is considered as the criterion to determine the VSL. Simulations carried out in the given IEEE 39 bus test system, showed that the three previously reported indices i.e., Q-loss sensitivity index, V-Q sensitivity index gave some erroneous prediction. Therefore, looking at the accuracy of different indices, a new index known as WASI is defined. Properly selected weighting factors when multiplied to formulate WASI, gave better accuracy of prediction with the same. However, the variation of ENVCI with load increase was found to be more conforming to the P-V curves obtained for load increase at a particular bus. Moreover, due to the advantage of ease of calculation of ENVCI, and the non requirement of load flow solution for an online evaluation and application, it can be preferred over other indices.

After examining the accuracy of different indices and selecting ENVCI as the criterion for the determination of voltage instability, the weak bus ranking of the system is done, similar to other indices. To alleviate the problem of instability, suitable amount of compensation needs to be done by different means at the weak buses. In the subsequent

Chapter-**3**, the fixed capacitor compensation is decided to be carried out within the framework of optimization for voltage stability study.

OPTIMAL PLACEMENT AND SIZING OF FIXED SHUNT REACTIVE COMPENSATION TO INCREASE LOAD MARGIN WITH MBFO ALORITHM

3.1. Introduction

Generally, the steady state static analysis of voltage instability in a large interconnected power system gives considerable idea about the vulnerability of the system [12]. A scenario of gradual load increase in some weak areas of the system as discussed in Chapter-2, gives an indication about the limits of loadability (using ENVCI [41]) in it, before the system breaches its own secure operation. For even more practical understanding few contingencies in the form of outage of lines, generators etc, gives a better idea about the system's load bearing capacities at some specific points in the network [29, 82]. As the system is continuously changing its operating conditions therefore, a close watch on the present operating regions is necessary. Because, a decision of specific corrective control measure that ensures a voltage secure operation of the system, largely depends on the operating condition. In this regard, the speed of decision making also plays an important role. Moreover, voltage stability margin can be improved by suitably sizing and placing VAR compensating devices [85] in the system. The main issue of optimal size and location has been determined by several researchers after formulating the problem as an optimization problem [87, 88]. For solving them, conventional algorithms like interior point based methods and Sequential Quadratic Programming (SQP) [66, 67] and intelligent search algorithms like, Genetic Algorithm (GA) and Particle Swarm Optimization (PSO) [69, 85], have been applied. This work aims at optimizing the suitable location and capacity of fixed compensation (FC) in the IEEE 39-Bus New England power system so as to increase the system load margin using a Modified Bacteria Foraging Optimization Algorithm (MBFOA) [89] that is different from original version [90] and has been tested in wide varieties of power system problems mentioned above.

3.2. Problem Formulation

The problem is formulated, as an optimization problem in the same IEEE 39 bus Test system as in Chapter 2. The objective of this work is to determine the most suitable two locations in the system where a suitable amount of injected reactive power would maximize the loadability limit or VSL of the system when the same is subjected to load increase at some weak buses of the system one after other. To limit the numbers of optimizing variables only two locations are chosen for the purpose. With this, there are in total four different optimizing variables, *i.e.*, two numbers of locations with their respective percentage of compensations. It may be recalled that the maximum loadability limit of the system is maximum possible increase in real power flow at some load buses, before the system witnesses a voltage collapse condition. The load buses are already ranked from the perspective of relative weakness, utilizing ENVCI as the criteria.

3.2.1. Statement of the problem

The optimization problem may be stated in a general form as explained in Equation 3.1. Similar to most of the problems of optimization, there are sets of equality and inequality constraints that needs to be satisfied simultaneously.

$$F = F_1 + F_2 + xF_C \tag{3.1}$$

The parts F_1 and F_2 of the objective function F, take into account respectively, the maximization of VSL and minimization of real power loss of the system under the maximum load condition. Each part of the objective function is suitably normalized, so that they can be added together. It may be recalled that both the individual objectives essentially aid one another and they are not contradictory in nature. However, the third part F_C consists of penalty factor that gets added to the objective functions in the case of any limit violation. The details of these three components of the objective function F is explained below.

3.2.1.1. Maximization of steady state VSL of loading

Increasing the margin of loadability or VSL in a stressed operating condition without compromising on voltage stability, requires proper selection of location and amount of FC in the system by external means. Therefore, the primary objective F_1 of the work aims to maximize the VSL of the system, considering locations of system buses and the amounts of percentage compensation at those locations as two types of variables of optimization. The loads are increased in the weakest bus for determining the VSL of the system. The objective function F_1 is therefore defined as follows in Equation 3.2.

$$F_1 = min \ (\lambda_i^{Max}) \tag{3.2}$$

where, λ_i^{Max} = set of maximum load parameter, λ for i^{th} bus. λ_i = Load parameter of ith bus, i = 1,..., 5 for the 5 numbers of selected weak buses considered for load increase during optimization. The minimum value among the set, λ_i^{Max} corresponds to the weakest bus and if the VSL of weakest of the selected buses is improved then there can be overall improvement in the system VSL.

3.2.1.2. Minimization of active power loss

It is well known that, when the real power loss of the transmission lines in the system increases due to increase in line currents. Then the reactive power loss also increases thereby increasing the overall line voltage drops in the system. This results in overall reduction in system bus voltages. By choosing suitable locations and amounts of capacitive reactive power injection in the system, the loss can be reduced and voltage profile can be improved for the same condition of load increase [81]. Therefore, one of the two objectives is to reduce system real power loss. Hence, F_2 can be written as follows.

$$F_2 = P_{loss}(x, u) = P_{loss} \tag{3.3}$$

where, P_{loss} is the real power loss in the system for all i numbers of transmission lines in the system for a particular operating condition. In the same equation,

$x = \{V_1,$ all node voltages$\}$ where x is set of all the node voltages V_n and node angles δ_n

$u =$ Vector of control variable comprising of the position and size of shunt FC in the system.

As the system is operating with constraints, and the solution needs to satisfy them. The remaining objective is avoid the violation of any of the inequality constraints, which is fulfilled with the help of the penalty factors, formed by taking into account the operational constraints of the system as defined in the following section.

3.2.2. Equality and inequality constraints

Any problem of optimization needs to be solved within the limits of different types of equality and inequality constraints. For the present problem, they are detailed below.

3.2.2.1. Equality constraints

The equality constraints are the active and reactive power balance described by a set of power flow equations as explained in Equations **3.4** and **3.5** respectively and in general form as in Equation in **3.6**

(i) Real power balance equation

The real power balance equation for load in i^{th} bus can be expressed as

$$P_i - V_i \sum_{j=1}^{N_g} V_j \left[G_{ij} \cos \delta_{ij} + B_{ij} \sin \delta_{ij} \right] = 0 \qquad i = 1, 2, 3, 4, \ldots N_{g-1} \tag{3.4}$$

Assuming

(ii) Reactive power balance equation

The reactive power balance equation for load in i^{th} bus can be expressed as

$$Q_i - V_i \sum_{j=1}^{N_g} V_j \left[G_{ij} \cos \delta_{ij} - B_{ij} \sin \delta_{ij} \right] = 0 \qquad i = 1, 2, 3, 4, \ldots N_{PQ} \tag{3.5}$$

$$G(x, u, \lambda) = 0 \tag{3.6}$$

Where x and u are the set of state and control variables. Similarly, λ is the load parameter related to the condition of load increase. The equality constraint in this case is achieved by solving the power flow equations with the help of NRLF method explained earlier in Chapter **2.**

3.2.2.2. Inequality constraints

The, transformer apparent power S_T, line apparent power S_{line}, bus voltage magnitude V_L are considered as follows:

(i) Transformer apparent power (S_T) limit

The ith transformer apparent power can be expressed in the following equation as

$$S_{Ti_{\min}} \leq S_{Ti} \leq S_{Ti_{\max}}, \quad for \quad i = 1......N_T \tag{3.7}$$

(ii) Transmission line apparent power (S_{Line}) limits

The ith transmission line apparent power limit can be expressed by the following equation as

$$S_{i_{Line\,\min}} \leq S_{i_{Line}} \leq S_{i_{Line\,\max}}, \quad for \quad i = 1...N_{Line} \tag{3.8}$$

(iii) Bus voltage limit

The ith bus voltage limits can also be expressed in the following equation as

$$V_{Li_{\min}} \leq V_{Li} \leq V_{Li_{\max}}, \quad for \quad i = 1...N_L \tag{3.9}$$

The set of inequality constraints defined by the same sets of state, control variables and the load parameter, can be written in a general form as follows.

$$H(x, u, \lambda) \leq 0 \tag{3.10}$$

In this work, the transformer apparent power S_T, line apparent power $S_{Ti\ line}$, bus voltage magnitude V_L, are required to remain within their respective maximum and minimum limits as

follows. where, the above constraints are included in the objective function, in the form of penalty factors as explained in the subsequent section.

3.2.2.3. Penalty factors

Three penalty factors are considered to take care of any violation limits of bus voltage, line flow and transformer capacity limit violations. In the event of any violation a large valued factor gets added up with the original objective function thereby penalizing its objective of minimization. Each of them is explained below.

$F_3 = Pf_1 =$ Penalty factor for limit violation of bus voltages.

$$Pf_1 = 10 * abs\left(sign\left(V^{rated}_{min} - 0.9\right) - 1\right) + 10 * abs\left(sign\left(V^{rated}_{max} - 1.1\right) + 1\right) \tag{3.11}$$

$F_4 = Pf_2 =$ Penalty factor for limit violation of transformer MVA capacity violation.

$$pf_2 = 10 * abs\left(sign\left(trans^{rated}_{max} - 15\right) + 1\right) \tag{3.12}$$

$F_5 = Pf_3 =$ Penalty factor for limit violation of line flow capacities of all the lines in the system.

$$pf_3 = 10 * abs\left(sign\left(line^{rated}_{max} - 20\right) + 1\right) \tag{3.13}$$

$F_C =$ penalty factor = $F_3 + F_4 + F_5$, \tag{3.14}

Min F(x, u, λ) is designed as below.

$$F = max\ f_1 + min\ f_2 + Pf_1 + Pf_2 + Pf_3 \tag{3.15}$$

The problem is formulated as a static constrained non-linear optimization problem. Where, λ_i^{Max} is a set of 5 values corresponds to maximum loading capacity among the **17** load buses when the bus is subjected to load increase scenarios. The first and second parts of the objective functions formulated in Equation **3.15** allow the *P*-loss minimization and improvement in load

margin respectively. Each part of the objective function is suitably scaled. When the limits are violated then there is a penalty factors. The penalty factors pf_1, pf_2, and, pf_3 will be zero as long as there is no violation of limit. The load parameter of the load bus evaluated by increasing the loads in steps and the load is equally shared by the generators till the unstable point is reached. This is illustrated as

$$\left.\begin{aligned} P_{Li} &= P_{Lio}\,(1+\lambda) \\ Q_{Li} &= Q_{Lio}\,(1+\lambda) \\ P_{Gi} &= P_{Gio}\,(1+\lambda) \end{aligned}\right\} \tag{3.16}$$

where, P_{Li}, Q_{Li} are the active power, reactive power of the load and P_{Gi} is the active power of the generator of the ith bus. λ is the load parameter, multiplied in steps of 2% to increase the real and reactive powers from their respective nominal values. The system load margin is evaluated with the help of ENVCI. With the increase in load, ENVCI value reduces reaching towards zero near the LM. Hence the corresponding λ value is the LM of the system.

3.3 Optimization Algorithms

Any problem of constrained optimization can be solved with the help of numbers of conventional and modern heuristic optimization techniques. However, as discussed previously, if the problem is highly non-linear and non convex with numbers of *epistatic* (interdependent) variables required to be optimized, then a conventional gradient based optimization method or even many of heuristic optimization algorithms fail to produce promising results. The computational burden and duration increases considerably with large dimension like that of a multi generator power system. Therefore, this work focuses on MBFOA, which has been employed in optimization of numerous power system problems and compared its performance with that of the Genetic Algorithm (GA). Before proceeding to the methodology of the optimization problem, brief overviews of the two algorithms are discussed here.

3.3.1. Genetic Algorithm

The Genetic algorithm [86] is a search based optimization algorithms, inspired from the phenomena found in living life. They always produce high quality solutions because they are independent of the choice of the initial configurations. Moreover, they are computationally simple and easy to implement. Based on stochastic techniques, the mechanism of the algorithm is influenced from natural selection and genetics. GA starts with an initial set of random solutions called *population*, whose every individual is called a *chromosome*, that can be a solution to the problem. A chromosome is a binary or real valued string structure that is an aggregated list of binary digits representing the code of control parameters in the problem. The chromosomes evolve through successive iterations, called generations. During each generation, the chromosomes are evaluated, using some measure of fitness. To create the next generation, new chromosomes called offspring are formed by either (a) merging two chromosomes from the current generation using a *crossover* operator or (b) replacing one bit from the parent chromosome by its complement using the *mutation* operator. A new generation is formed by selecting, a few of the parents and offspring according to the fitness value and rejecting others, to keep the population size constant. Suitable chromosomes having higher probabilities are being selected for the mating pool. The selection rule used is a roulette-wheel selection. After several generations, the algorithms converge to the best chromosome, which represents the optimal or near optimal solution to the problem [86]. To obtain optimality the algorithms combine the solution evaluation and randomized, structured exchanges of information between the results. One of the drawbacks is their possibility to converge prematurely to a suboptimal solution.

The goal here is to allow the ''fittest'' individuals to be selected more often to reproduce. There are a number of operators proposed for selection operation. Hence, each individual in the population consists of a combination of these variables. Then the genetic operators are applied on the genetic population to improve the solution. This process is continued until the convergence criterion is satisfied. This is pictorially represented in Figure **3.1** The crossover operator is principally responsible for the global search property of the GA, and its probability usually in the range of 0.7-1.0. The parameters used for GA are given in Table **3.1**. The GA has a tendency to converge in sub-optimal solution.

Initialize Population

Run Power Flow and Evaluate fitness value

select parents for reproduction

Apply crossover and mutation

Evaluate fitness of chromosomes

Converged ?

NO

Yes

Stop
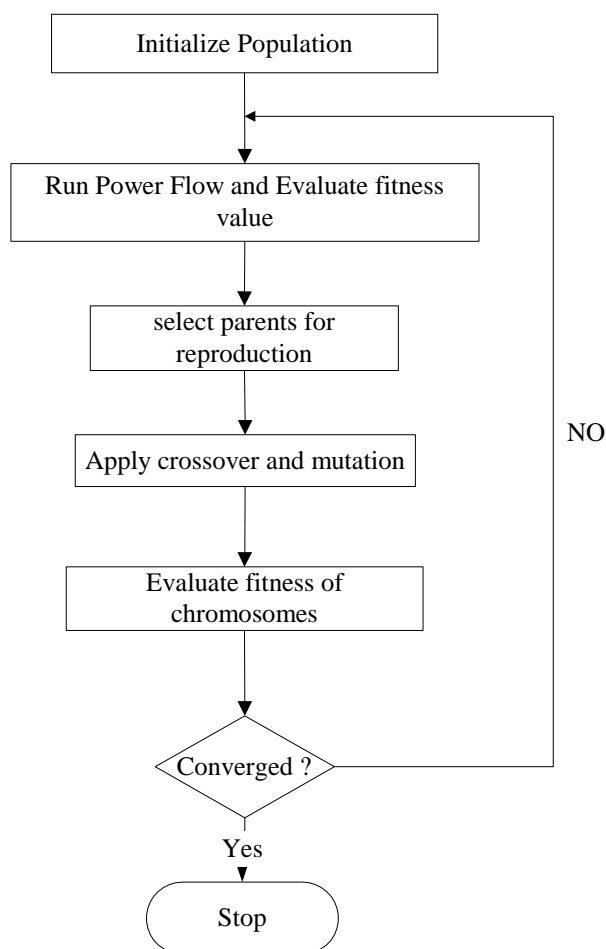
Figure 3.1 Flow chart for Genetic Algorithm.

Table 3.1. Parameters used in GA.

Parameters	Value/Type
Population size	50
Maximum generations	100
Selection operator	Roulette wheel
Crossover probability	0.85
Mutation probability	0.05
Termination method	Maximum generation

3.3.2. Modified bacteria foraging optimization algorithm:

Modified Bacteria Foraging Optimization Algorithm (MBFOA) [89], is a modified version of the BFOA proposed by Passino [90]. Although BFOA is developed, and applied in optimization problems in many fields including some in the field of power system, the work gets its motivation to use the same algorithm with some modifications in original BFOA [90], for having better efficiency and quicker convergence of the result. A real *E.coli* bacterium (denoted by $\theta \in \Re^p$) performs two basic operations in its process of foraging. It either tumbles or swims with help of flagella [89]. When the flagella rotate in the clockwise direction, a bacterium *tumbles*, whereas in counter clockwise rotation the same gets the indication to *swim*. This important process is known as *chemotaxis.*

The bacteria undergo *chemotaxis*, when they move towards richer nutrient locations (favourable solution space). The bacteria replicate themselves over the process of chemotaxis when they find favourable nutrient space. This occurrence has motivated Passino to set up the process of *reproduction* in MBFOA. In the process of evolution, the newer bacteria try to follow the most successful ones, by the process of *swarming*. But the most unique feature in the entire process involves the concept of *elimination and dispersal*, in which the entire set of bacteria might get eliminated altogether due to unfavorable ecological changes, and get dispersed to a newer region of nutrient. This uniqueness of the algorithm when done with a lesser probability of elimination and dispersal, improves the overall chemotactic growth of the bacteria instead of adversely affecting the solution. Therefore, the MBFOA essentially mimics the four primary mechanisms observed in a real *E. Coli* bacterial system, in the form of chemotaxis, swarming, reproduction, and elimination dispersal.

A virtual bacterium is one trial solution that moves on the functional surface to locate the global optimum. Let us define a chemotactic step to be a tumble followed by a tumble or a tumble followed by a swim or run. Let *j* be the index for the chemotactic step. Let *k* be the index for the reproduction step. Let *l* be the index of the elimination-dispersal event. The algorithm begins with the process of initialization. That is to let

p: Dimension of the search space

S: Total number of bacteria in the population,

N_c : The number of chemotactic steps,

N_s: The swimming length.

N_{re} : The number of reproduction steps,

N_{ed} : The number of elimination-dispersal trials,

P_{ed} : Probability of elimination-dispersal,

C (i): The size of the step taken in the random direction specified by the tumble.

Let $P(j,k,l) = \{\theta^i(j,k,l) | i = 1, 2, ..., S\}$

is the position of each member of S bacteria at the jth chemotactic step, k^{th} reproduction step, and l^{th} elimination-dispersal event in the population of the S bacteria. Here, let J (i, j, k, l) denote the value of objective function at the location of the ith bacterium denoted by $\theta^i(j,k,l) \in \Re^P$. For actual bacterial populations, S can be very large, but the choice is problem specific and varies for different problems. $\theta = \left[\theta_1, \theta_2, \theta_3, ...\theta_p, \right]^T$ denote the P dimensional positions in the search space. The main four prime processes in MBFOA are described below.

3.3.2.1. Chemotaxis

As explained earlier, this process simulates the progress of an *E.coli* bacterium through swimming and tumbling by the use of flagella $\theta^i(j,k,l)$ represents i^{th} bacterium at j^{th} chemotactic, k^{th} reproductive and l^{th} elimination-dispersal step. $C(i)$ is the size of the step taken in the random direction specified by the run length unit. Then in computation of chemotaxis the movement of the bacterium may be represented as below

$$\theta^i(j+1,k,l) = \theta^i(j,k,l) + C(i)\frac{\Delta(i)}{\sqrt{\Delta^T(i)\Delta(i)}}$$
(3.17)

Where, Δ represent the vector in random direction whose element lie in a range of -1 and 1.

3.3.2.2. Swarming

The group behavior of swarm is found in many evolutionary motile species, and the characteristic of the one seen in E.coli bacteria is closer to that of S. typhimurium. The cells

release an attractant aspertate, the magnitude of which is modeled by the values of $d_{attractant}$, $W_{attractant}$. The process helps them to combine into groups and thus move as concentric patterns of swarms with high bacterial density. Similarly, the opposite process of repelling is modeled by, h $_{repellant}$, $W_{repellant}$. The cell-to-cell signaling in *E.coli* swarm may be represented by the following function.

$$J_{cc}(\theta, P(j,k,l)) = \min J_{cc}(\theta, \theta^i(j,k,l))$$

$$= \sum_{i=1}^{s}(-d_{attractant}e^{-w_{attractant}\sum_{m=1}^{p}(\theta^{op}_m - \theta^i_m)^2}) + \sum_{i=1}^{s}(h_{repellant}e^{-w_{repellant}\sum_{m=1}^{p}(\theta^{op}_m - \theta^i_m)^2}) \qquad (3.18)$$

Where, $J_{cc}(\theta, P(j,k,l))$ is the objective function value to be added to the actual objective function *J*, to be minimized. $d_{attractant}$, $W_{attractant}$, h $_{repellant}$, $W_{repellant}$ are different attractant and repellent coefficients that needs to be chosen properly.

3.3.2.3. Reproduction

The least healthy bacteria ultimately die while the healthier bacteria (those yielding lower value of the objective function) replicate into another set of bacteria, which are then placed in the same location. This keeps the bacterial size constant.

3.3.2.4. Elimination and dispersal

Gradual or sudden unforeseen event similar to rise in temperature may annihilate the entire group of bacteria which have evolved till now and currently in favourable region of nutrient gradients. These events may subsequently disperse the original set into a new location. Instead of destroying the process of evolution, this process is unique feature of MBFOA and tend to speed up convergence as the population of newly created species may find themselves in more favourable environment. The probability P_{ed} of this process is kept low, to avoid the natural cycle of chemotaxis. The flowchart of MBFOA is presented in Figure 3.2 [89]. The details of the algorithm steps of the original version are as follows.

[**Step 1**] Initialize parameters *p, S, N_s, N_c, N_{re}, N_{ed}, P_{ed}, C(i)=(i=1,2,3....S)*, and Algorithm: θ_i

[**Step 2**] Elimination-dispersal loop: *l=l+1*

[**Step 3**] Reproduction loop: *k=k+1*

[**Step 4**] Chemotaxis loop: *j=j+1*

[a] For i =1,2…S. take a chemotactic step for bacterium i as follows.

[b] Compute fitness function. $J(i, j,k,l)$ add on the cell-to cell attractant–repellant profile to simulate the swarming behavior.

$$J_c(i, j,k,l) = J(i, j,k,l) + J_{cc}(\theta^i(j,k,l), P(j,k,l))$$
(3.19)

[c] Let $J_{last} = J_c(i, j,k,l)$ to save this value since we may find a better health or cost via a run.

[d] Tumble: Generate a random $\Delta(i) \in \mathfrak{R}^p$ vector with each $\Delta_m(i), m=1,2,...,P$ element a random number on [0, 1].

[e] Move: Let

$$\theta^i(j+1,k,l) = \theta^i(j,k,l) + C(i)\frac{\Delta(i)}{\sqrt{\Delta^T(i)\Delta(i)}}$$
(3.20)

This results in a step size in the tumble direction.

[f].compute $J(i, j+1,k,l)$ and let
$$J(i, j+1,k,l) = J(i, j,k,l) + J_{cc}(\theta^i(j+1,k,l), P(j+1,k,l))$$
(3.21)

[g] Swim

    i) Let *m=0* (counter for swim length).

    ii) While $m < N_s$ (if have not climbed down too long).

• Let $m=m+1$.

• If $J_c(i, j+1, k, l) < J_{last}$ (if doing better), let $J_{last} = J_c(i, j+1, k, l)$ and let

$$\theta^i(j+1, k, l) = \theta^i(j, k, l) + C(i)\frac{\Delta(i)}{\sqrt{\Delta^T(i)\Delta(i)}} \tag{3.22}$$

and take $\theta^i(j+1, k, l)$ to compute new $J(i, j+1, k, l)$ as done in [f]

Else, let $m = N_s$. This is the end of the while statement.

[h] Go to next bacterium $i+1$, if $i \neq S$ (*i.e.,* go to [b] to process the next bacterium).

[Step 5] If j <Nc , go to step 4.

[**Step 6**] Reproduction

[a] For the given k and l, and for each i =1, 2,..., S , let

$$J^i_{health} = \min_{j \in \{1....x_c\}} \{J(i, j, k, l)\} \tag{3.23}$$

be the health of the bacterium *i*. Sort bacteria and chemotactic parameters *C(i)* in order of ascending cost *J* $_{health}$ (higher cost means lower health).

[b] The S_r bacteria with the highest J_{health} values die and the remaining S_r bacteria with the best values split.

[**Step 7**] If $k < N_{re}$ go to step 3. In this case, the number of specified reproduction steps is not reached; start the next generation of the chemotactic loop.
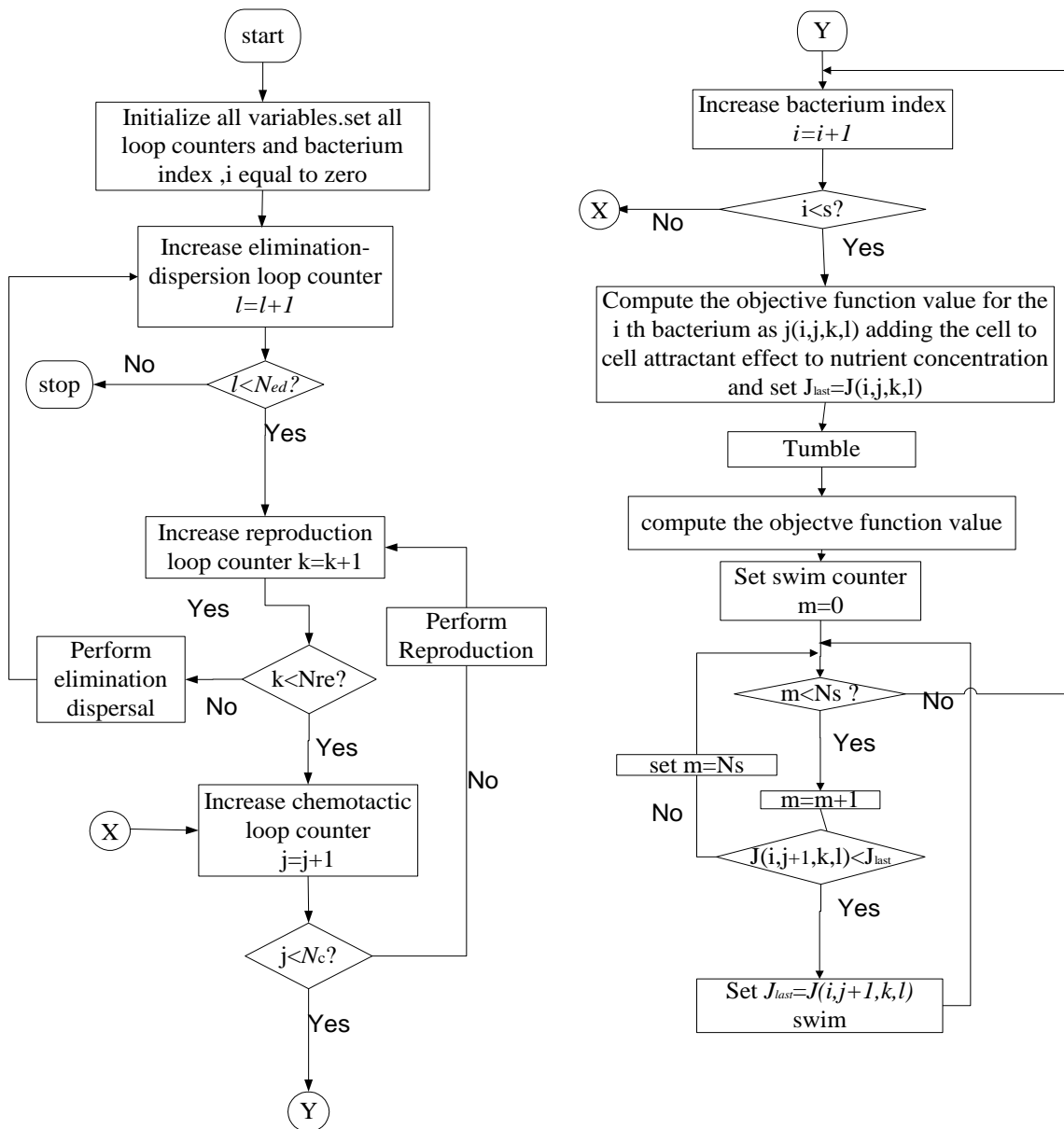
Figure 3.2. Flow chart of MBFOA.

[**Step 8**] Elimination-dispersal: For $i =1, 2..., S$ with probability P_{ed}, eliminate and disperse each bacterium (this keeping a constant number of bacteria in the population). To do this, if a bacterium is eliminated, simply disperse another one to a random location on the optimization domain. If $l <N_{ed}$, then go to step 2, otherwise end.

The parameters used for simulation discussed above problem are given in Table **3.2**.

Table 3. 2. Parameters used in MBFOA

Parameters	Value/type
Depth attractant	1.8
Width attractant	0.06
Width repellant	10
Height repellant	1.8
Run length unit	0.06
Elimination probability	0.25
Elimination dispersal probability	0.25

3.3.3. Differential evolution

Differential Evolution (DE) algorithm is a population-based stochastic optimization algorithm recently introduced [120]. DE works with two populations such as: old generation and new generation of the same population. The population size is adjusted by the parameter N_P. The population having real valued vectors of dimension D is equal to the number of control variables. The population is initialized within random initial factor bounds. The optimization process is accomplished by use of three key operations, namely mutation, crossover and selection. In every generation, individuals of the current population develop into target vectors. For every target vector, the mutation operation generates a mutant vector, by means of addition of the weighted difference between two randomly chosen vectors to a third vector. In crossover operation, a new vector is generated, called trial vector, which is the result of combination of the parameters of the mutant vector and that of the target vector. If the trial vector obtains a better fitness value than the target vector, then the trial vector replaces the target vector in the next generation. The evolutionary operators are described below [121-124]. The flow chart is given in Fig. 3.3.

3.3.3.1. *Initialization*

For each parameter j with lower bound X_j^L and upper bound X_j^U, initial parameter values are usually randomly selected uniformly in the interval [X_j^L, X_j^U].
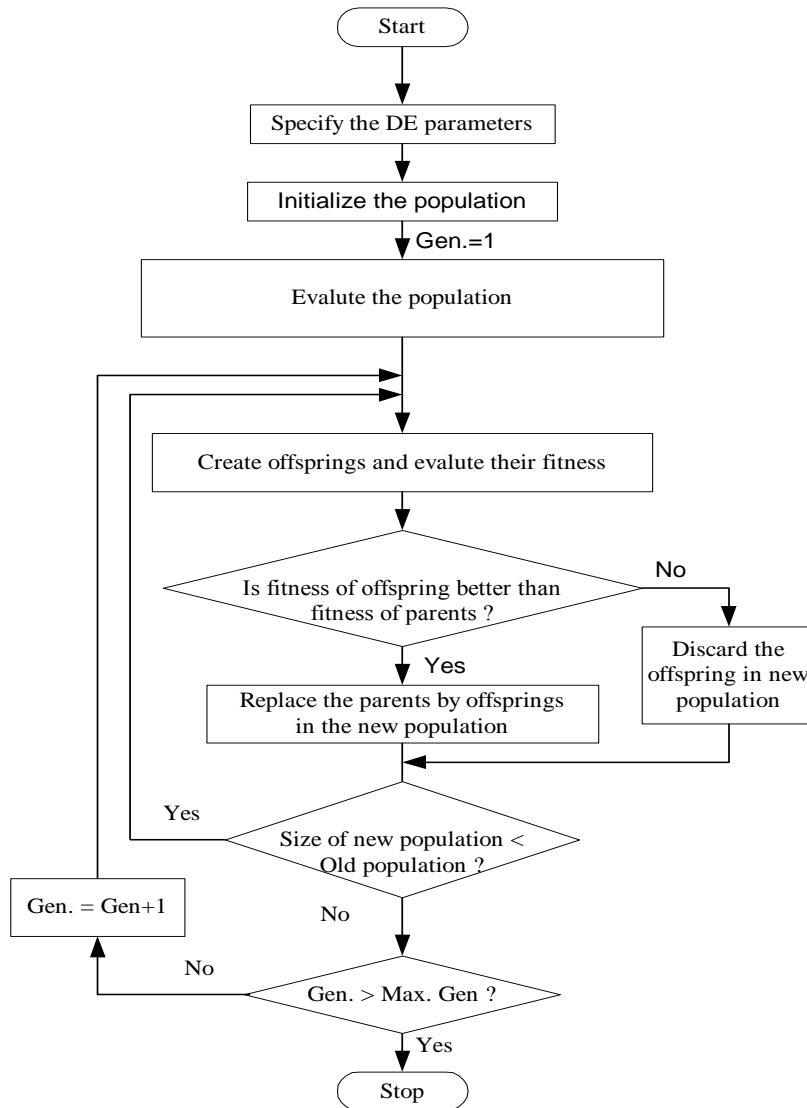
Fig.3. 3. *Flow chart for DE*

3.3.3.2.   *Mutation*

For a given parameter vector $X_{i,G}$, three vectors ($X_{r1,G}, X_{r2,G}, X_{r3,G}$) are randomly selected such that the indices i, r_1, r_2 and r_3 are distinct. A donor vector $V_{i,G+1}$ is created by adding the weighted difference between the two vectors to the third vector as:

$$V_{i,G+1} = X_{r1,G} + F.(X_{r2,G} - X_{r3,G})$$
(3.24)

Where *F* is a constant ranges between (0-2)

3.3.3.3. *Crossover*

Three parents are selected for crossover and the child is a perturbation of one of them. The trial vector $U_{i,G+1}$ is developed from the elements of the target vector ($X_{i,G}$) and the elements of the donor vector

($X_{i,G}$).Elements of the donor vector enters the trial vector with probability *CR* as:

$$U_{j,i,G+1} = \begin{cases} V_{j,i,G+1} & if \quad rand_{j,i} \le CR \quad or \quad j = I_{rand} \\ X_{j,i,G+1} & if \quad rand_{j,i} > CR \quad or \quad j \neq I_{rand} \end{cases}$$

$$U_{j,i,G+1} = \begin{cases} V_{j,i,G+1} & if \quad rand_{j,i} \le CR \quad or \quad j = I_{rand} \\ X_{j,i,G+1} & if \quad rand_{j,i} > CR \quad or \quad j \neq I_{rand} \end{cases} \tag{3.25}$$

With $rand_{j,i} \sim U(0,1)$, I_{rand} is a random integer from $(1,2,.....D)$ where D is the solution's dimension i.e. number of control variables. I_{rand} ensures that $V_{i,G+1} \neq X_{i,G}$.

3.3.3.4. *Selection*

The target vector $X_{i,G}$ is compared with the trial vector $V_{i,G+1}$ and the one with the better fitness value is admitted to the next generation. The selection operation in DE can be represented by the following equation:

$$X_{i,G+1} = \begin{cases} U_{i,G+1} & if \quad f(U_{i,G+1}) < f(X_{i,G}) \\ X_{i,G} & otherwise. \end{cases} \tag{3.26}$$

where $i \in [1, N_P]$.

3.3.4. Particle swarm optimization algorithm

The PSO method is a member of wide category of Swarm Intelligence methods for solving the optimization problems. It is a population based search algorithm where each individual is referred to as particle and represents a candidate solution. Each particle in PSO flies through the search space with an adaptable velocity that is dynamically modified according to its own flying experience and also to the flying experience of the other particles. In PSO each particles strive to improve themselves by imitating traits from their successful peers. Further, each particle has a memory and hence it is capable of remembering the best position in the

search space ever visited by it. The position corresponding to the best fitness is known as p_{best} and the overall best out of all the particles in the population is called g_{best}. The features of the searching procedure can be summarized as follows [121, 125]:

- Initial positions of p_{best} and g_{best} are different. However, using the different direction of p_{best} and g_{best}, all agents gradually get close to the global optimum.

- The modified value of the agent position is continuous and the method can be applied to the continuous problem. However, the method can be applied to the discrete problem using grids for XY position and its velocity.

- There are no inconsistency in searching procedures even if continuous and discrete state variables are utilized with continuous axes and grids for XY positions and velocities. Namely, the method can be applied to mixed integer nonlinear optimization problems with continuous and discrete state variables naturally and easily.

The modified velocity and position of each particle can be calculated using the current velocity and the distance from the $pbest_{j,g}$ to $gbest_g$ as shown in the following equations :

$$v_{j,g}^{(t+1)} = w \times v_{j,g}^{(t)} + c_1 \times r_1() \times (p_{best_{j,g}} - x_{j,g}^{(t)}) + c_2 \times r_2() \times (g_{best_g} - x_{j,g}^{(t)}) \qquad (3.27)$$

$$x_{j,g}^{(t+1)} = x_{j,g}^{(t)} + v_{j,g}^{(t+1)} \qquad (3.28)$$

With $\quad j = 1,2,....n \quad$ and $\quad g = 1,2,....m$

Where $\quad V_g^{min} \leq v_{j,g}^{(t)} \leq V_g^{max}$

n = number of particles in a swarm;

m = number of components in a particle;

t = number of iterations (generations);

$v_{j,g}^{(t)}$ = g-th component of velocity of particle j at iteration t, ;

w = inertia weight factor;

c_1, c_2 = cognitive and social acceleration factors respectively;

r_1, r_2 = random numbers uniformly distributed in the range (0, 1);

$x_{j,g}^{(t)}$ = g-th component of position of particle j at iteration t;

$pbest_j$ = p_{best} of particle j;

g_{best_g} = g_{best} of the group.

The j-th particle in the swarm is represented by a d-dimensional vector $x_j=(x_{j,1}, x_{j,2}, \ldots\ldots, x_{j,d})$ and its rate of position change (velocity) is denoted by another d-dimensional vector $v_j = (v_{j,1}, v_{j,2}, \ldots\ldots, v_{j,d})$. The best previous position of the j-th particle is represented as $pbest_j=(pbest_{j,1}, pbest_{j,2}, \ldots\ldots, pbest_{j,d})$. The index of best particle among all of the particles in the swarm is represented by the $gbest_g$. In PSO, each particle moves in the search space with a velocity according to its own previous best solution and its group's previous best solution. The velocity update in a PSO consists of three parts; namely momentum, cognitive and social parts. The balance among these parts determines the performance of a PSO algorithm. The parameters c_1 and c_2 determine the relative pull of p_{best} and g_{best} and the parameters r_1 and r_2 help in stochastically varying these pulls. In the above equations, superscripts denote the iteration number. The flow chart of PSO is shown in Fig. 3.4.

```
                    ┌─────────────┐
                    │    Start     │
                    └─────────────┘
                           │
              ┌──────────────────────────┐
              │ Initialize Population with random │
              │    position and vectors   │
              └──────────────────────────┘
                           │
              ┌──────────────────────────┐
              │ for each particle's position (x) │
              │   Evaluate objective function  J │
              └──────────────────────────┘
```

if $J(x)$ is better than Jp_{best}
then $x = p_{best}$

set best of $p_{best} = g_{best}$

update

$$v_{j,g}^{(t+1)} = w \times v_{j,g}^{(t)} + c_1 \times r_1() \times (p_{best\ j.g} - x_{j,g}^{(t)}) + c_2 \times r_2() \times (g_{best\ j.g} - x_{j,g}^{(t)})$$

$$x_{j,g}^{(t+1)}) = x_{j,g}^{(t)}) + v_{j,g}^{(t+1)})$$

NO

Is iter= max iter ??
Is adequate objective
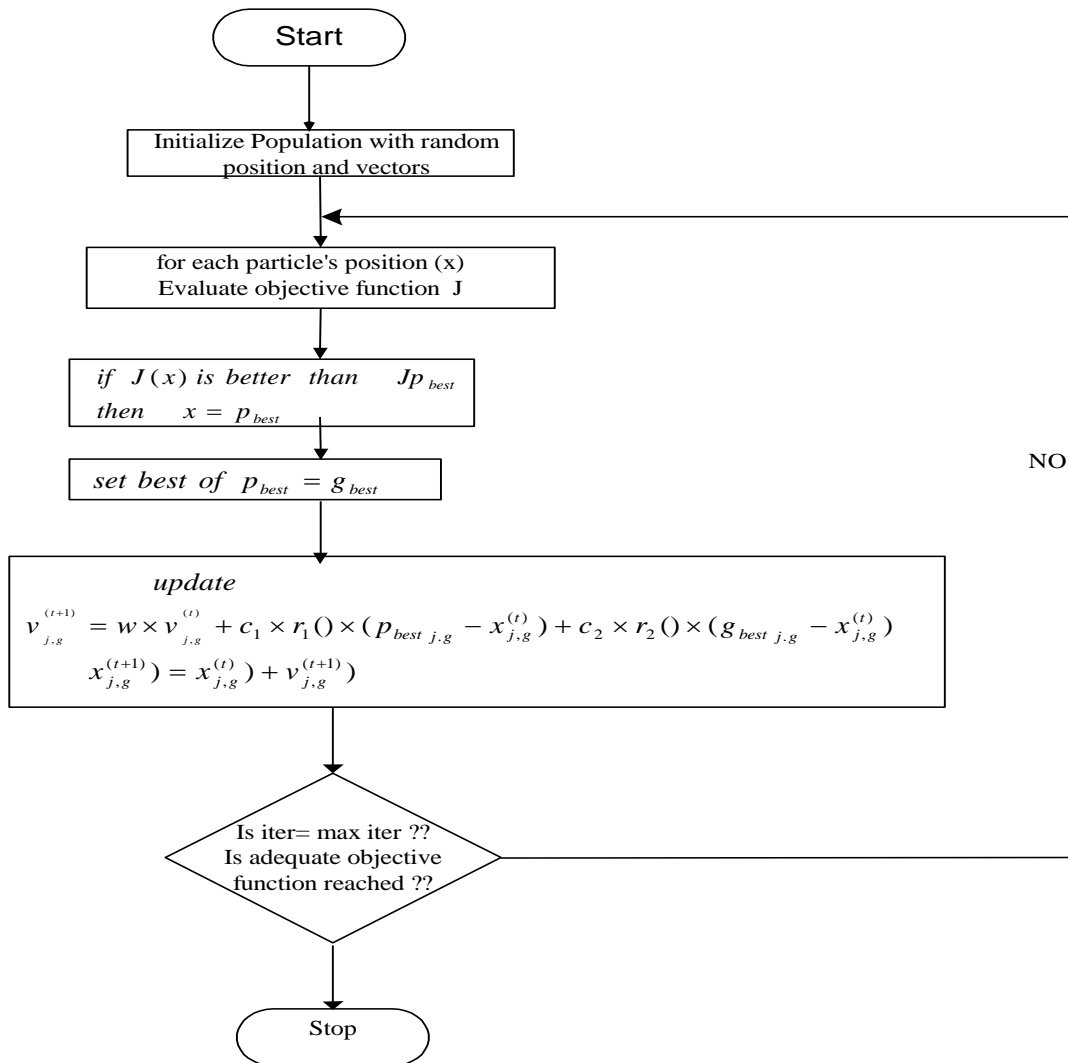function reached ??

Stop

Fig. 3.4 . Flow chart of PSO algorithm.

3.4. Simulation Results and Discussions

The methodology adopted to determine the optimum size and location of VAR compensating devices at two different locations in the system is with the help of optimization. Five numbers of weakest buses according to the ranking of the system load buses (found in Chapter-2) are selected. This is done to simulate the scenarios of worst case loading in the system.The loads of these 5 buses are increased gradually in steps of 2% of their respective nominal values one by one until VSL for each bus in terms of λ_i is reached. Obtaining the values of λ_i for all the five bus numbers $i=1$ to 5 the value of $\boldsymbol{min}$ (λ_i^{Max}) representing the least load increase among them is retained to maximize F_1 explained in Equation **3.3**. Other cost functions defined in Equations **3.4** and **3.5** are also obtained for every run. It is to be noted that, the above procedure is repeated for each bacterium, which are four randomly generated numbers. Two of them represent the location and two for the amounts in terms of percentages of compensation at these load buses. Proper scaling is done before these random numbers can be used. Moreover, the load increase at the weak buses is done along with the simultaneous compensation at the random locations being operational. Therefore, the load increase essentially denotes the same for a compensated condition.

The maximum size of the compensating device is 90 MVAr (Q_{max}). The 17 load buses, *i.e* **3, 4, 7, 8, 12, 15, 18, 20, 21, 22, 23, 24, 25, 26, 27, 28,** and **29** are chosen for this purpose. Similarly, for the amount of compensation at any particular load bus, a maximum of **50%** compensation is chosen. The optimization carried out with MBFOA and GA and the system with optimized condition compensation are tested finally for accuracy. Methodology adopted in each of the optimization algorithm is explained below.

3.4.1 Optimization using GA

Conventional GA with binary coded *chromosomes* is used for optimization. The location and amount of reactive power compensation at two locations are randomly initialized, to represent a single chromosome. For each location two random numbers are generated. One random number represents the location and the other represents the amount of reactive power compensation in terms of percentage (-40% to +40%) of nominal load at that location. Therefore

4 random numbers represent randomly selected location and amount at two locations in the system. Each random number is then converted to a binary string, by multiplying the number with a large number $\Omega = (2^{17}-1)$. All the 4 random numbers converted to binary strings having a length of 17 bits each, are then joined together to form a chromosome. 50 such randomly initialized chromosomes constitute the initial set to represent the *population* set in the first generation.

The crossover and mutation probabilities are assumed to be 0.85 and 0.05 respectively. Similarly, a maximum of 100 generations of the algorithm solution produce convergence to optimized result. The convergence characteristic is represented in terms of numbers of objective function evaluations to have a better possible comparison with MBFOA. Because, in each generation GA and MBFOA evaluate the objective function different number of times, but the duration of a function evaluation remains constant. Therefore a comparison in terms of function evaluation instead of generation would give better idea of speed of optimization in both the algorithms.

3.4.2. Optimizing with DE and PSO

With the DE optimization it is seen that the objective function is not converging as compared to the MBFOA and GA . Also the result obtained with PSO technique, the optimization characteristic is not promising one when compared with the GA and MBFOA and DE . as shown in Fig.**3. 5.** Also it is found that with DE the compensation required at bus no 29 with 42.84 % of ratedVAR compensation and 42.88% of the installed VAR compensator is required at bus no 28 with PSO as shown in Table 3.3.

Table.3. 3. Optimized compensation results with GA, MBFOA, DE, and PSO

Compensation Specifications	(Constant Q-Load)			
	GA	MBFOA	DE	PSO
1st location of static compensation	Bus No. **28**	Bus No. **24**	Bus No.**29**	Bus No.**28**
1st amount of static compensation	**43.35%**	**42.78%**	**42.84%**	**42.88%**
2nd location of static compensation	Bus No. **20**	Bus No. **15**	Bus No.**25**	Bus No.**27**
2nd amount of static compensation	**31.57%**	**08.68%**	**20.25%**	**9.78%**
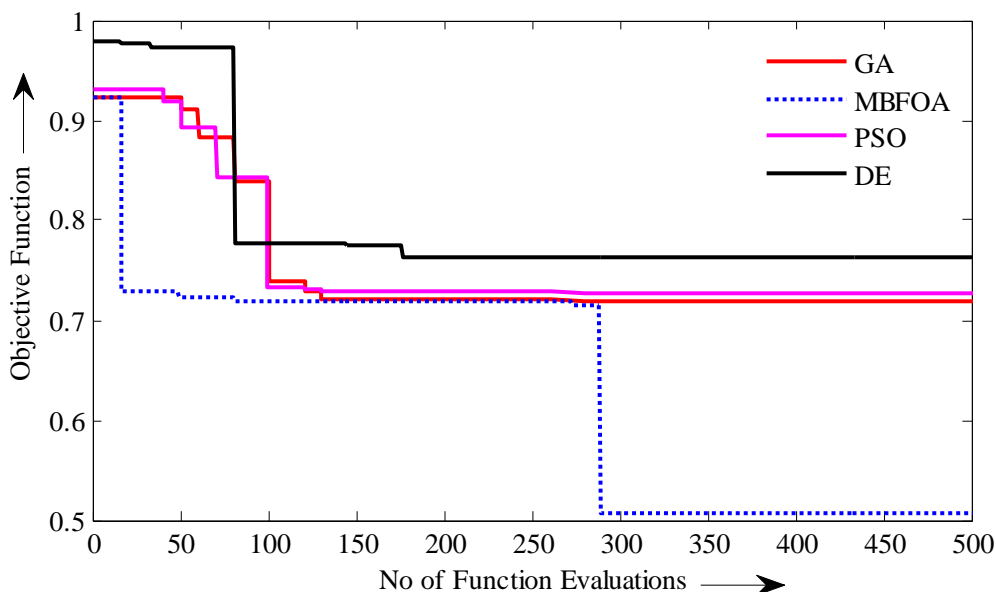
Figure 3.5. Convergence characteristics for increased load.

From the convergence characteristics shown in Figure **3.5**, it can be seen that the algorithm converges to solution after 10 generations with GA. The optimized results, which give the two locations and the corresponding amount of compensation, are shown in Table **3.3**. The load margin is increased to **4.51** times of the nominal load with GA. The optimization with GA for this case gives the two optimal locations and sizes of FC which are at bus no. **28** with compensation of + **45.35%** of Q_{max} (= 90 MVAr) and at bus no. **20** with compensation required to be + **31.57%** of Q_{max} respectively.

3.4.3. Optimization using MBFOA

Four random solutions represent a single bacterium, and 4 such bacteria are evolved in the process of chemotaxis for several generations. Unlike GA, the binary coded strings are not required. The parameters of MBFOA used for the sake of optimization are given in Table.**3.1.** From the convergence curves shown in Figure **3.5**, it can be seen that MBFOA converges faster than GA optimization. The final solution with MBFOA proposes a **42.78 %** of rated FC at bus number **24** and **8.68%** of rated compensation at load bus number **15**. Keeping the location and

amounts of compensation obtained with both the methods, separate PV curves are drawn when the load was increased in the weakest bus of the system, *i.e.,* bus number **20**.

It shows that for this bus the VSL with both the optimization results have improved upon the value of VSL obtained without compensation. Moreover, MBFOA solution has provided better compensation with respect to GA. Similar PV curves are also drawn for all the five weak buses. The results for load increase shown five weak buses **8, 20, 27, 28 and 29** are depicted in Figure **3.6** to **3.10** respectively. From all the results the MBFOA case compensation has shown improved performance compared to GA, even though the amount of improvement is only marginal for other four weak buses. The voltage profiles obtained one step prior to the VSL conditions for load increased at bus numbers **8, 20, 27, 28** and **29** separately. The result obtained with the GA and MBFOA is shown in Figure **3.6 (a)** as the load increased in the weak bus no.8, the voltage profile of all 29 buses are depicting the nominal loading and maximum loading without compensation, with GA and MBFOA at optimized compensations. Similarly the load margin for the same bus is depicted in the Figure **3.6 (b)**.
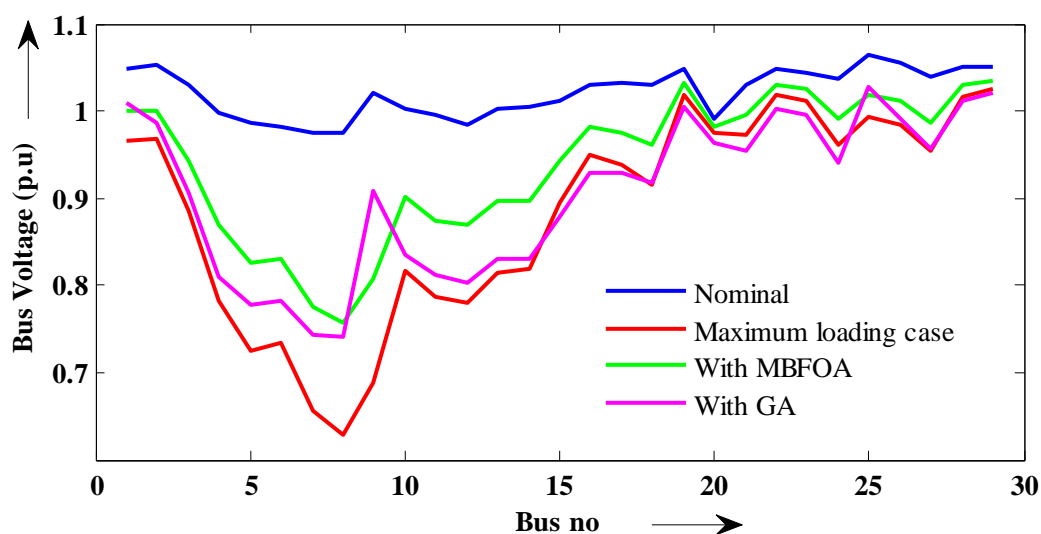
Figure 3.6.(a) System voltage profile for P increase in weak bus (bus No 08).
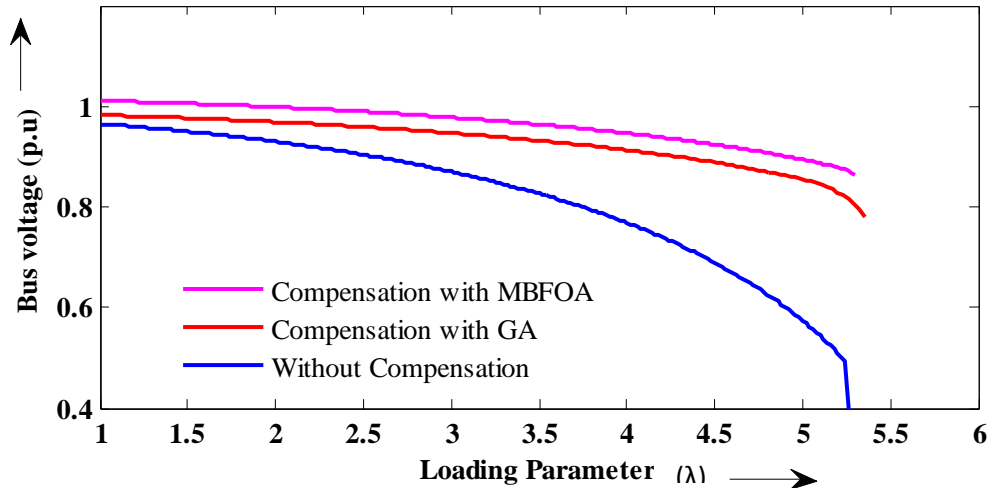
Figure 3.6 (b). Loadability limit of weak bus 8.

The voltage profile of load bus 20 is observed with the simulation results that there is a chance of overvoltage in the bus 20 can cause voltage instability when the bus is at maximum LP (λ). In nominal case all the bus operate close to the standard value 1.0 pu. As load increased in bus 20 gradually to a maximum load shown in **Fig.3.7 (a)**, the voltage became close to 1.5, which is the upper limit of operating voltage assumed. This can violate the operating voltage limit. This voltage is brought back close to nominal value with compensation by MBFOA method. It is clear that the MBFOA makes the operating voltage very much close to the nominal operating compared to GA. Thus MBFOA is better than the GA optimisation technique.

Figure 3.7 (a). System voltage profile for P increase in weak bus (bus No 20).

The load margin in this bus was 4.08 without compensation, where as it can be increased to 4.5 with GA but can further be increased to 4.55 with MBFOA shown in **Fig.3.7(b)** .
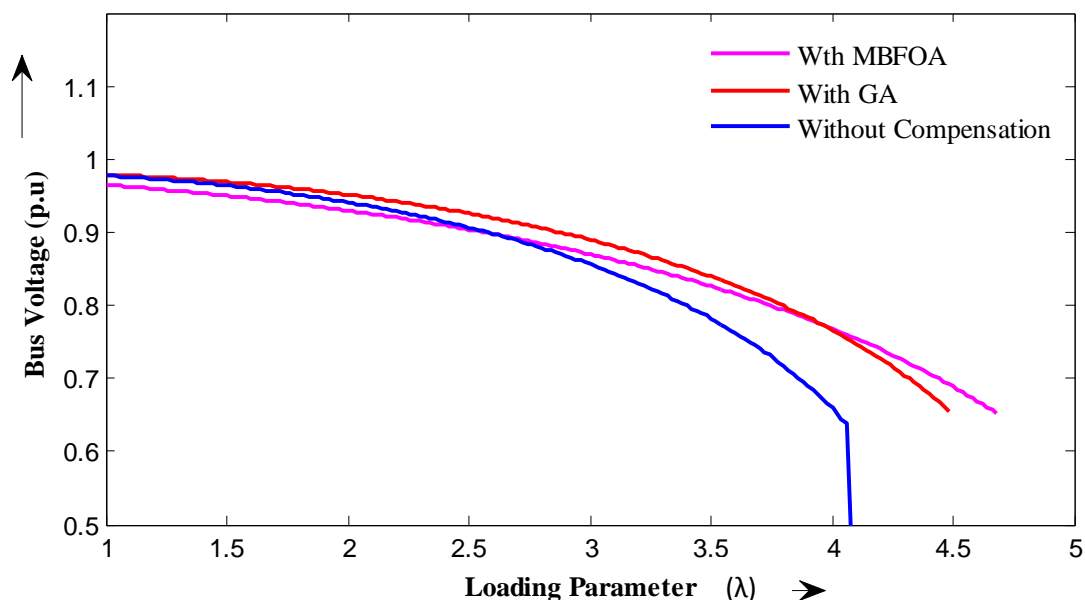
Figure 3.7 (b). Loadability limit of weak bus 20.

In **Fig 3.8(a)** the voltage profile of bus 27 at nominal case is very much in the stable state as compared to the maximum loading which is more than 1.1 pu causing over voltage leading to voltage instability. The voltage instability is avoided by reactive power compensation with GA and MBFOA optimisation techniques. But MBFOA gives more stable value(0.95pu) than GA 0.9 pu. The load margin for load bus 27 was 8.9 without compensation , which was enhanced to 9.4 as compensation made with GA. But with MBFOA technique for compensation the load margin enhanced to 9.5.this is shown in **Fig. 3.8 (b)**
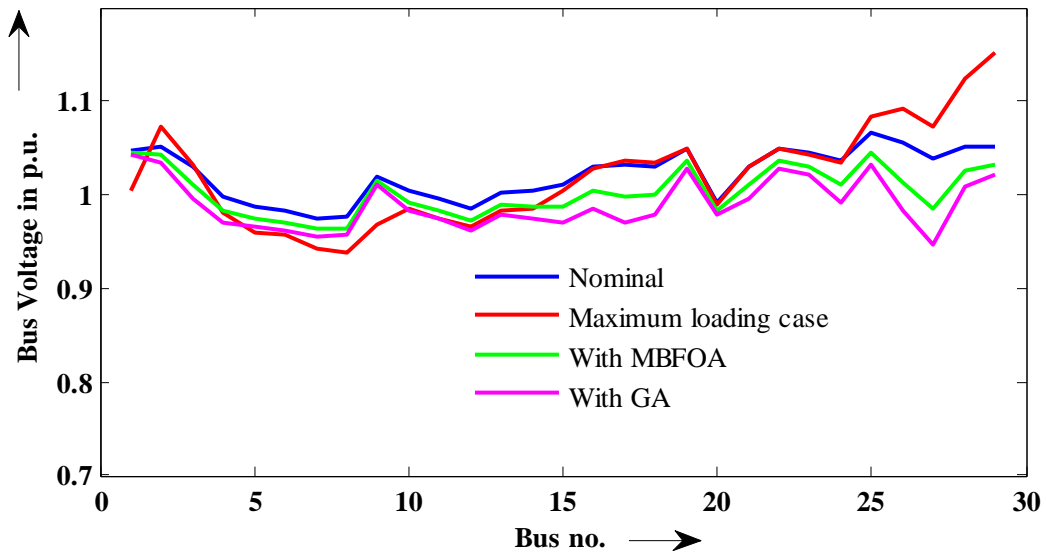
Figure 3.8 (a). System voltage profile for P increase in weak bus (bus No 27).
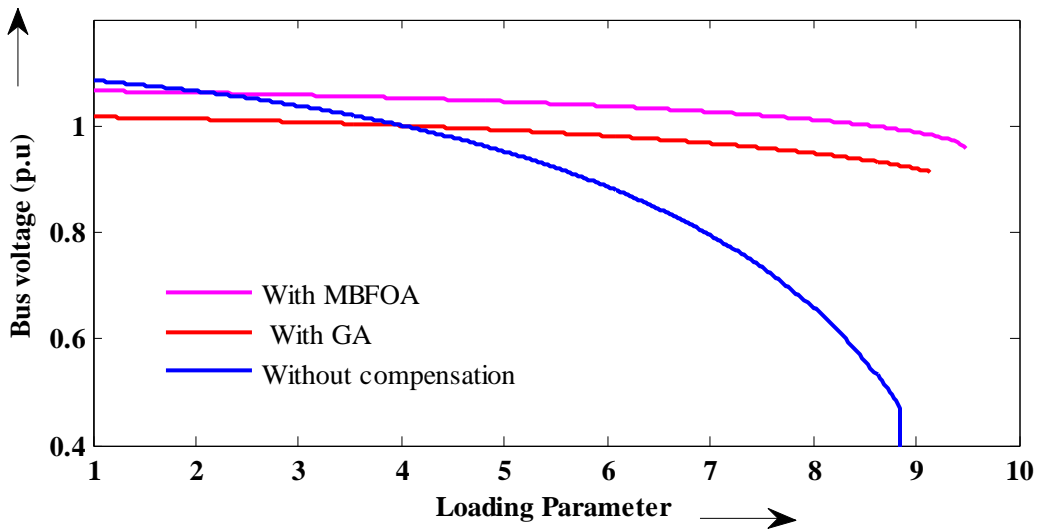
Figure 3.8 (b). Loadability limit of weak bus 27.

In **Fig 3.9(a)** , it is seen that bus no 28 becomes very small (0.89 pu)at maximum loading than the nominal loading (1.05pu). the voltage in the bus 28 becomes 1 pu when it is optimally fed with reactive power using MBFOA. This is stable operating voltage than that of voltage(1.1 pu) obtained with GA optimisation technique. The load margin of bus 28 increased to 8.8 in optimisation case from 8.7 in nominal case. Although the load margin is same for the both GA and MBFOA techniques but the voltage is more stable in MBFOA than the GA.this is shown in **Fig. 3.9(b) .**
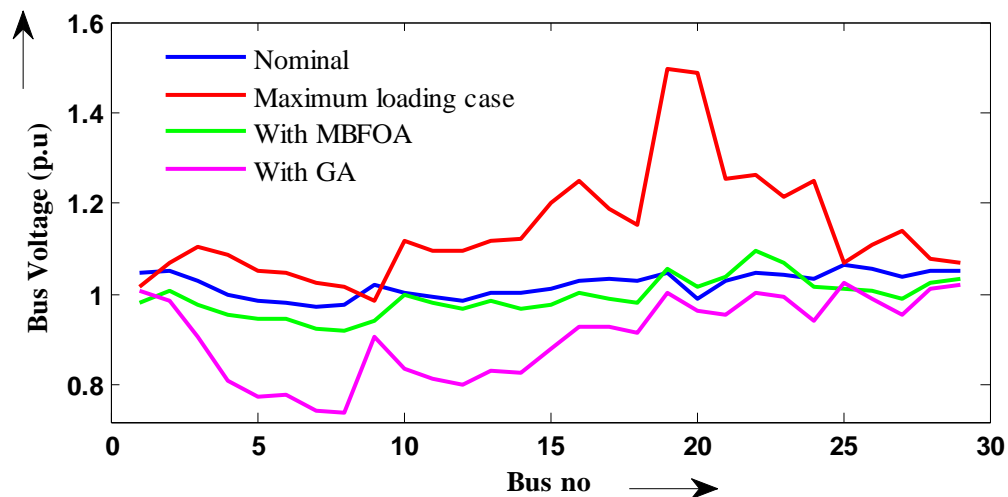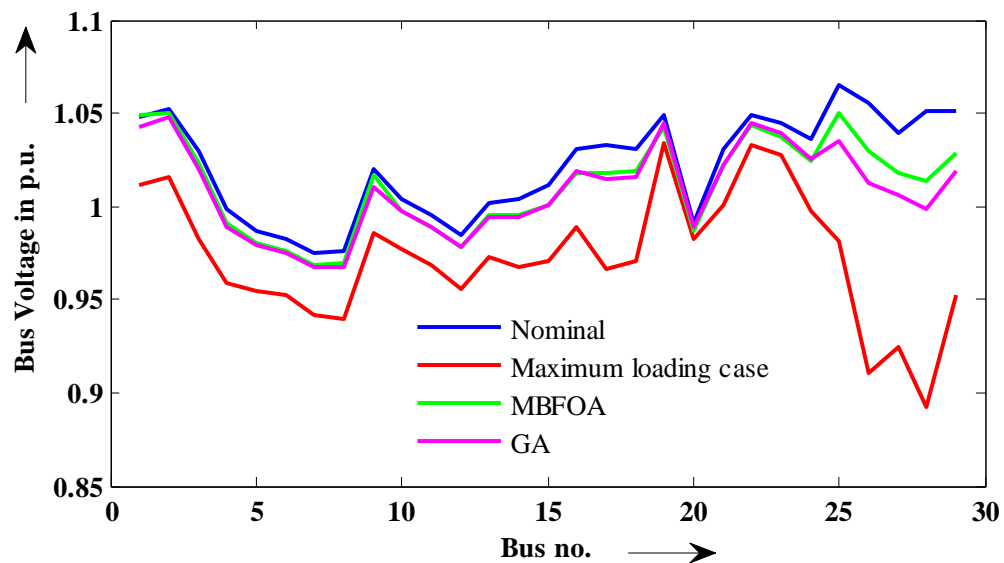

Figure 3.9 (a). System voltage profile for P increase in weak bus (bus No 28).
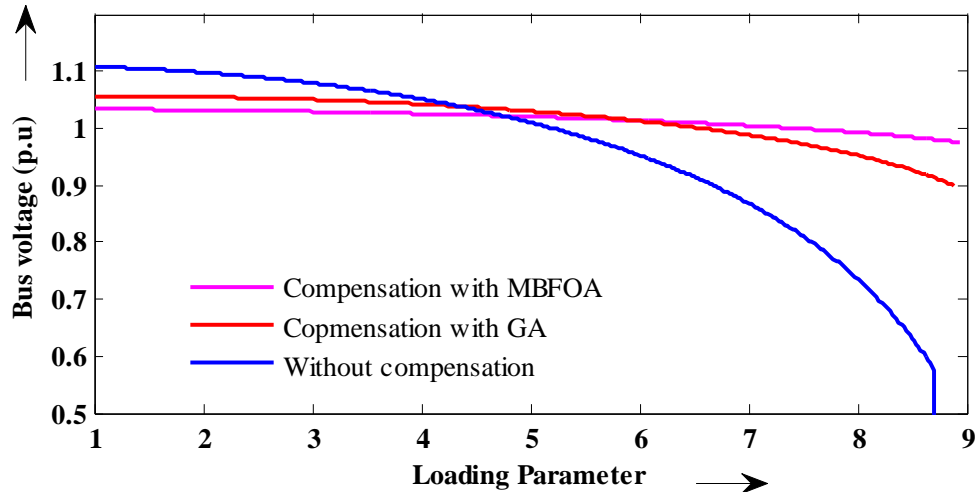
Figure 3.9 (b). Loadability limit of weak bus 28.

In **Fig 3.10(a)** the voltage of load bus 29 is 1.15pu at maximum loading from 1.05 pu at nominal loading. The voltage becomes 0.95pu with MBFOA technique where as with GA it is 0.96 pu. Further the load margin is increased to 7.2 with GA and enhanced further to 7.3 with MBFOA from 7.1 without any compensation as shown in **Fig. 3.10(b)** shows the load margin study.
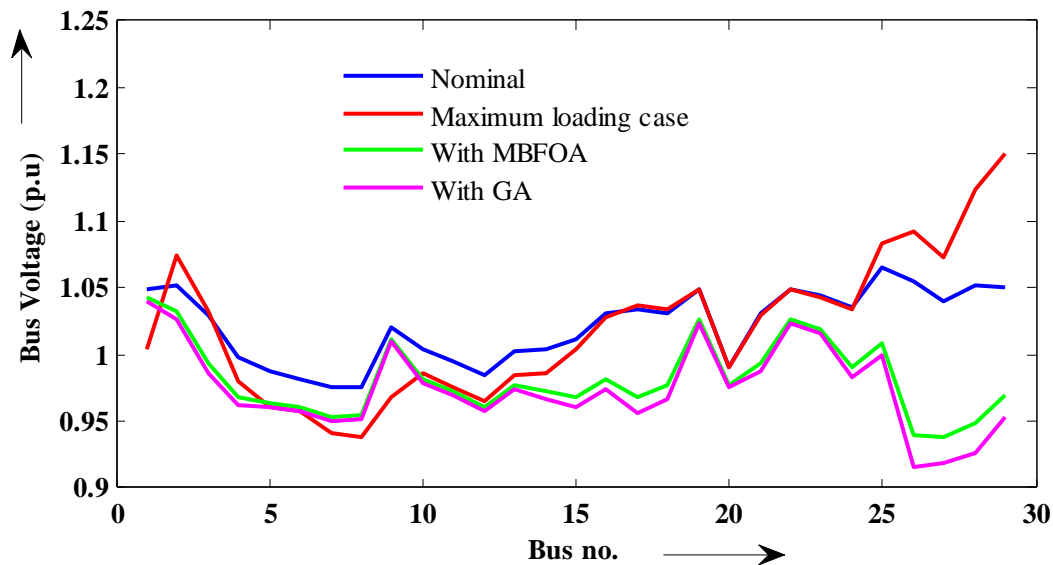
Figure 3.10 (a). System voltage profile for P increase in weak bus (bus No 29).
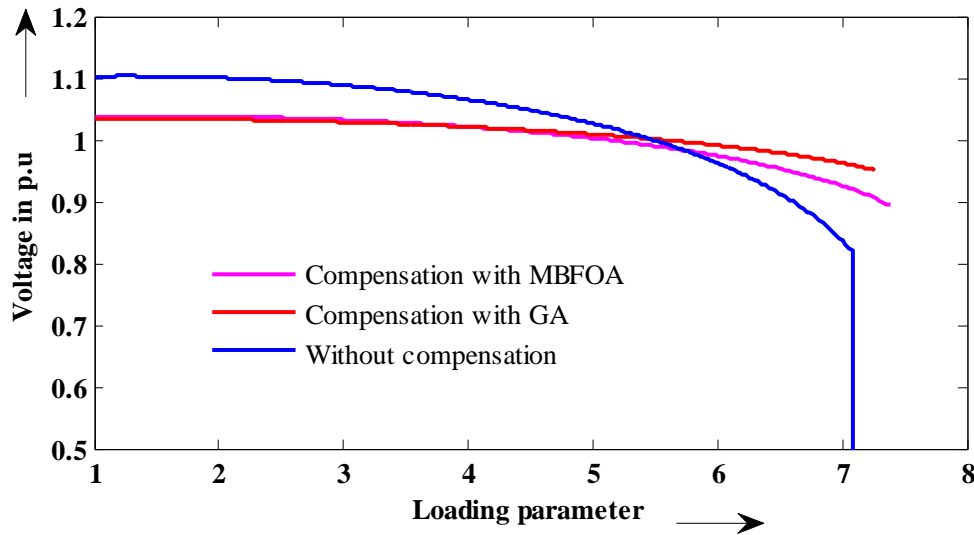
Figure 3.10. (b). Loadability limit of weak bus 29.

The compensation parameters with GA and MBFOA are shown in Figure **3.11.** It clearly shows the compensation amount be very less (9% and 30%) in two capacitors for MBFOA than GA which are (45 % and 46 %) . The ENVCI –Lambda(λ) curve after optimisation is shown in Figure **3.12** and justifies increase in **06**% (in p.u system of 100 MVA base) of LM with MBFOA than GA.
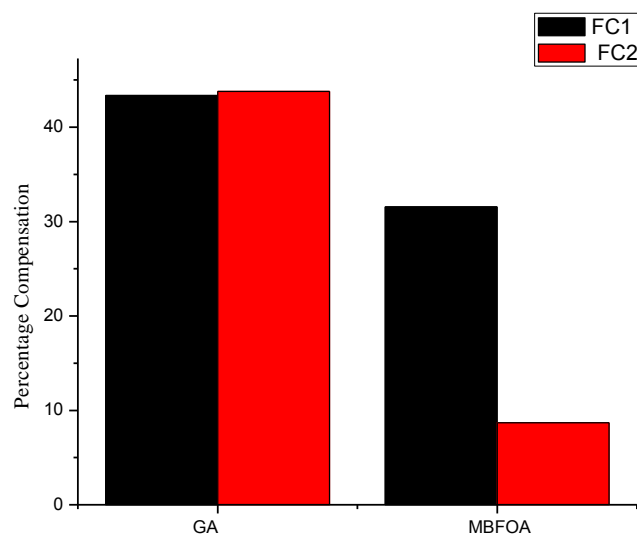
Figure 3.11. Compensation with GA and MBFOA.
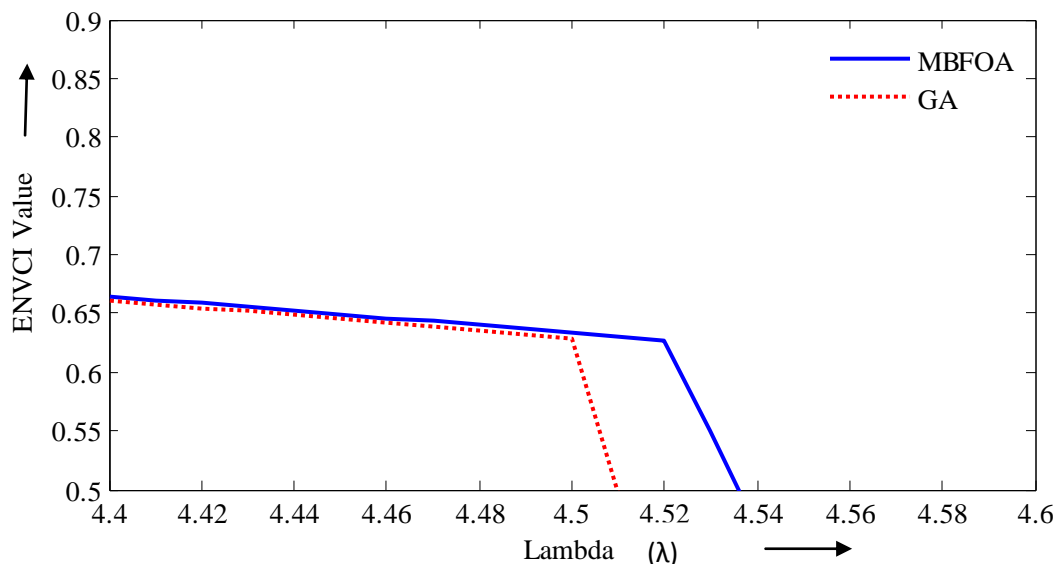
Figure 3.12. ENVCI-Lambda curve for load increase after optimization.

3.7. Conclusions

With the increasing power demand and reduced opportunity of generation and transmission system expansion available to the system operator, the power system is operating in ever increasing stressful condition. In this scenario, the systems are operating very near their loadability limits. To relieve the system operation and improve the operating voltages in it proper optimized compensation of reactive power resources has become mandatory for secure operation. To alleviate the problem, fixed capacitive compensation of proper size at proper location in the system improves the operation increasing the VSL. In this work, some modifications are done in a basic intelligent optimization technique known as BFOA. With the proposed modifications, MBFOA is applied to optimize a suitably designed objective function to obtain the optimum location and size of FC, which can improve the system VSL. The optimization efficiency and accuracy is compared with the results obtained with GA, DE, and PSO and found to be better than the rest. The system PV curves in the case of loading done at almost all the buses improved, giving the best result when the loads are increased at the weakest bus in the system. The choice of the proposed algorithm is based on the fact that it has some unique characteristics of elimination and dispersal not found in other algorithms and that the original version of the algorithm has already been tested in many problems of power system.

Thus, the subsequent chapters are dealt with the MBFOA optimization techniques only with the modified models of the system.

However, by placing only FC at some optimum location may not solve the purpose of improvement in voltage profiles under wider ranges of system operating conditions. To improve upon the performance, the role of FACTs device in the form of a STATCOM placed at a suitable location in the system, is tested in Chapter-**4**.

IMPROVEMENT OF LOAD MARGIN WITH THE INCLUSION OF STATCOM IN TRANSMISSION SYSTEM

4.1. Introduction

Transmission network operation becomes stressful due to increase in the reactive power consuming loads, contingencies in the form of line outage and generator mal-operation, over load etc, leading to voltage insecure operation. The solution to the problem is addressed by supplementing the shortfall in reactive power by external means to the network at desired locations. Further, the optimized VAR supplement will make the system operation much healthier. The optimized value of reactive power can be obtained if the VAR generating systems are variable type. According to the continuously changing reactive power needs of the system due to the changes in the operating conditions, if the amount of required VAR support can be supplied by external means then the problem is best alleviated. The planning for reactive power compensation in maintaining the operating voltage to increase the loadability of the system is the main objective. In chapter 3 only fixed capacitors were taken into account as the simplest and first form of reactive power support. As the fixed capacitors have limitations of having fixed values but not of variable capacity, to a varying load the fixed capacitor cannot provide variable value. Practically variable reactive power cannot be provided from a fixed capacitor. Thus switched capacitors are better option than fixed capacitors which are used to operate quickly and swiftly to supply the optimized value of reactive power.

Different types of FACTs devices can meet the above requirement. Among the category of series devices in the family of FACTs, the concept of TCSC was introduced in [50]. However, for the purpose of control of system voltage, the category of shunt devices is found to be more suitable compared to the series devices. In [110], the usefulness of STATCOM for alleviating issues related to voltage stability was probed. For obtaining the suitable settings of the devices for effective operation of the same in a stressed power system, different techniques of optimization have been applied. In [108], GA is used to optimal location of four devices namely

TCSC, TCPST, TCVR and SVC to compare the efficiency of each device in a multi generator power system to study the problems of voltage stability in the same. Similarly, a widely accepted optimization algorithm, enhanced-PSO [111] is utilized to determine optimal value and location of STATCOM the extent of improvement in the system loadability margin. In this work a STATCOM is placed at the weakest bus in the test system (introduced earlier in Chapter 2) to improve upon the performance of fixed capacitor (FC) compensation scheme in Chapter 3. Further, to have even better performance the generator PV bus settings of all the 10 generators are also considered as control variables during optimization. The problem is identically formulated with the same objective as considered in the previous chapter. Before, going to the details of formulation of the problem, some more elucidation on the operation of STATCOM is presented at the outset.

4.2. Fundamental Concept of STATCOM

The static synchronous compensator (STATCOM) is a GTO based device of Flexible AC Transmission Systems (FACTS) family. The STATCOM is a static synchronous generator operated as a static VAR compensator which can inject lagging or leading VAR into the system when connected in shunt. Simple diagram of STATCOM is shown in Figure **4.1 (a)** and **(b)** respectively. The DC source voltage is converted into AC voltage by the voltage source converter using GTO and AC voltage is inserted into the line through the transformer. In a heavily loaded condition, if output of VSC is more than the line voltage, converter supplies lagging VARs to the transmission line. During light load condition, if line voltage is more than the line voltage then converter absorbs lagging VAR from the system. If output voltage of converter is equal to line voltage, then the STATCOM is in floating condition and this shunt device does not supply or absorb reactive power to the system or from the system.
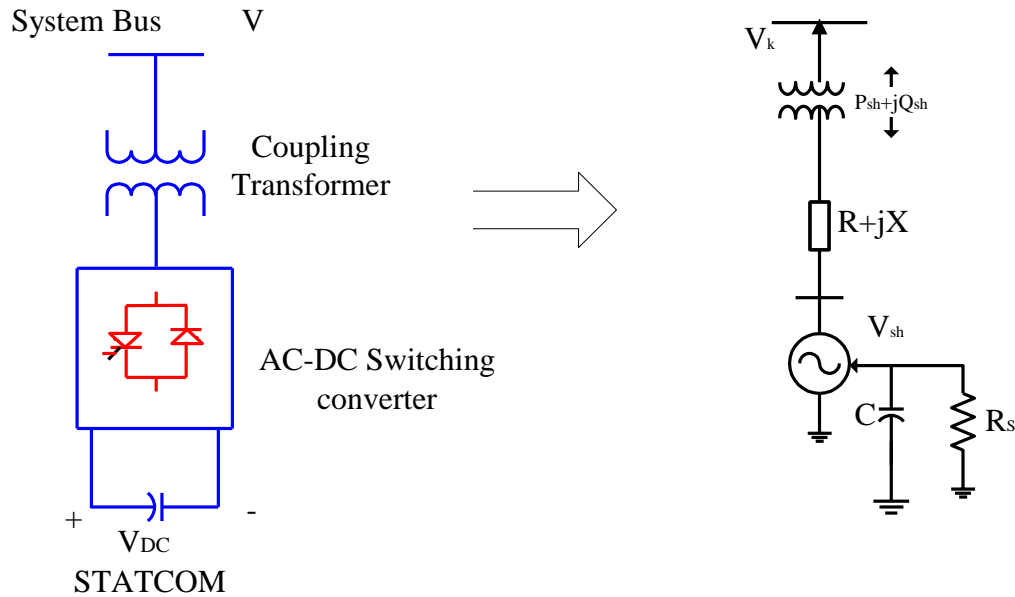
Figure 4.1. (a) & (b). Schematic diagram of STATCOM.

4.2.1. Operating principle of the STATCOM

The STATCOM regulates voltage at its terminal by controlling the amount of reactive power injected into or absorbed from the power system. It is to note that for the system voltage being low, the STATCOM generates reactive power (STATCOM capacitive) and with the system voltage being high, the latter absorbs reactive power (STATCOM inductive) as well. The variation of reactive power is performed by means of a Voltage-Sourced Converter (VSC) connected on the secondary side of a coupling transformer as shown in Figure **4.1 (a)**. The VSC uses forced-commutated power electronic devices (GTOs, IGBTs or IGCTs) to synthesize a voltage from a DC voltage source. The schematic diagram and equivalent circuit of the STATCOM is shown in the Figure **4.1 (a)** and Figure **4.1 (b)** above. In this figure, V_k represents the system voltage to be controlled and V_{sh} is the voltage generated by the VSC. The active and reactive power transfer between sources V_k and V_{sh} are given by the following two equations.

$$P = \frac{V_k V_{sh} \sin \delta}{X} \tag{4.1}$$

$$Q = \frac{V_k(V_k - V_{sh}\cos\delta)}{X} \tag{4.2}$$

In steady state operation, the voltage V_{sh} generated by the VSC is in phase with V_k ($\delta = 0$), so that only reactive power is flowing ($P = 0$) and the reactive power is given by the equation

$$Q = \frac{V_k(V_k - V_{sh})}{X} \tag{4.3}$$

If V_{sh} is lower than V_k, Q is flowing from V_k to V_{sh} (STATCOM is absorbing reactive power). On the reverse, if V_{sh} is higher than V_k, Q is flowing from V_{sh} to V_k (STATCOM is generating reactive power). The amount of reactive power is given by the same above equation. A capacitor connected on the DC side of the VSC acts as a DC voltage source. In steady state the voltage V_{sh} has to be phase shifted slightly behind V_k in order to compensate for transformer and VSC losses and to keep the capacitor charged.

4.2.2. V-I characteristic of STATCOM in different modes of operation

The STATCOM can be operated in two different modes:

- In voltage regulation mode (the voltage is regulated within limits as explained below),
- In VAR control mode (the STATCOM reactive power output is kept constant).

When the STATCOM is operated in voltage regulation mode, it implements the following V-I characteristic. As long as the reactive current stays within the maximum and minimum current values ($-I_{max}$, I_{max}) imposed by the converter rating, the voltage is regulated at the reference voltage V_{ref}. However, a voltage drop is normally used (usually between 1% and 4% at maximum reactive power output), and the V-I characteristic has the slope indicated in the Figure **4.2**. In the voltage regulation mode, the V-I characteristic is shown in the same figure and is described by the following equation:

$$V = V_{ref} + X_{SL}I \tag{4.4}$$
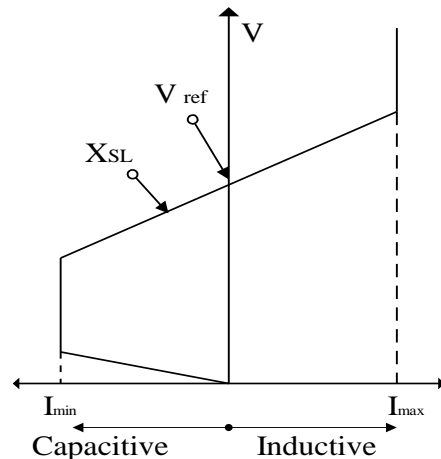
Figure 4.2. V-I characteristic of STATCOM.

4.2.3. Advantages of STATCOM over SVC

The STATCOM has several advantages. It has no rotating parts, very fast in response, requires less space as bulky passive components are eliminated, inherently modular and re-locatable, less maintenance and no problem as loss of synchronism [50]. The STATCOM performs the same function as the SVC. However at voltages lower than the normal voltage regulation range, the STATCOM can generate more reactive power than the SVC [92]. This is due to the fact that the maximum capacitive power generated by a SVC is proportional to the square of the system voltage (constant susceptance) while the maximum capacitive power generated by a STATCOM decreases linearly with voltage (constant current). This ability to provide more capacitive reactive power during a condition of fault, is one of the important advantages of STATCOM over the SVC. In addition, the STATCOM will normally exhibit a faster response than the SVC because with the VSC, the STATCOM has no delay associated with the thyristor firing (in the order of 4 ms for a SVC).

4.3. STATCOM in the Test System

The STATCOM provides effective voltage support at the bus which it is connected to. The STATCOM is placed as close as possible to the load bus for various reasons. The first reason is that the location of the reactive power support should be as close as possible to the

point at which the support is needed. Secondly, in the test system under consideration the location of the STATCOM at the load bus is more appropriate because the effect of voltage deviation is the highest at this point. Finally, the 20th bus in the test system is the weakest bus that is most vulnerable to the possibility of voltage collapse condition. Therefore, STATCOM is located on the same bus and the structure of the new system *i.e.* STATCOM in the system is shown in Figure **4.3**. The size of the STATCOM taken here is 200MVAR.

Before formulation of the problem, the fundamental concepts of the power flow condition model of STATCOM is elaborated in some detail here.
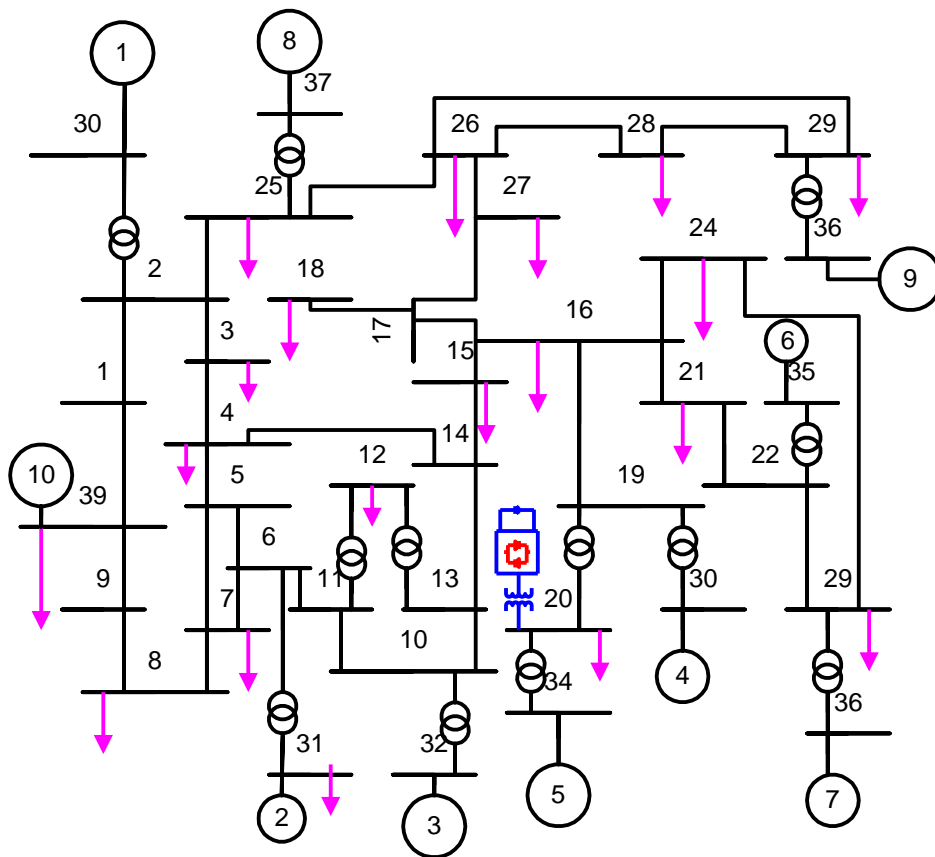
Figure 4.3. STATCOM in IEEE-39 Bus system.

4.3.1. Power flow model of STATCOM

A schematic representation of the STATCOM is shown in Figure **4.1(a)** and the equivalent circuit is shown in Figure **4.1 (b)** respectively. The equivalent circuit represents the Thevenin equivalent when seen from bus *k*, with the voltage source E_{sh} being the fundamental frequency component of the VSC output voltage. In steady-state fundamental frequency studies the STATCOM may be represented in the same way as a synchronous condenser, which in most cases is the model of a synchronous generator with zero active power generation. A more flexible model may be realized by representing the STATCOM as a variable voltage source E_{sh}, for which the magnitude and phase angle may be adjusted, using a suitable iterative algorithm to satisfy a specified voltage magnitude at the point of connection with the AC network. The shunt voltage source of the three-phase STATCOM may be represented by

$$E_{sh} = V_{sh} \left(\cos \delta_{sh} + j \sin \delta_{sh} \right) \tag{4.5}$$

The voltage magnitude, V_{sh}, is given maximum and minimum limits, which are a function of the STATCOM capacitor rating. However, δ_{sh} may take any value between 0 and 2π radians. With reference to the equivalent circuit shown in Figure **4.1(b)**, and assuming three phase parameters, the following transfer admittance equation can be written:

$$[I_k] = [Y_{sh} \quad -Y_{sh}] \begin{bmatrix} V_k \\ E_{sh} \end{bmatrix} \tag{4.6}$$

The bus at which the STATCOM is connected is represented as a **PQ** bus. In such a case, the generated or absorbed reactive power would correspond to the violated limit. Unlike the SVC, the STATCOM is represented as a voltage source for the full range of operation, enabling a more robust voltage support mechanism. The STATCOM equivalent circuit shown in Figure **4.1(b)** is used to derive the mathematical model of the controller for inclusion in power flow algorithms. The power flow equations for the STATCOM [93] are mentioned below assuming the following voltage source representation. Based on the shunt connection shown in Figure **4.1(b)**, the following may be written using [93]

$$S_{sh} = V_{sh} I_{sh}{}^* = V_{sh} Y_{sh}{}^* \left(V_{sh}{}^* - V_k{}^* \right)$$

(4.7)

The expression for active and reactive power equations is obtained for the converter and bus k, respectively.

$$P_{sh} = V_{sh}^2 G_{sh} + V_{sh} V_k \left[G_{sh} \cos(\delta_{sh} - \delta_k) + B_{sh} \sin(\delta_{sh} - \delta_k) \right]$$

(4.8)

$$Q_{sh} = -V_{sh}^2 B_{sh} + V_{sh} V_k \left[B_{sh} \cos(\delta_{sh} - \delta_k) - G_{sh} \sin(\delta_{sh} - \delta_k) \right]$$

(4.9)

$$P_k = V_k^2 G_{sh} + V_{sh} V_k \left[G_{sh} \cos(\delta_k - \delta_{sh}) + B_{sh} \sin(\delta_k - \delta_{sh}) \right]$$

(4.10)

$$Q_k = -V_k^2 G_{sh} + V_{sh} V_k \left[B_{sh} \cos(\delta_k - \delta_{sh}) - G_{sh} \sin(\delta_k - \delta_{sh}) \right]$$

(4.11)

Using these power equations, the linearized STATCOM model is given below, where the voltage magnitude V_{sh} and phase angle δ_{sh} are taken to be the state variables:

$$
\begin{bmatrix} \Delta P_k \\ \Delta Q_k \\ \Delta P_{sh} \\ \Delta Q_{sh} \end{bmatrix}
=
\begin{bmatrix}
\dfrac{\partial P_k}{\partial \delta_k} & \dfrac{\partial P_k}{\partial V_k} V_k & \dfrac{\partial P_k}{\partial \delta_{sh}} & \dfrac{\partial P_k}{\partial V_{sh}} V_{sh} \\[2mm]
\dfrac{\partial Q_k}{\partial \delta_k} & \dfrac{\partial Q_k}{\partial V_k} V_k & \dfrac{\partial Q_k}{\partial \delta_{sh}} & \dfrac{\partial Q_k}{\partial V_{sh}} V_{sh} \\[2mm]
\dfrac{\partial P_{sh}}{\partial \delta_k} & \dfrac{\partial P_{sh}}{\partial V_k} V_k & \dfrac{\partial P_{sh}}{\partial \delta_{sh}} & \dfrac{\partial P_{sh}}{\partial V_{sh}} V_{sh} \\[2mm]
\dfrac{\partial Q_{sh}}{\partial \delta_k} & \dfrac{\partial Q_{sh}}{\partial V_k} V_k & \dfrac{\partial Q_{sh}}{\partial \delta_{sh}} & \dfrac{\partial Q_{sh}}{\partial V_{sh}} V_{sh}
\end{bmatrix}
\begin{bmatrix} \Delta \delta_k \\ \Delta V_k / V_k \\ \Delta \delta_{sh} \\ \Delta V_{sh} / V_{sh} \end{bmatrix}
$$

(4.12)

Where the augmented Jacobian is given by

$$
\begin{bmatrix}
\dfrac{\partial P_k}{\partial \delta_k} & \dfrac{\partial P_k}{\partial V_k} V_k & \dfrac{\partial P_k}{\partial \delta_{sh}} & \dfrac{\partial P_k}{\partial V_{sh}} V_{sh} \\[2mm]
\dfrac{\partial Q_k}{\partial \delta_k} & \dfrac{\partial Q_k}{\partial V_k} V_k & \dfrac{\partial Q_k}{\partial \delta_{sh}} & \dfrac{\partial Q_k}{\partial V_{sh}} V_{sh} \\[2mm]
\dfrac{\partial P_{sh}}{\partial \delta_k} & \dfrac{\partial P_{sh}}{\partial V_k} V_k & \dfrac{\partial P_{sh}}{\partial \delta_{sh}} & \dfrac{\partial P_{sh}}{\partial V_{sh}} V_{sh} \\[2mm]
\dfrac{\partial Q_{sh}}{\partial \delta_k} & \dfrac{\partial Q_{sh}}{\partial V_k} V_k & \dfrac{\partial Q_{sh}}{\partial \delta_{sh}} & \dfrac{\partial Q_{sh}}{\partial V_{sh}} V_{sh}
\end{bmatrix}
$$

(4.13)

With the above modifications in the Jacobian matrix of power flow, the STATCOM is included in the test system and the load flow is performed to study behavior of the system under condition of load increase. In summary, the power flow of the system is performed with NRLF involving the above modifications in the power flow equations and the Jacobian matrix.

4.4. Problem Formulation

The problem is formulated with the three objectives same as considered in Chapter **3** and taking into the account of the operating constraints as mentioned in the same chapter as expressed below:

$$\begin{cases} Minimize & F(x,u,\lambda) \\ subject\ to & G(x,u,\lambda)=0, \\ & and\ H(x,u,\lambda)\leq0 \end{cases} \qquad \textbf{(4.14)}$$

$F(x,u,\lambda)$ is expressed below

$F = max\ f_1 + min\ f_2 + Pf_1 + Pf_2 + Pf_3$ is the objective function (details already explained in section 3.2 of chapter 3, Equation No. 3.15)

$G(x,u,\lambda)=0$ is the equality constrained (explained in section 3.2 , Ch.- 3, Equation No. 3.6)

$H(x,u,\lambda)\leq0$ is the compact form of the inequality constraints (explained in sec.3.2 Ch- 3, Equation 3.10)

4.5. Optimization

The problem formulated in the previous section is optimized with modified bacteria foraging optimization algorithm (MBFOA) technique as it is seen in the last chapter that MBFOA performs better than GA. The problem is taken up as described below. The weakness sensitivity is estimated by the ENVCI calculation. Further simply the weakest bus (in this case bus 20) is connected with a STATCOM. More active power load is increased (as demand load) in the weakest bus and the optimized value of two reactive power as well as two optimal location

of these compensators are achieved. For a load increase in 50% from the nominal value the voltage stability is studied and the VSL is enhanced with proper optimized value of reactive power support at optimal location. Load flow study is made with NRLF method. The width attractant, repellant are 1.05 and 1.03 respectively. The run length unit is 0.07.

4.6. Simulation Results and Discussions

The simulation was carried out in Intel® core IV quad processor using **Matlab**® software. The proposed MBFOA was applied to solve the problem formulated above.
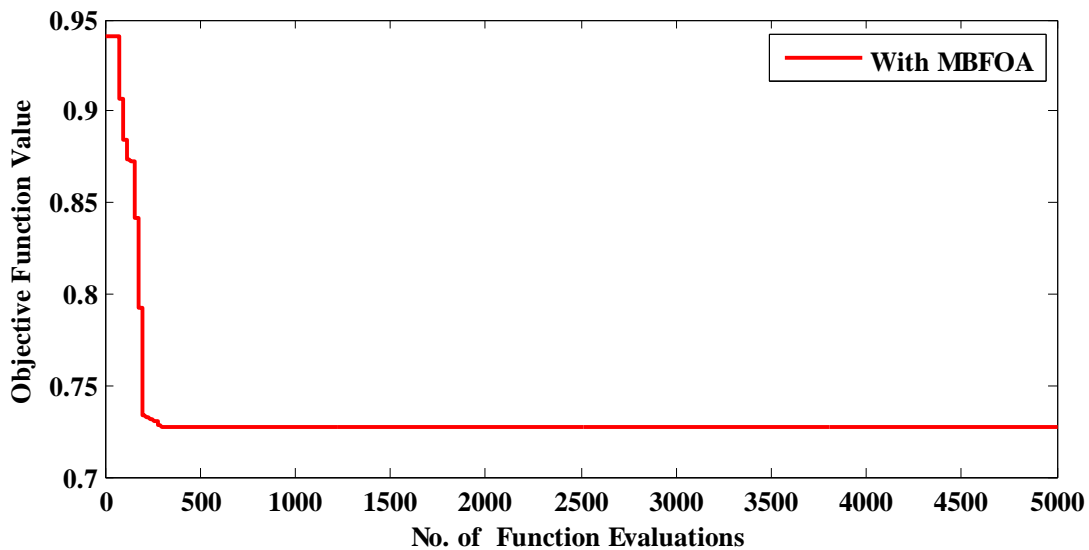
Figure 4.4. Convergence characteristic.

As done in the previous problem, the ENVCI is retained as the criterion to determine VSL of the system. As per the formulation the problem aims at maximizing the minimum value of VSL obtained among the weak buses, *i.e.* **8, 20, 27, 28, 29.** The result of optimization is shown in the convergence characteristics depicted in Figure **4.4**. Function calculations means calculations in local search procedure. Let 30 seconds to run for a function evaluation then it might take few minutes (0 to 3 minutes) for one iteration depending upon the no of variables This means a solver begins at an initial value x_0, performs some intermediate calculations that eventually lead to a new point x_1, and then repeats the process to find successive approximations x_2, x_3, ... of the local minimum. Processing stops after some number of iterations k. At any step, intermediate

calculations may involve evaluating the objective function and constraints, if any, at points near the current iterate x_i. For example, the solver may estimate a gradient by finite differences. At each of these nearby points, the function count (F-count) is increased by one.

- If there are no constraints, the F-count reports the total number of objective function evaluations.
- If there are constraints, the F-count reports only the number of points where function evaluations took place, not the total number of evaluations of constraint functions.
- If there are many constraints, the F-count can be significantly less than the total number of function evaluations.

F-count is a header in the iterative display for many solvers. For an example, see interpreting the results. F-count appears in the output structure as output func Count. This enables you to access the evaluation count programmatically. For more information on output structures, sometimes a solver attempts a step, and rejects the attempt. The trust-region, trust-region-reflective, and trust-region-dogleg algorithms count these failed attempts as iterations, and report the (unchanged) result in the iterative display. The interior-point, active-set, and levenberg-marquardt algorithms do not count such an attempt as iteration, and do not report the attempt in the iterative display. All attempted steps increase the F-count, regardless of the algorithm. The optimum values of generator bus voltages and amount and locations of compensation at two locations are given in Table.**4.1**. The profiles of system bus voltages obtained for different conditions of arbitrary load increases at some weak buses are discussed below

Table 4.1. Compensation for load increase in bus 20.

Compensation Specifications	Constant Q-Load
1st location of compensation	Bus no 21
1st amount of compensation	25.86%
2nd location of compensation	Bus No.25
2nd amount of compensation	14.2 %
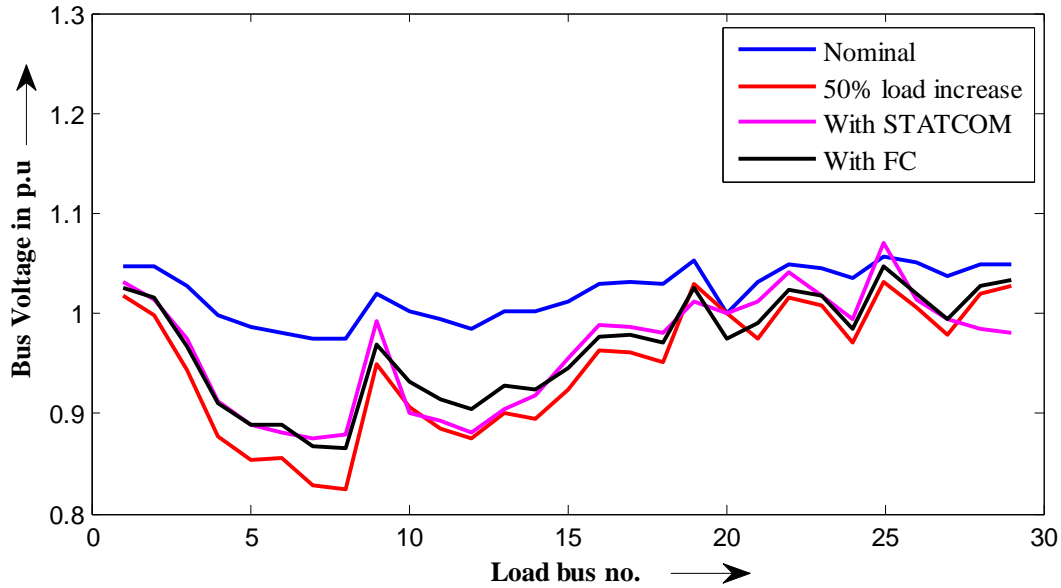
Figure 4.5. Voltage profile for load increase in bus no 8 with STATCOM in bus 20.

The system bus voltage (voltage in other buses also vary) as shown in Figures **4.5** to **4.12** respectively. In Figure **4.5** the load increased by **50%** of its rated value and the simulation result shows that the voltage at the same bus is very much close to the lower limit 0.8 p.u. The value of lower limit (0.8 p.u.) is considered for in depth study only. It means the system has crossed too far the limit of voltage violations. With the reactive power support the voltage is improved by **3**% (with FC) and **6**% with STATCOM.
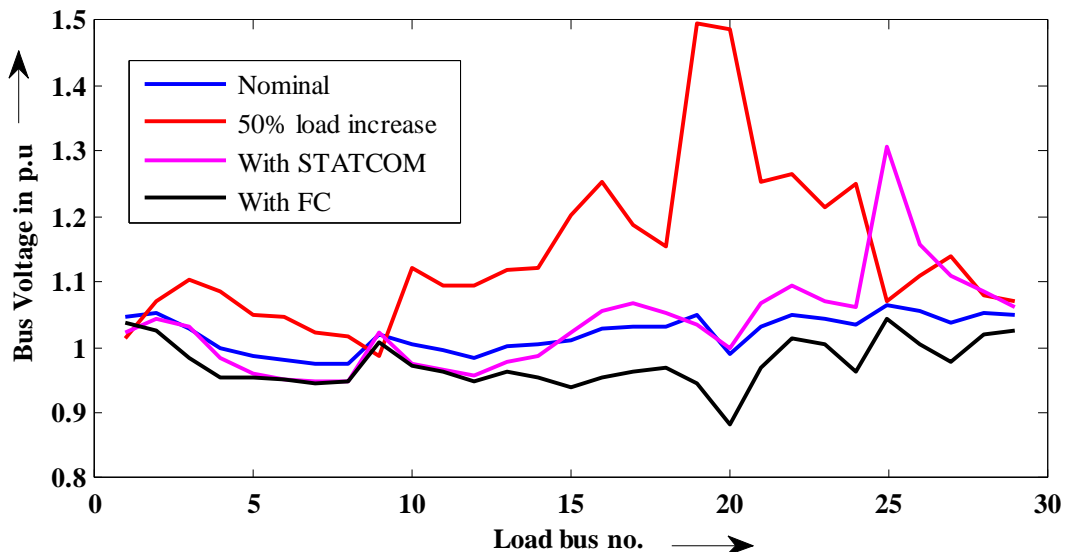
Figure 4.6. Voltage profile for load increases in bus no 20 with STATCOM in bus 20.
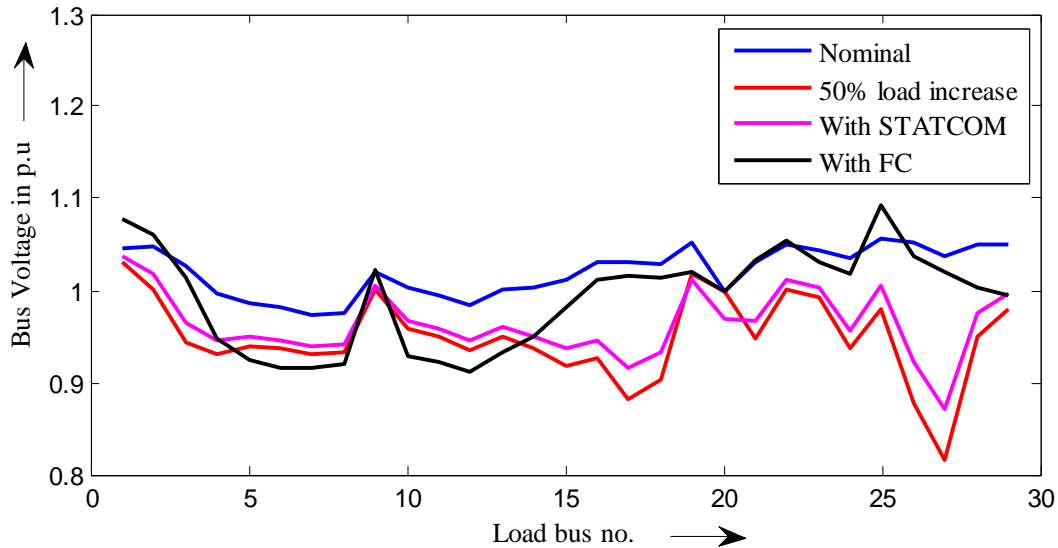
Figure 4.7. Voltage profile for load increases in bus no 27 with STATCOM in bus 20.

Similarly in bus **20**, the bus voltage at bus **20** is constant (1 p.u) as it is connected with STATCOM, treated as PV bus as shown in Figure **4.6**. The compensation made by STATCOM as well as FC enhance the voltage profile in the other buses also, where as keeping the voltage of bus no **8** to be almost same except for a negligible change. Similarly the voltage profile of the system indicating the better performance of STATCOM over FC for the load increase in bus no **27, 28,** and **29** are depicted in Figure **4.7** to Figure **4.9** .

Figure 4.8. Voltage profile for load increases in bus no 28 with STATCOM in bus 20.
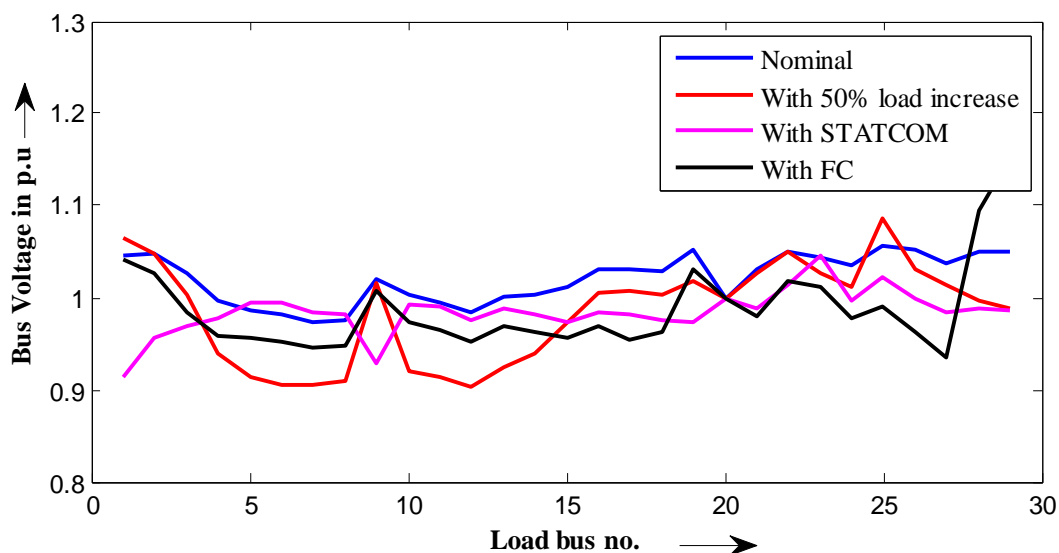
Figure 4.9. Voltage profiles for load increase in bus no 29 with STATCOM in bus 20.

Also the system is studied for some contingencies in the system along with increased load in a bus as shown in Figures **4.10**, **4.11**, and **4.12** respectively. Before optimisation, for **50%** load increase in load bus **23** with line outage of **10-11,** the system load bus voltage profile is observed. Then after optimization, the voltage magnitude obtained with use of STATCOM and FC which is plotted in Figure **4.10**. Comparison between the two compensators justifies the better result with STATCOM. In Figure **4.11**, the voltage profile of the load buses obtained in the same manner as discussed above, the system is stressed for 50% real power load increase in load bus **4** with a line outage of **2-3** in all the buses the voltage dip was seen (before optimization). Although the results obtained after optimization with FC shows the voltage dip is improved but with STATCOM the voltage level is improved more after optimization. The voltage in all the **29** load buses are plotted from the simulation made in the Figure **4.12** for 50% load increase in the load bus **16** with a line outage of **15-16**. The profile at nominal case is in stable condition where as in the contingency case it shows the closeness towards the lower hit limit, but the profile after optimization with STATCOM improves the voltage level in all the load buses and also with FC, the same is improved but less improvement compared to STATCOM.
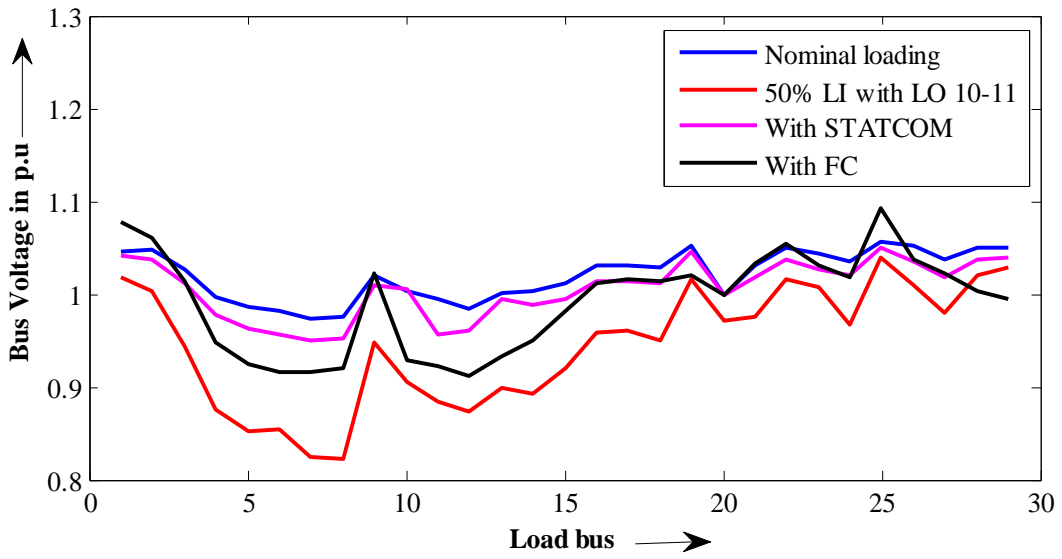
Figure 4.10. Voltage profile for load increase in bus no 23 with LO 10-11.

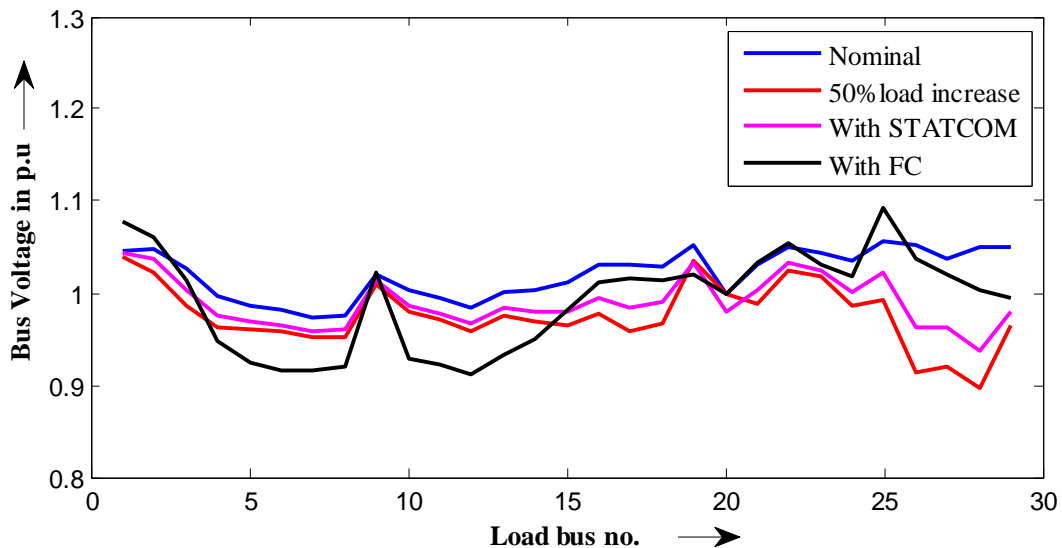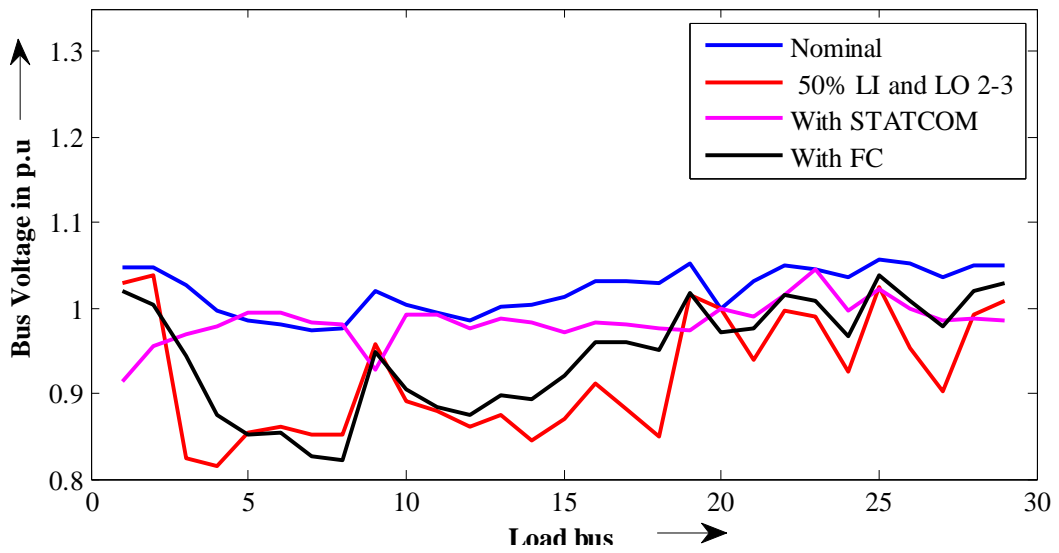***Figure 4.11.*** Voltage profile for load increase in bus no 4 with LO 2-3.
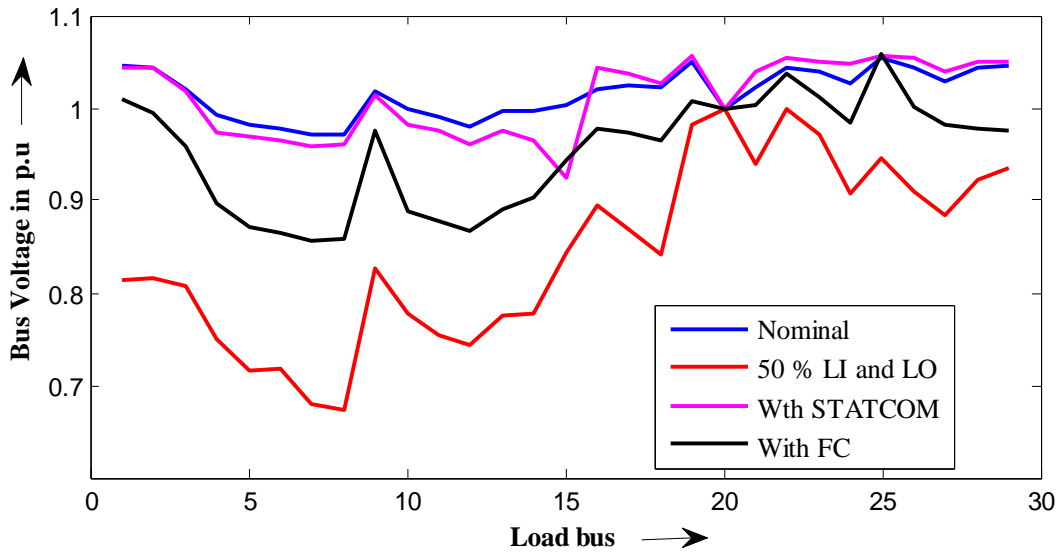
Figure 4.12. Voltage profile for load increase in bus no 16 with LO 15-16.
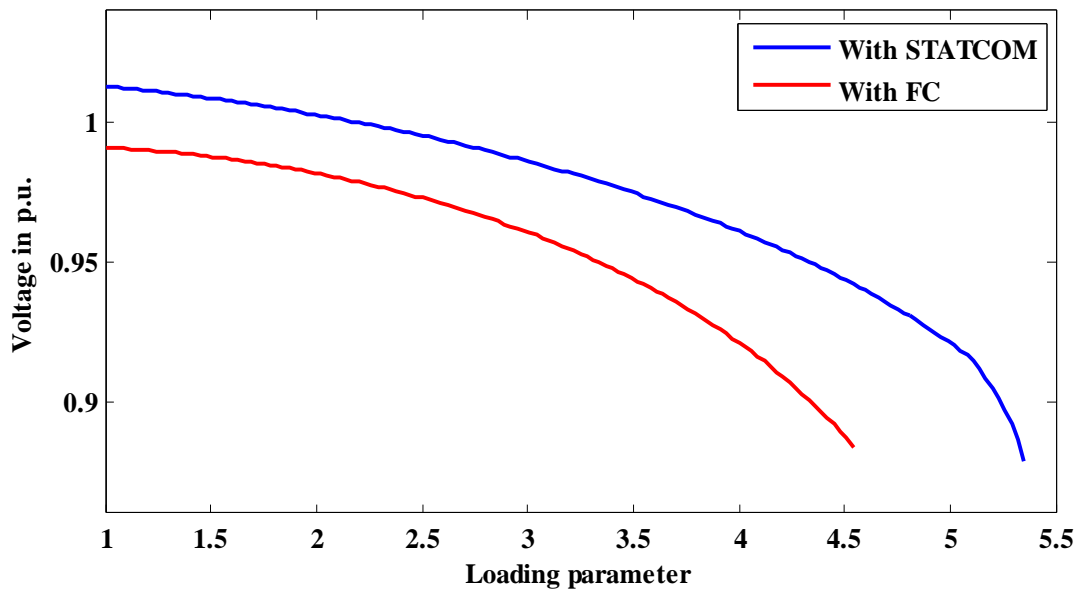
Figure 4.13. Loading limit of bus 8 with FC and with STATCOM.

In Figure **4.13**, the load margin of bus no **8** is shown after optimization with FC as well as with STATCOM. It shows that the increased LM to be **5.47** from **4.52**.
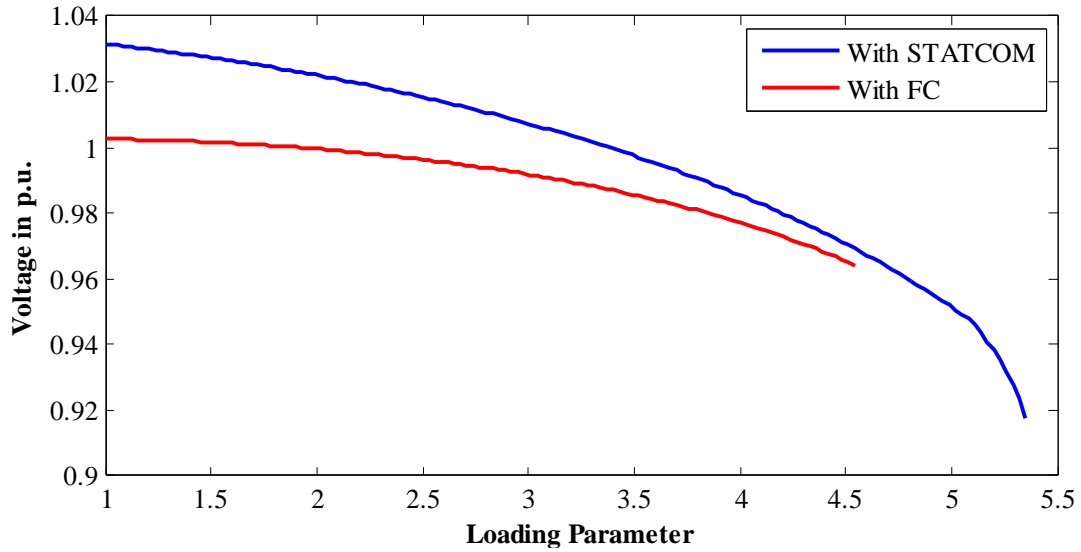
Figure 4.14. Load margin of bus 20.

The results obtained for bus **20** is shown in Figure **4.14**. It is very much evident that the load margin of the bus **20** is also increased with STATCOM compared to the FC. Similarly for load bus **27, 28** and **29** the results obtained are shown in Figure **4.15** to Figure **4.17**.
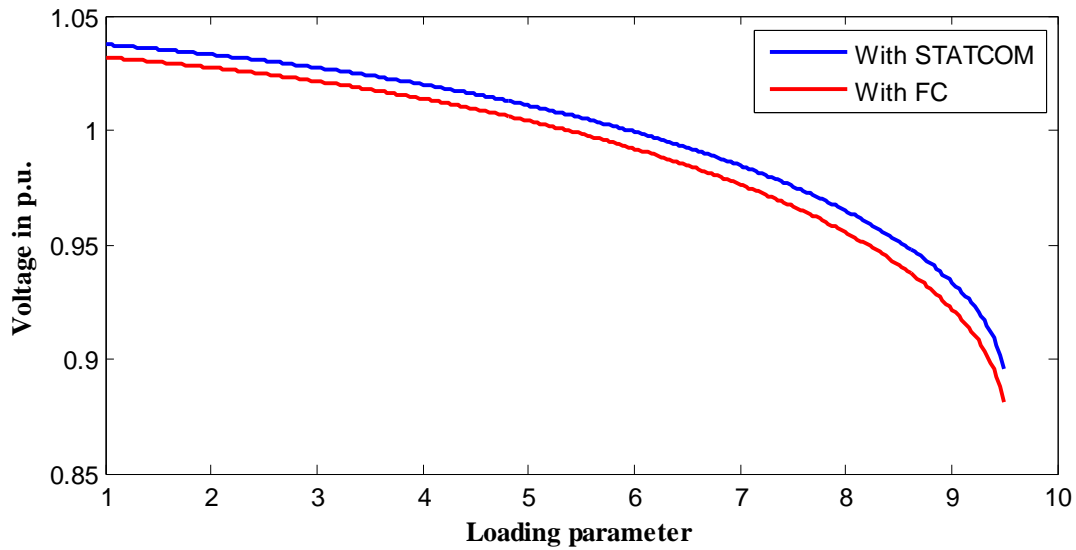
Figure 4.15. Load margin of bus 27.
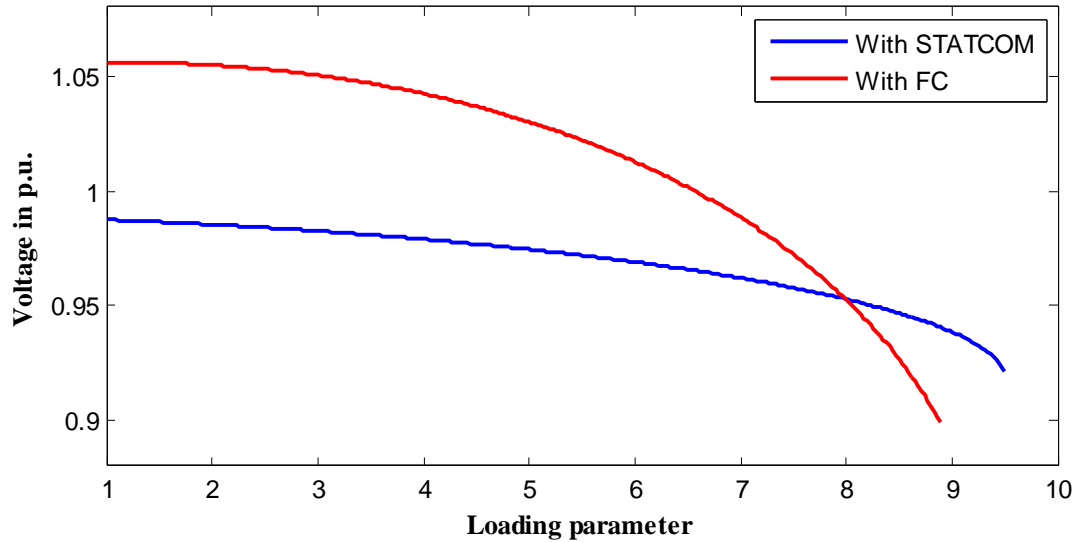
Figure 4.16. Load margin of bus 28.
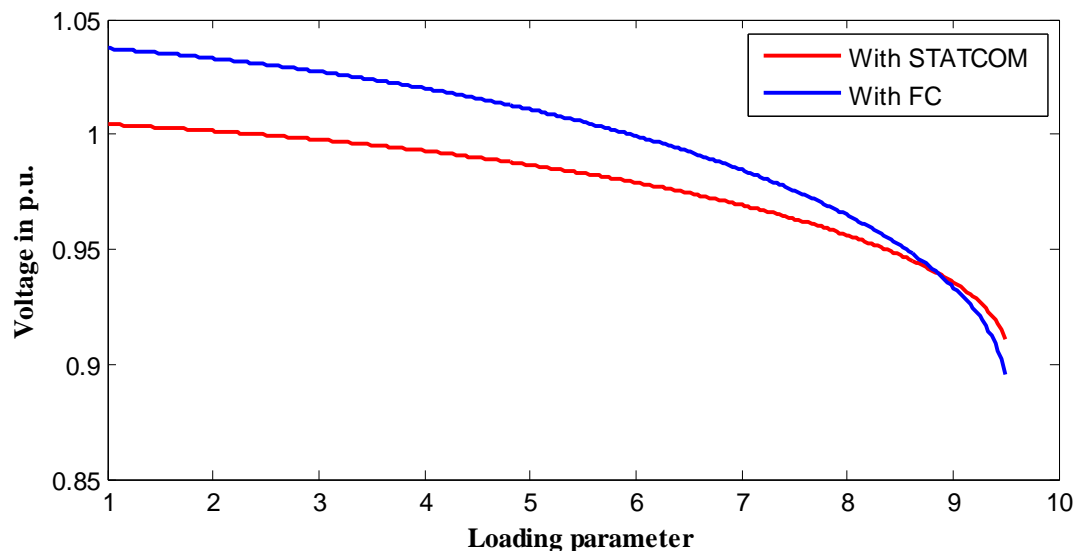
Figure 4.17. Load margin of bus 29.

In **Fig. 4.16** the comparison of the two curves obtained are of different behavior with the use of fixed capacitor the optimized value for bus 28 has voltage (when load parameter is 1) 1.05p.u. But with use of statcom, the voltage is equal to 0.99 p.u. With STATCOM the bus can be loaded upto 9.5 times of its normal operating conditions where as with FC it is less i.e, loading parameter is 9. The main objective is to bring back the operating voltage close to 1which is in the case of STATCOM the voltage variation is less than the FC case.

The loading limit versus ENVCI curve obtained after optimization of the load bus **20** with the STATCOM in it as one of the candidate buses is shown in Figure **4.18** giving good reason for the use of STATCOM over FC.
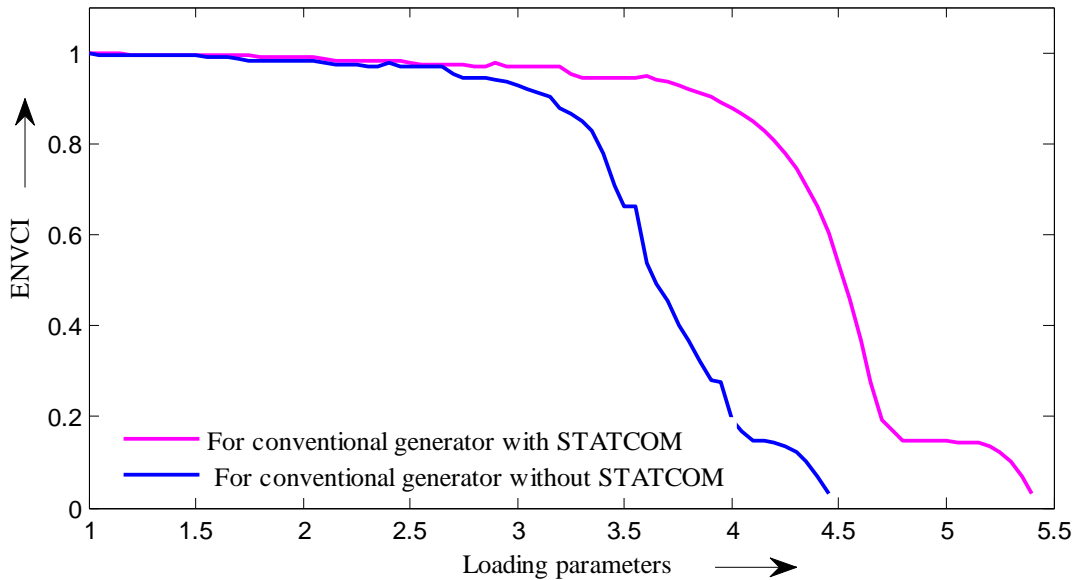
Figure 4.18. Loading limit of the load bus 20 with the STATCOM and without STATCOM.

4.7. Conclusions

Transmission network operation becomes stressful due to increase in the reactive power consuming loads, contingencies in the form of line outage, generator outage, sudden load increase etc. These will lead to voltage insecure operation of the system. The problem discussed in Chapter **3** is extended in this chapter, by connecting a STATCOM at weakest bus to provide additional support of reactive power in the network during increased levels of stress in operation. Further, apart from giving only fixed compensation at two locations, the generator voltages settings are also simultaneously optimized to improve the system operation. A optimum settings obtained with MBFOA is then tested for their operational efficiency. The performance of optimized condition settings along with the STATCOM depicts further improved voltage profiles for different conditions of contingencies.

To reduce the dependency on thermal power, which leads to increased cost and environmental pollution, renewable energy sources are gaining ground. One such sources is wind power. When the penetration level of wind power increases, due to the operating constraints of power electronics based converter used in these systems, the reactive power capacity of the system gets degraded. In the subsequent chapter, wind generators are integrated in the test system to test the efficacies of wind power in providing secure operation. In that chapter some more test cases of contingencies are compared when the STATCOM is operating with wind power or without it.

VOLTAGE STABILITY STUDY OF TRANSMISSION SYSTEM WITH WIND GENERATION

5.1. Introduction

Among various sources of generation of electrical power, fossil fuel based plants share the largest percentage. However, due to combustion of fast depleting fossil fuel and the related emission of greenhouse gas, their use needs to be discouraged. Therefore, renewable energy sources are gaining ground to have larger share in the overall energy mix. Among many sources of renewable energy, there is good potential for wind energy to generate electrical power [95-98]. According to the experts, global wind energy has the potential to supply more than 20% of electricity demand of the globe. In order to meet the challenge of the ever increasing power demand, larger generation capacity expansion is required. In this scenario, wind energy conversion system (WECS) can be integrated with the electrical grid, which is primarily sustained by conventional power sources. There are numerous approaches of designing the WECS. There are different types of synchronous and induction generator based systems proposed for the power generation [99, 100]. However, as the nature of wind flow is uncertain, therefore the variable speed type of induction generator has been the preferred choice due to many advantages. Among them, double fed induction generator (DFIG) has gained more interest. The concept of DFIG is discussed in later section. It consists of a wind turbine that is connected via a gear train to the rotor shaft of the induction generator. The rotor terminals of the induction machine are connected to the four-quadrant power electronic converter capable of supplying both real and reactive powers from the grid to the rotor as well as supplying power from the rotor to the grid [101,102]. Moreover, the nature of intermittency of wind flow needs a complex and challenging task of scheduling both conventional and wind powered units in a wind integrated system. There is always a chance of erroneous estimation of available wind power during actual

operation. During the stage of under estimation, there may be actual shortfall in the overall capacity of reactive power resources in the system. This is due to the fact that the DFIG based WECS has limited capacity of reactive power [103, 104] as it depends on the limited current carrying capacity of converters which are connected to the grid. Therefore, during the operational stage of DFIG integrated system, these practical or physical constraints of the later cannot be neglected. This would give incorrect picture of voltage instability in a DFIG integrated system. Taking these factors into account, this chapter focuses on modeling of reactive power capability limits of DFIG based WECS, as some of the conventional units of the IEEE 39 bus test system are replaced with DFIG based wind farm of equivalent capacities. During the modeling of real and reactive power generations of these units, the uncertainty of wind flow is taken into consideration. For better voltage control, the presence of STATCOM at the weakest bus of the system is also modeled. The chapter is organized by beginning with the need of wind power in general proceeding gradually with its modeling concepts with regards to its real and reactive power output when DFIG based systems are integrated. Various optimization techniques are applied for the study of voltage stability [104, 105] with index analysis [106, 107]. The recent study is carried out applying MBFOA to avoid voltage instability with ENVCI.

5.2 Advantages of Wind Power

The following advantages studied for consideration of the wind system as a non conventional source of electricity for the analysis of the voltage stability.

It is one of the least-cost renewable energy tools available in modern world as shown in Figure **5.1**, costing about 0.1 to 0.14 US dollar per kilowatt-hour, depending on the wind speed availability and installation cost at a particular project site. Wind energy system pollution free unlike thermal power plants that rely on combustion of coal. Wind generators don't produce atmospheric emissions that cause acid rain or greenhouse gasses. The statistics of the wind power is shown in Figure **5.2**. The wind generation (WG) promotes the economy in rural areas, where the finest sites for wind generators are found. Farmers and ranchers can continue to work on the land, as the wind generators need a fraction of the land. Wind power plant owners make payments to the farmer for the use of the land on rent basis, supplying the landowners with extra income.
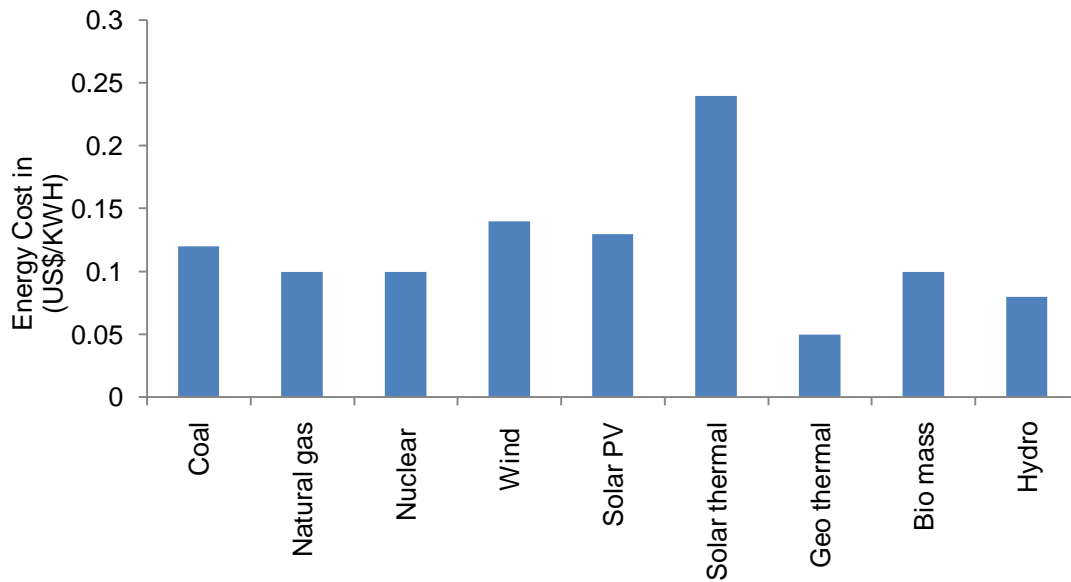
Figure 5.1. Average energy cost per KW-hour [94].
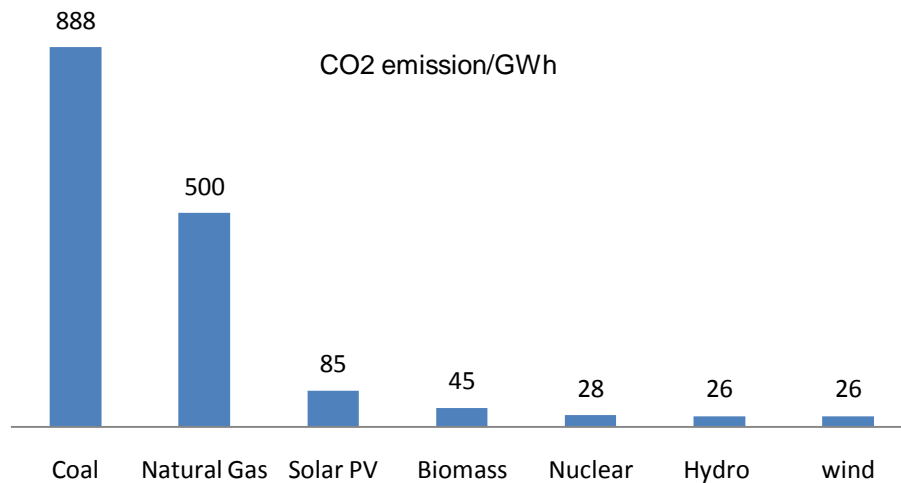
Figure 5.2. Carbon Dioxide emission per GW-Hour [94].

5.3. Generation of Wind Power

The concept of WECS is to convert the kinetic energy from the wind source to the mechanical energy through a wind turbine. Further this mechanical energy to electrical energy conversion is achieved by the generator coupled with the wind turbine. The generator converts

the mechanical energy to the electrical form. Due to intermittent nature of wind flow, the low speed shaft of the rotor blades need an arrangement of gear box to convert the speed to higher levels for the shaft of the generator. The use of multi-pole generator sometimes is a good alternative approach of a gearless system. The electrical power generated from the generator is transferred to the transmission level utilizing a transformer that steps up the voltages of the generator. Generally the voltages from the generator are typically in a hundreds of volts. The kinetic energy of the blowing air with mass m at velocity v_w is expressed as

$$E = \frac{1}{2} m v_w^{\,2} \tag{5.1}$$

The instantaneous power of the wind flowing in an area 'A' with air density ρ is expressed as

$$P_w = \frac{1}{2} \rho_a A v_w^{\,3} \tag{5.2}$$

In the view point of variable speed wind turbines, the rotor blades rotates with a speed ranging between 12 m/s to 20 m/s. The power drawn from the wind is dependent on the rotor power efficiency. As per Betz limit, the mechanical power captured by the wind turbine depends on the rotor power efficiency of the turbine and expressed as

$$P_{turb} = \frac{1}{2} C_p(\lambda) \rho_a A v_w^{\,3} \tag{5.3}$$

The rotor power efficiency of the turbine C_p is a function of the blade tip speed ratio λ and blade pitch angle β. In order to avoid the effects of *wake*, the turbines are placed at distances nearly three times of their rotor radius. When the tip speed ratio is less than 3, the wake effect reduces the maximum rotor power efficiency. The tip speed ratio can be calculated as

$$\lambda = \frac{\omega_b R}{v_w} \tag{5.4}$$

where ω_b is the rotor speed in radian/sec and R is the rotor radius from axis to tip in meter.

The variability of wind speed and therefore the power output from it is the most challenging aspect for a successful grid interconnection. Thus the accurate forecasting of wind power is an important role in the system integration of the large-scale wind farms. Wind power generation is mostly dependent on the local wind resources. Hence the wind power distribution is a seasonal as well as the environmental issue that is specific to the area. Wind forecasting has been done following different approaches based on techniques using time series, fuzzy logic, neural network etc. Each method has its own uniqueness and features and therefore gives definite degree of accuracy in the prediction result. But, the statistical data can have weak variations and changes, leading to much incorrect results. The wind forecasting programs can be broadly divided into two types, *i.e.,* physical and statistical methods. Physical processes try to model the wind farm equations according to the aero dynamical performance of wind turbines and local effects of wind speed in the real site. Statistical methods try to reproduce the behavior of the wind farm from previous data in different condition. Although various probability distribution models were proposed for the statistical analysis of documented wind speeds, the most widely used probability density function (PDF) to describe the wind speed is the Weibull functions [95] as wind speed profile at a given location follow a Weibull distribution over time. The PDF for Weibull distribution is given by

$$f_v(v) = \left(\frac{k}{c}\right)\left(\frac{k}{c}\right)^{k-1} e^{\left(-(v/c)^k\right)} \tag{5.5}$$

The Weibull distribution function with a shape factor k of 2 is also known as the Rayleigh distribution. In [98], the advantages of the Weibull distribution are noted as

i. It gives a good fit to the observed wind speed data

ii. For known shape factor k and scale factor c parameters at one height, there are methods accessible to get the equivalent parameters at another height. Normally the shape parameter ranges from 1 to 3 and the scale factor range between 5 and 25 for any wind speed characteristics.

5.3.1. Relation between wind power and the wind speed

The wind speed is assumed as a random variable and the output power of the WECS can also be characterized as a random variable during a transformation from wind speed to wind power. Generally, the power output of the wind generator will be in three ranges as below

(i) $v_o < v < v_i$. In this range the power output is zero.

(ii) $v_i < v < v_r$. In this range the power output increases linearly towards the rated power.

(iii) $v_r < v < v_o$. In this range the power output remains constant at the rated value.

where, v_o = cut out wind speed and v_i = cut in wind speed, v_r = rated wind speed. Mathematically the above ranges power output from WECS can be expressed as

$$\left. \begin{array}{l} p = 0, \quad for \quad v < v_i \quad and \quad v > v_o \\[2em] p = p_r \times \dfrac{(v - v_i)}{v_r - v_i} \quad , \quad for \ v_i \le v \le v_r \\[2em] p = p_r \quad , \quad for \ v_r \le v \le v_o \end{array} \right\} \tag{5.6}$$

5.4. Doubly Fed Induction Generator (DFIG)

The schematic layout of a DFIG is shown in Figure **5.3** consisting of a wind turbine connected by means of a gear box to the rotor shaft of the induction generator [99]. The rotor terminals of the induction machine are connected to the converter capable of receiving and supplying real and reactive power from the grid [99]. There are two converter systems namely the grid side converter (GSC) and the generator or the rotor side converter (RSC). The GSC maintains the DC link capacitor voltage. On the contrary, the RSC is assigned with the job of controlling the active and reactive power output from the machine. Each of the converters is coupled in decoupled manner by two independent controllers. In addition the DFIG also has a wind turbine control to maximize the output power from the turbine with the help of pitch angle controller thereby guiding the power output control of the RSC. The machine is connected to the

grid via a step up transformer at the GSC. If required, additional reactive power compensating unit may be connected at the point of interconnection. The DFIG is a three phase induction generator with rotor containing three phase windings, which are fed from the RSC through slip rings. The power electronic converter is able to handle power flow in both directions permitting the DFIG to work at both sub-synchronous and super synchronous speeds. The DFIG produces controlled voltage V_1 at grid frequency f_1 at the stator with the help of the GSC. However, variable voltage V_2 is provided at the rotor due to variable frequency f_2, as it is dependent on the rotor speed that is affected by the variation of angular velocity of the turbine due to a variable wind speed. Considering f_r to be the slip frequency of the rotor, it is defined as follows.

$$f_r = f_1 \pm f_2 \tag{5.7}$$

The positive sign in Equation 5.7 implies a super synchronous operation and a negative sign is meant for the sub synchronous operation. At super synchronous speed the phase sequence of the rotor currents being in the same direction to that of the stator, the rotor now supplies power to the grid along with the stator. For sub synchronous operation, power is drawn by the rotor like an induction motor. The DC link capacitor forms a common link that maintains DC bus voltage for both the converters at their interconnection. The steady state operation of the DFIG is restricted by the ratings of the RSC and GSC. The maximum power rating P_{max} of the RSC is normally 25% - 30% of the rating of the induction machine and can be expressed by the following equation

$$S_{max} = \frac{P_{max}}{P_{rated}} \tag{5 8}$$

Where, the P_{max} maximum rotor power supplied/absorbed, P_{rated} is the rated power output of the DFIG and S_{max} the maximum magnitude of slip.
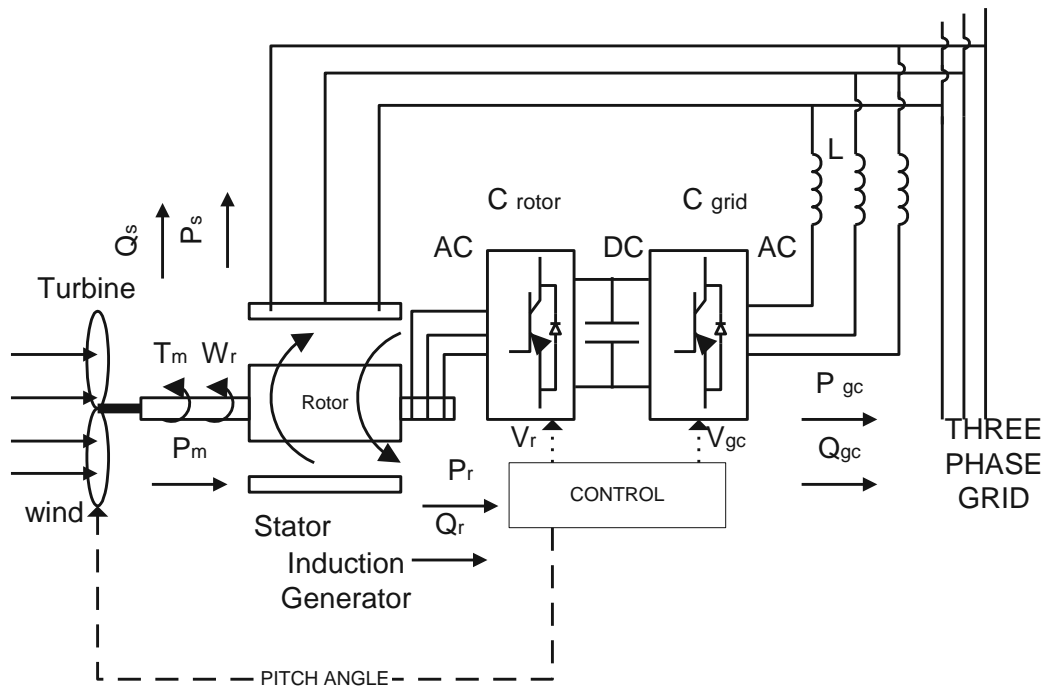
Figure 5.3. Variable-speed wind turbine with a doubly-fed induction generator (DFIG).

5.4.1. Reactive power capabilities of conventional generator and DFIG

The reactive power capability of a generation unit on the power system is crucial in the study of voltage stability. The synchronous generators have limitations in terms of maximum current and heating of the machines. The active power of the machine is restricted by the prime mover capability. The reactive current output capability is dependent on the limits of armature and field currents and the temperature. Therefore, the reactive capability of the synchronous generator depends on the machine limitations.

Similarly, the reactive power capability limit of the DFIG depends on the electromechanical characteristics of the generator and the power supplying capacity of the converters. Since the DFIG is a variable speed machine the rotor speed and the slip play an important role. The three limiting parameters for the reactive power capability of the DFIG are [98]:

a. stator current,

b. rotor current , and

c. rotor voltage.

The stator voltage is supplied from the grid, and is not affected by the design of the wind turbine. Similarly the stator current limit relies on the design of the generator, while the constraint of the rotor voltage and rotor current depend on the design of the generator and power converters. The rotor voltage varies with rotor speed and therefore the required rotor voltage is directly proportional to the slip.

Further, the effects of wind variation on the real and reactive power capability characteristics of DFIG systems must be analysed [100]. The GSC is based on power electronics switches which operate with voltage and current limits. Therefore, the generator real and reactive power capacities are also constrained by these limits. During the under estimation of wind power, the available power is more than the estimated value of real power output. This results in reduction of reactive power generating capacity of DFIG system. Modeling the DFIG system in *d-q* reference frame, the instantaneous values of real and reactive powers output from the system is expressed in terms of stator, rotor voltages and currents. These quantities may be represented as follows:

$$v_{ds} = -R_s i_{ds} + \omega_s [(L_s + L_m)i_{qs} + L_m i_{qr}] \tag{5.9}$$

$$v_{qs} = -R_s i_{qs} - \omega_s [(L_s + L_m)i_{ds} + L_m i_{dr}] \tag{5.10}$$

$$v_{dr} = -R_r i_{dr} + s\omega_s [(L_s + L_m)i_{qr} + L_m i_{qs}] \tag{5.11}$$

$$v_{qr} = -R_r i_{dr} - s\omega_s [(L_r + L_m)i_{dr} + L_m i_{ds}] \tag{5.12}$$

$$P = P_s + P_r = v_{ds} i_{ds} + v_{qs} i_{qs} + v_{dr} i_{dr} + v_{qr} i_{qr} \tag{5.13}$$

$$Q = Q_s + Q_r = v_{qs} i_{ds} - v_{ds} i_{qs} + v_{qr} i_{dr} - v_{dr} i_{qr} \tag{5.14}$$

In the above expressions subscript r and s represent the rotor and stator side quantities respectively. Similarly, the subscripts d and q represent the direct and quadrature axis components respectively. Where, ω_s is the synchronous speed, R_s, is the stator resistance, L_s is self inductance, R_r, denotes the rotor resistance, L_r denotes the self inductance and L_m represents the magnetizing inductance of the DFIG system. The value of v_{qs} is made equal to the stator terminal voltage, by assuming the d-axis aligning with the axis of maximum stator flux. R_s is neglected in the study. The rotor current can be expressed as

$$I_r = \sqrt{i_{dr}{}^2 + i_{qr}{}^2} \qquad (5.15)$$

The reactive power required by the stator (Q_s) is delivered by the GSC, and therefore, the lower and upper bounds of reactive power generating capacity limits of GSC puts constraints on the capability of DFIG system to supply Q_s. As the converters are based on power electronics switches, therefore a stator current limit is also imposed. To determine the maximum and minimum limits of Q_s the following approach is adopted. As the q axis is aligned with the grid voltage vector, it makes the v_{ds} equals to zero and therefore, v_{qs} equals to v_s. Substituting these values in Equations 5.13 and 5.14 respectively, the values of P_s and Q_s may be expressed as

$$P_s = v_{qs} i_{qs} \qquad (5.16)$$

$$Q_s = v_{qs} i_{ds} \qquad (5.17)$$

From the Equation 5.17, it can be observed that as Q_s is dependent on direct axis component i_{ds} alone, therefore the limits depend on the limits of i_{ds}. Keeping v_{qs} at 1 $p.u.$, the range of Q_s between sub-synchronous and super-synchronous conditions can be expressed as follows, considering the sign of i_{qs}

$$\sqrt{I_{s_{max}}{}^2 - (i_{qs})^2} \leq Q_s \leq \sqrt{I_{s_{max}}{}^2 + (i_{qs})^2} \qquad (5.18)$$

where $I_{s_{max}}$ is the maximum limit of i_s. Moreover, obtaining i_{ds} from Equation 5.10 and replacing in Equation 5.17, the expression of reactive power exchanged with the grid at the stator terminal is represented as follows

$$Q_s = -\frac{v_{qs}^2}{\omega_s[(L_s + L_m)]} - \frac{L_m v_{qs} i_{dr}}{L_s + L_m} \tag{5.19}$$

In the above equation the first and second terms represent the magnetization of the stator and the net reactive power exchanged with the grid. As v_{qs} is maintained at 1 *p.u*, the Q_s is controlled by i_{dr} alone. Substituting Equation 5.16 in Equation 5.9, the i_q is expressed as

$$i_{qr} = -\frac{P_s(L_s + L_m)}{L_m v_{qs}} \tag{5.20}$$

Represented by the maximum limit of i_r as $i_{r_{max}}$, thus i_{dr} may be expressed as

$$i_{dr} = \sqrt{i_{r_{max}}^2 - i_{qr}^2} \tag{5.21}$$

Finally, substituting the values of i_{dr}, and i_{qr} from Equations 5.20 and 5.21 in Equation 5.19, the upper and lower limits of Q_s can be expressed in terms of $i_{r_{max}}$ as

$$Q_s \geq -\frac{v_s^2}{\omega_s[(L_s + L_m)]} - \frac{L_m v_s}{(L_s + L_m)}\sqrt{i_{r_{max}}^2 - \left[\frac{P_s(L_s + L_m)}{L_m v_s}\right]^2} \tag{5.22}$$

$$Q_s \leq -\frac{v_s^2}{\omega_s[(L_s + L_m)]} + \frac{L_m v_s}{(L_s + L_m)}\sqrt{i_{r_{max}}^2 - \left[\frac{P_s(L_s + L_m)}{L_m v_s}\right]^2} \tag{5.23}$$

5.5. Test System

IEEE-39 bus system is considered with the modification as shown in Figure **5.4**. A STATCOM is used at the bus number 20 has already been discussed in Chapter 4. In addition to this an equivalent wind farm is considered to be located at bus number 30 replacing the conventional generator No.10 at the same location. The real power rating of the same is kept as that given in the data sheet, that is 2.5 *p.u*. at 100 MVA base. Keeping all the system data unaltered, the simulation is carried out. The problem is formulated in the next section.
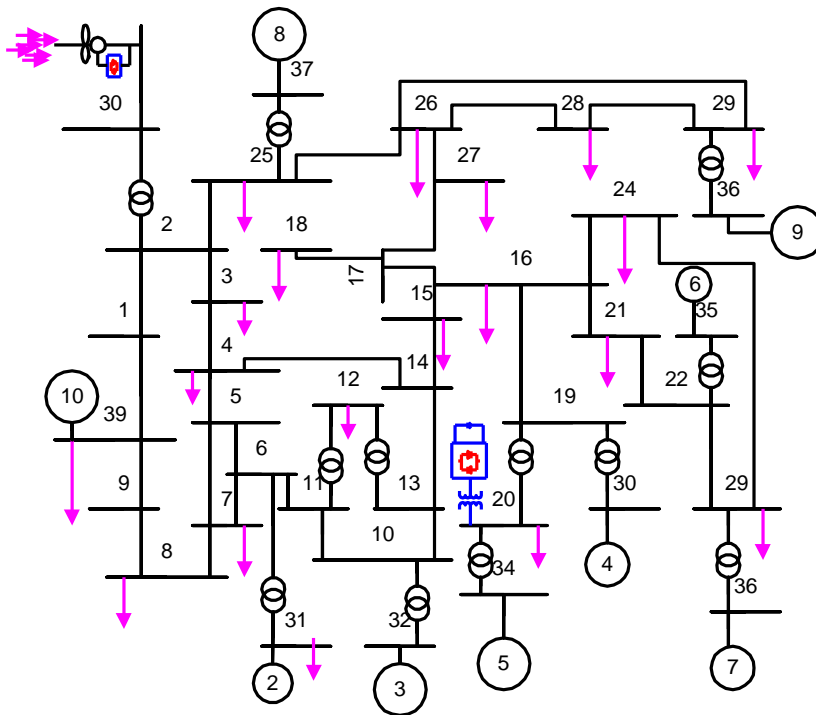
Figure 5.4. Schematic diagram of IEEE-39 bus test system with STATCOM and WG

5.6. Problem Formulation

When dealing with wind power, a very important factor to be taken into account is the system damping. When there are too many wind firms other conventional coal fired plants have to be reduced as such the overall damping of the system reduces, this causes serious problems in many power systems worldwide. To avoid such issue of damping, specific assumptions made for the WG as follows. The damping of the system improves as the inherent short-term storage that exists within the mechanical linkage includes the blade aero elasticity, the kinetic energy in and out of the rotating mass (shaft, gearbox, generator, blades), and potential energy within the shaft and gearbox stiffness. Short-term storage also includes the inherent damping in the blade-air interaction, the gear-to-gear in the oil bath of the gearbox, the windage from the air-cooled generator, and/or liquid friction losses in the water- or oil-cooled generator. All of these actually

provide some kind of buffer to smooth out the energy spikes presented to the turbines by the presence of turbulence or other sources. The problem is formulated with the same objective subjected to the same operating constraints as considered in the previous chapter. The subsequent section details the simulation and results along with their brief methodologies.

5.7. Simulation Results and Discussion

As discussed earlier, the 10th generator at bus number 30 in the test system is replaced by equivalent sized DFIG based wind farm. The system is subjected to same patterns of load increase at the five weak buses as done previously. Before proceeding for optimization, a test solution is obtained to verify the accuracy of modeling of the DFIG based wind farm at the 30th bus of the system. Three different load flows are carried out for the operating conditions of nominal, 30 % and 40% load increases at the 20th bus.
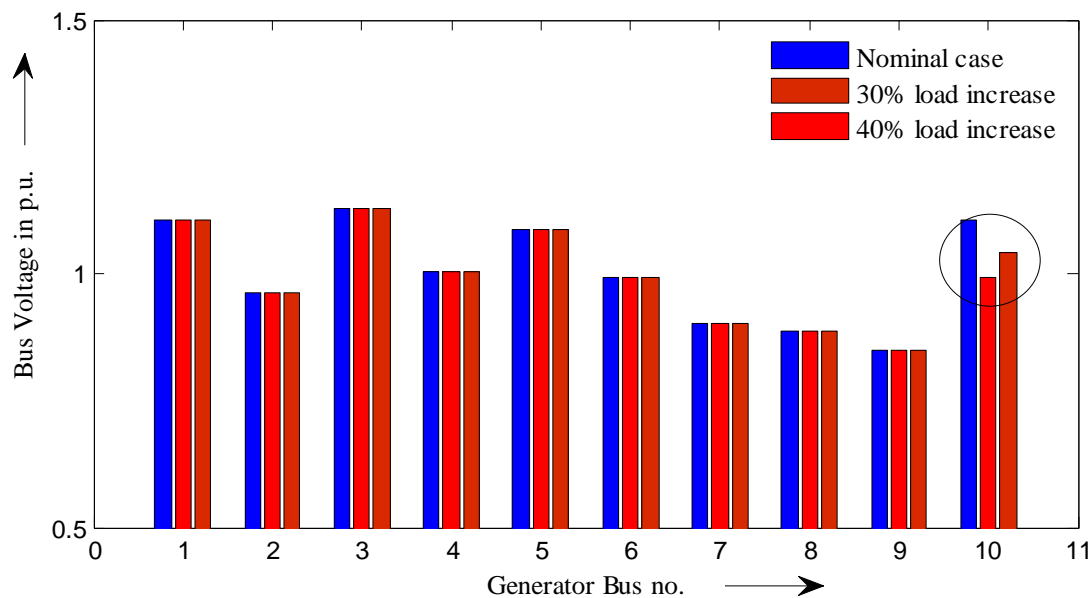
Figure 5.5. Voltage profiles of wind generator with load increase at the bus no 10.

As depicted in Figure **5.5**, the results of the ten generator bus voltage obtained after the power flow solutions done at the above three conditions gave same values, except in the DFIG. This was expected, as due to the reactive power supplied by DFIG iteratively corrects itself within the newer limits of Q_s, found after every iteration of NRLF. The process continues in every iteration

of load flow, till the later converges. After confirming the accuracy of the procedure to model the reactive power constraints of DFIG, the MBFOA algorithm is applied to optimize the generator bus voltages and the location and amount of compensations. The convergence characteristic is shown in Figure **5.6**. The result of the optimized variables is shown in the Table **5.1**.
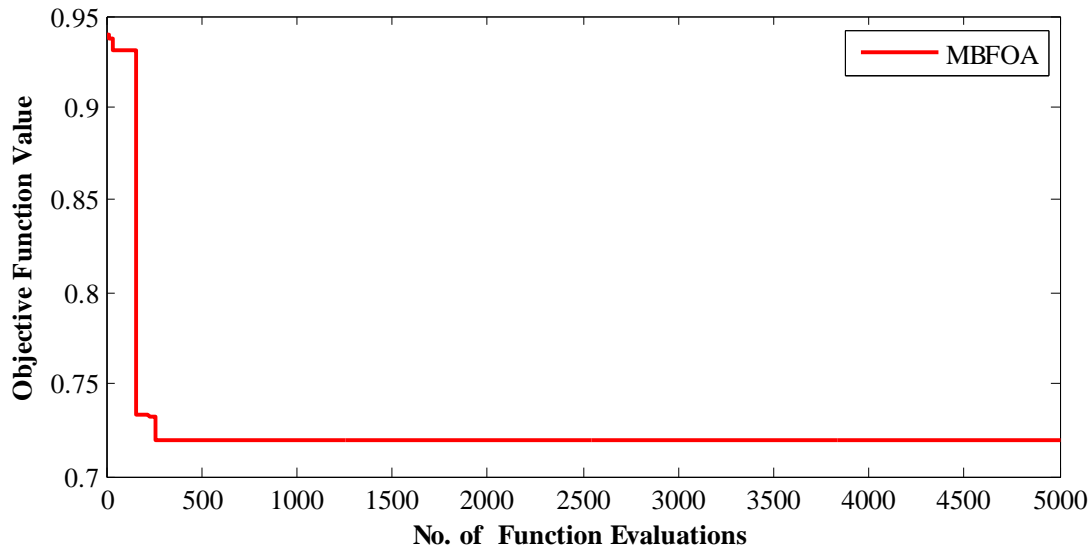
Figure 5.6. Convergence characteristic.

Table 5.1. Compensation for load increase in the system with WG and STATCOM.

Compensation Specifications	Constant Q-Load
1st location of compensation	Bus no 21
1st amount of compensation	57.87%
2nd location of compensation	Bus No.25
2nd amount of compensation	12.37%

Moreover, the PV Curves obtained at all the 5 weak buses, after setting the optimized operating values of generator voltages and compensation are shown in Figures **5.7-5.11**. The corresponding variation of ENVCI values with load increase is also depicted in Figure **5.12**. It can be seen that in this condition also the chosen index has proven its accuracy as it has given the same result as PV curves. Both from the PV-curves and ENVCI, it can be seen that, when DFIGs are operating in the system VSL of the system is getting reduced compared to STATCOM

operating in a conventional generator environment. Therefore, due to the limiting constraints of reactive power capability of DFIG, the system VSL is getting compromised.
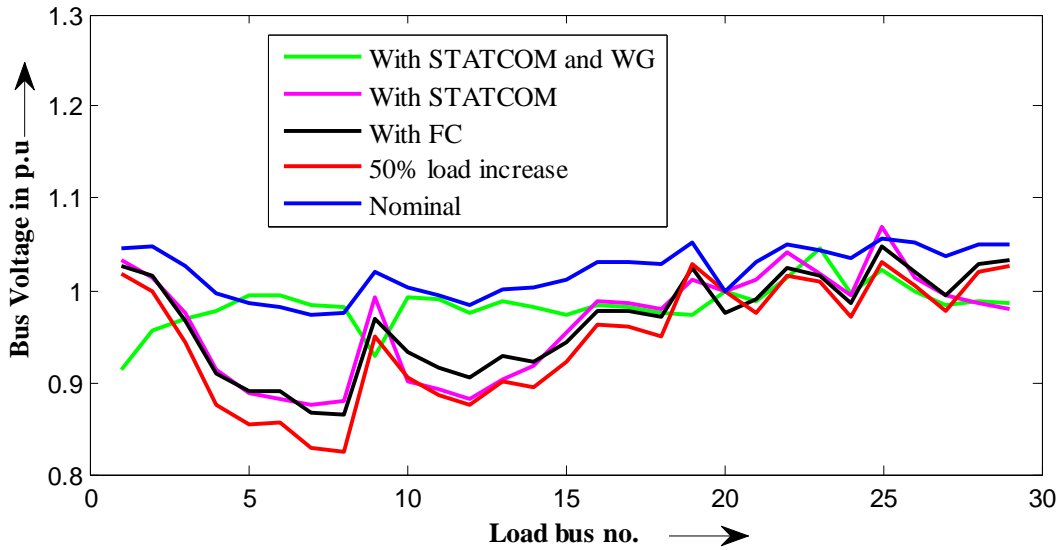
Figure 5.7. System load bus profile for 50% load increase in bus 8.
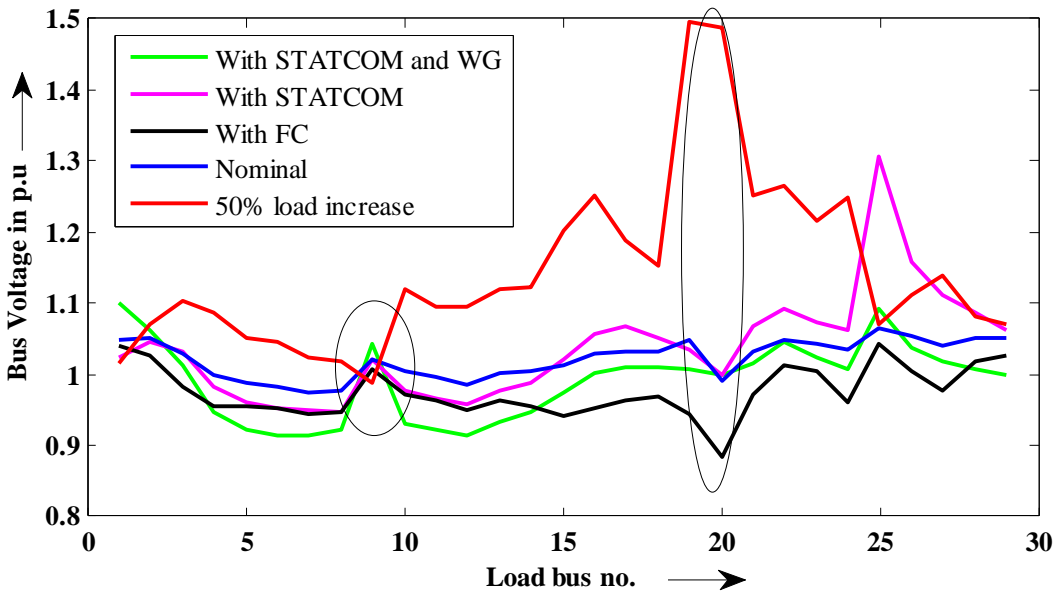
Figure 5.8. System load bus profile for 50% load increase in bus 20.
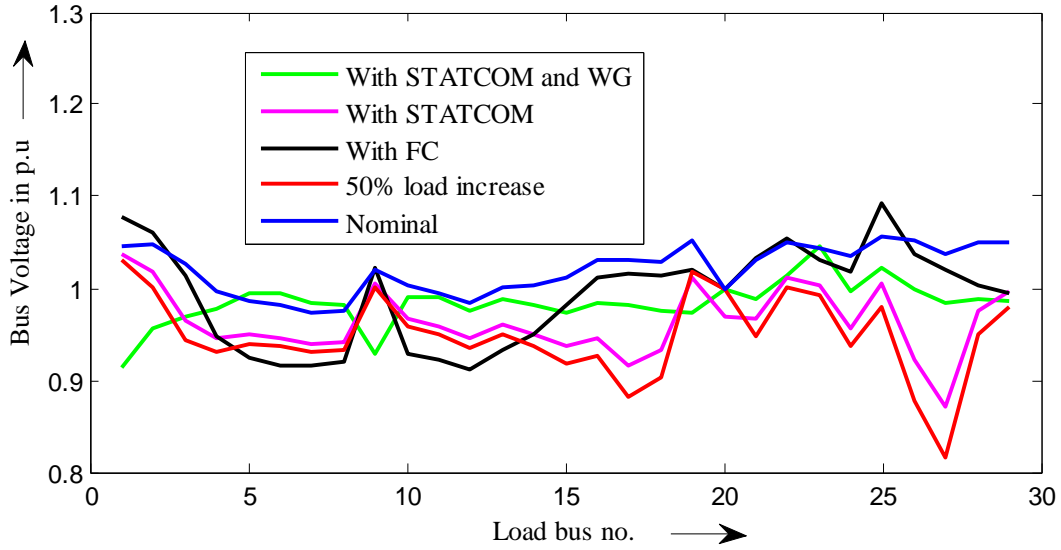
Figure 5.9. System load bus profile for 50% load increase in bus 27.
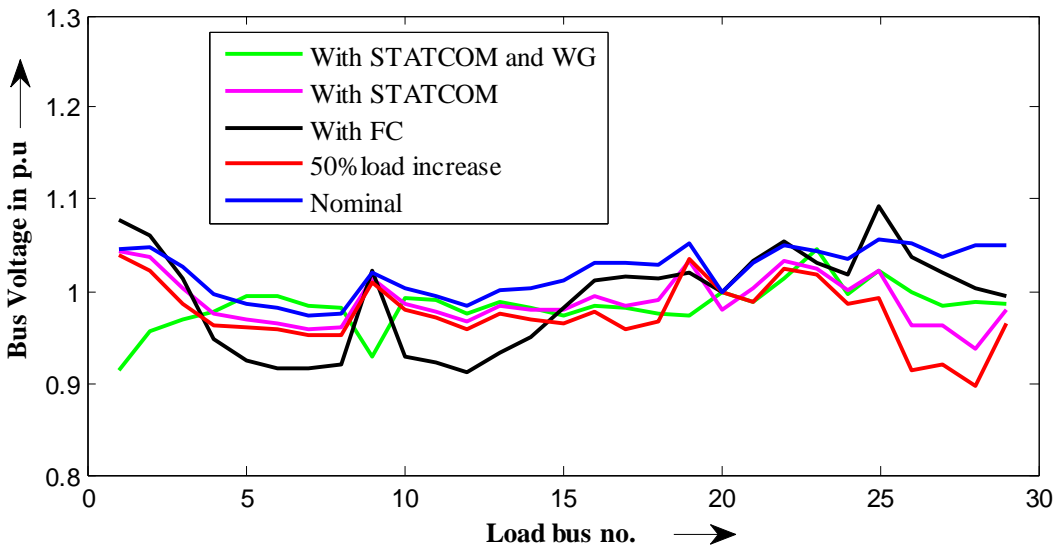
Figure 5.10. System load bus profile for 50% load increase in bus 28.
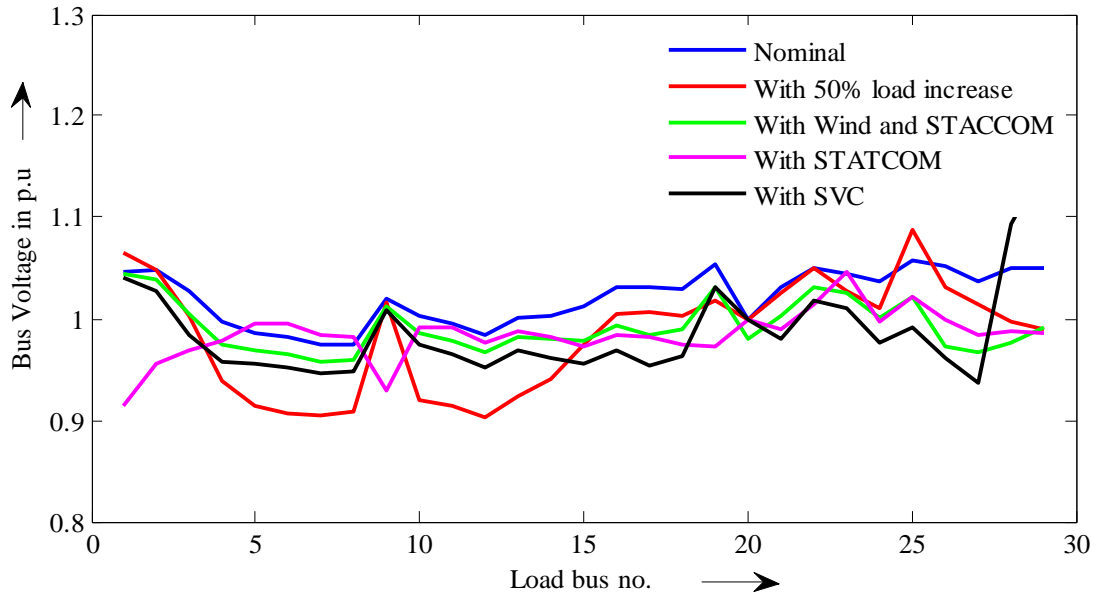
Figure 5.11. System load bus profile for 50% load increase in bus 29.
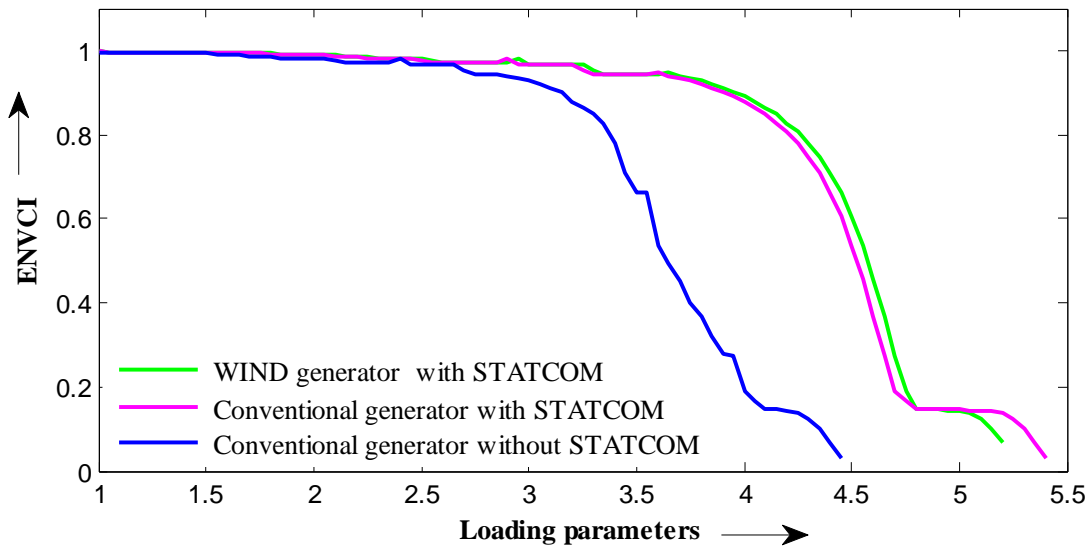
Figure 5.12. ENVCI- loading limit parameter curve for bus no 20 with MBFOA.

The profile of voltages for load increase cases at different locations, *i.e.*, a line outage with increased load at a particular bus. In all the cases of load increases at different weak buses, the profile of the condition of STATCOM and fixed compensation (obtained in Chapter 4) has given the best voltages. However, when the conventional generator is replaced by the wind generators, the constraints of reactive power have degraded the system voltages at some

locations. For the load increase in the bus number 8 when STATCOM was present only without the wind generator, the system voltages of all the bus numbers above 20 (*i.e.*, 20 to 29) have given better voltages, but between bus no 1 to 19 all the bus voltages have degraded. However, when the wind generator is connected then the overall bus voltages have remained more close to the nominal condition of loading compared to all other cases.

For the case of load increase at the 20th bus, the only STATCOM operation, the bus voltage of the 25th bus has increased to very high value as shown in Figure **5.8**. In this case without compensation, the bus voltage of the 20th bus has hit its limit showing instability. Analyzing all the conditions of load increase two distinct patterns are observed.

i)   The voltages of bus number 20 and 8 have not deteriorated by large amount when the STATCOM is in operation.

ii)   Even though the system loadability limit, obtained with STATCOM in the environment of conventional generators alone has given the best result, the connection of DFIG based WECS at the 30th bus operating with STATCOM has provided bus voltages closer to the nominal condition of loading.

After three arbitrary conditions of line outages along with load increase are simulated to verify the performance of different schemes of compensation and generator systems. They are as follows:

i)   *Case 1*:   With the optimized settings of bus voltages and compensation amounts and locations, different scheme voltage profiles are tested when the load at bus number 4 is increased by 50% along with a simultaneous line outage of line number 2-3. With this contingency, the wind generator system operating with STATCOM has given a degraded performance of voltages compared to the case when only STATCOM was connected in the conventional test system. The profile is shown in Figure **5.13.**
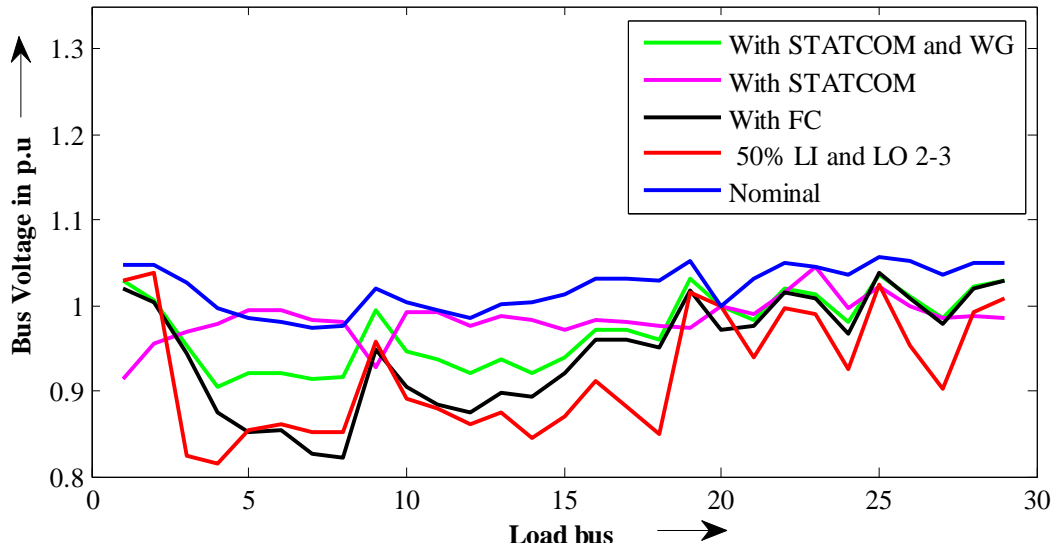
Figure 5.13. System load bus profiles for 50% load increase in bus 4 with line outage 2-3.
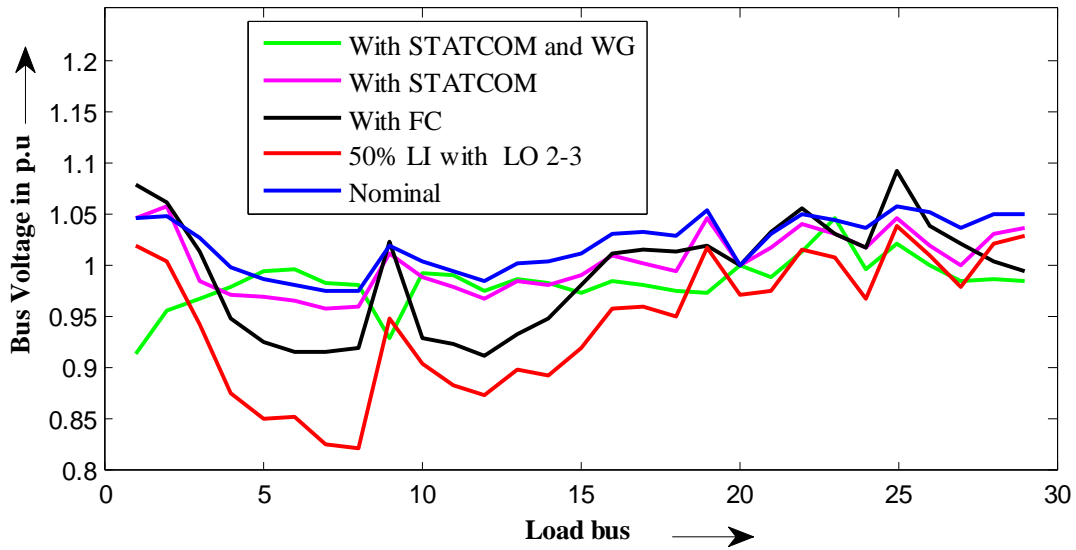
Figure 5.14. System load bus profiles for 50% load increase in bus 23 with line outage 2-3.
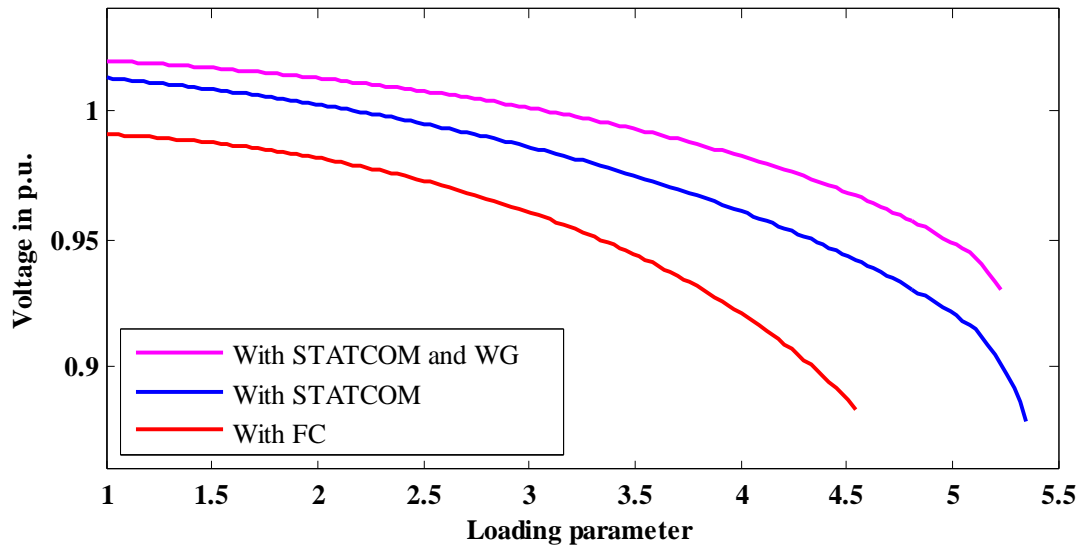
Figure 5. 15. Loading limit of bus no 8.
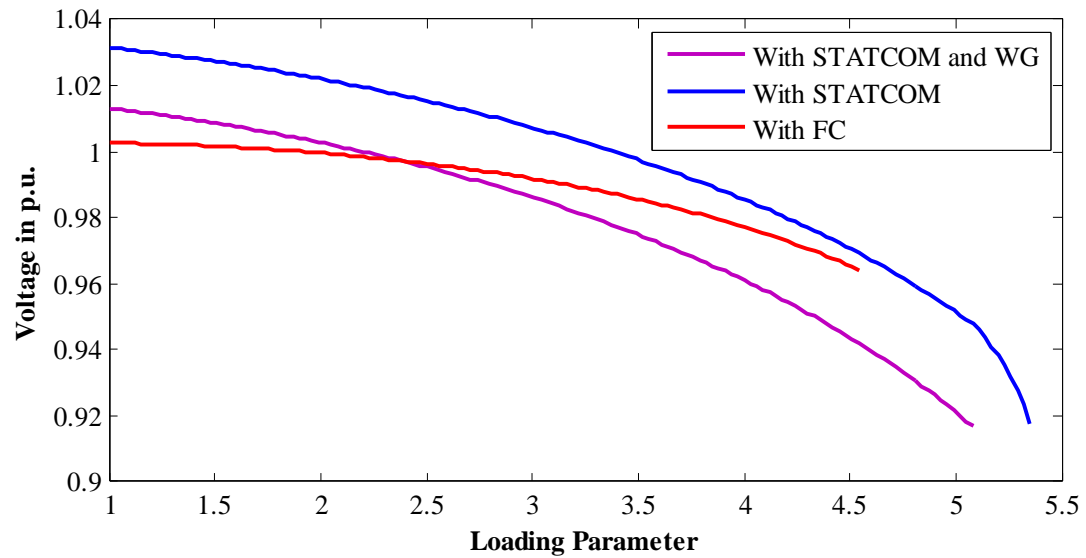
Figure 5. 16. Loading limit of bus no 20.
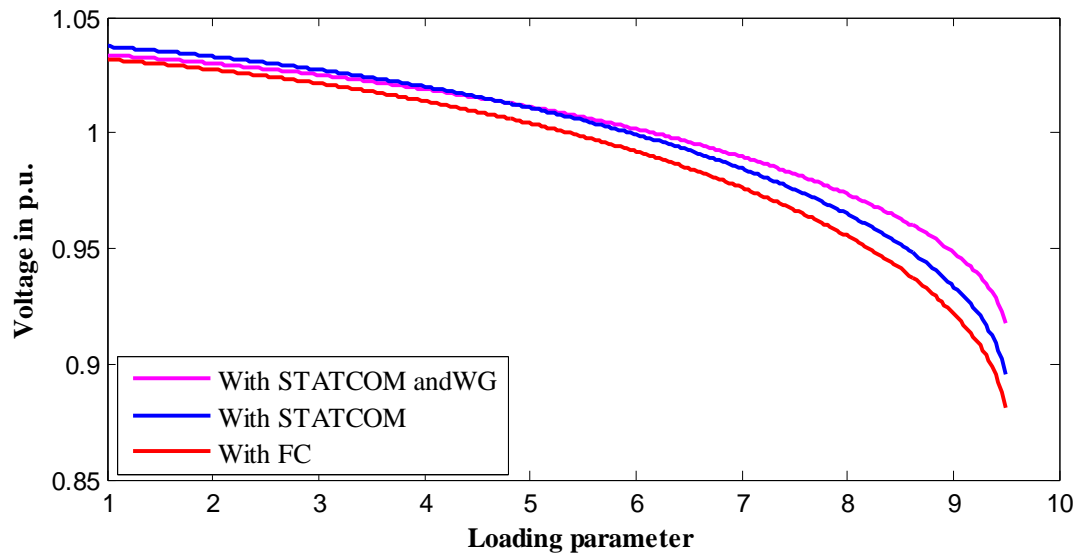
Figure 5. 17. Loading limit of bus no 27.

ii)   *Case 2*:   Finally, the line number 2-3 is removed to simulate an outage condition, when the load at the bus number 23 is raised by 50% from the nominal value. The pattern of voltage profile is similar to the one obtained in Case 1, where after connection of the DFIG, the system voltages have degraded marginally at some buses compared to STATCOM alone as depicted in Figure **5.14**.

Observing the results obtained for the condition of line outage along with load increase, the following points can be concluded.

i)   The performance of DFIG in terms of maintaining system voltages has degraded when the level of stress in the system is increased, even with the presence of STATCOM.

ii)   The fixed compensation scheme, has given the worst system voltages compared to the other two schemes of compensation. This is not only because of the presence of STATCOM, but also due to the fact that the generator bus voltages are optimized for improving the system voltages.
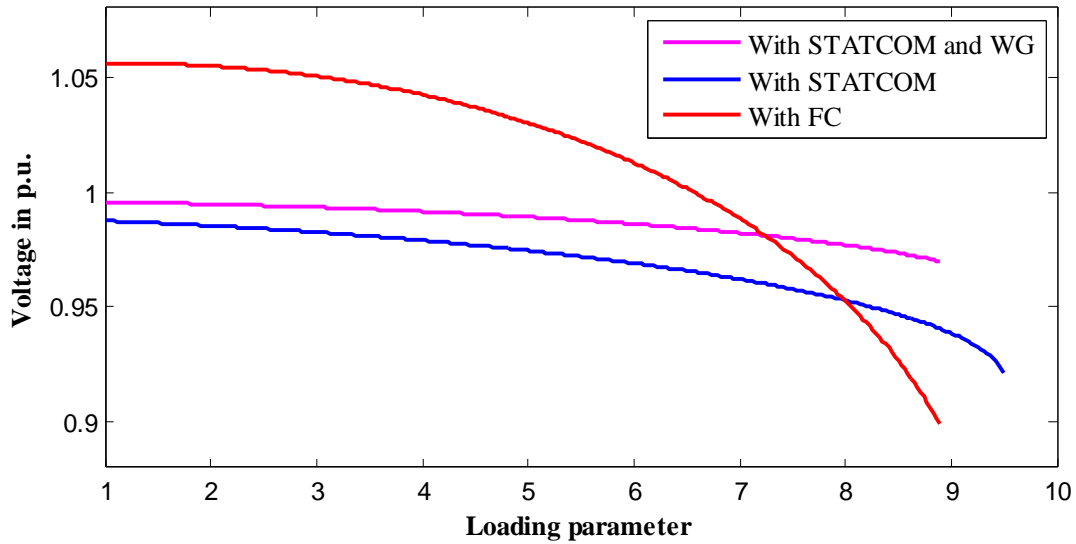
Figure 5. 18. Loading limit of bus no 28.

The loadability of bus no 8 is shown in the Figure **5.15** justifying the combinational performance of wind and STATCOM to be more effective than the FC and STATCOM respectively. The same is seen in the load buses namely 20, 27, 28, and 29 in the respective Figures **5.16 to 5.19**.
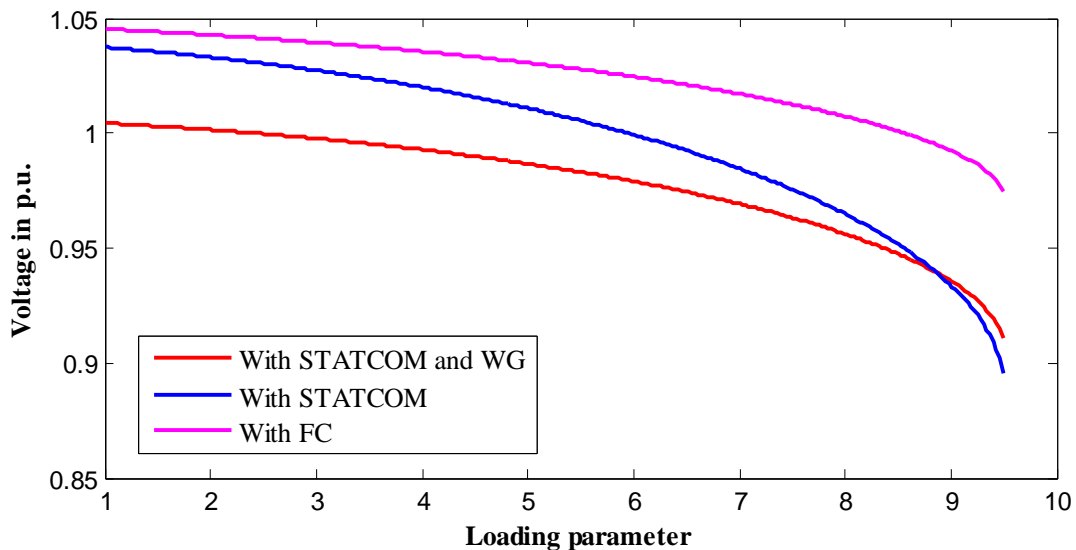
Figure 5. 19. Loading limit of bus no 29.

5.8. Conclusions

To reduce the dependency on fossil fuel based conventional generation system which pollutes the environment quite significantly; the renewable energy sources are increasing their percentage share in the overall generating capacities in modern power system. The abundance of wind power has come out as a potential candidate in this field. This study limits itself to the augmentation of DFIG based WECS in to a test system, replacing one of the conventional generator with it. A STATCOM is assumed to be present at the weakest bus as before. During the modeling the reactive power limits of the grid side converter is taken into consideration. Therefore, the solution is expected to get constrained even further in terms of getting a better VSL compared to the case as shown in Chapter 4, when the STATCOM was operating within the constraints of conventional system and generators. Optimizing the generator voltages and transformer taps after formulating the same objective function as done previously, it was found that the MBFOA converges to the final solution quickly. From the P-V curves, it is seen that the VSL of the system even though better than the fixed compensation scheme discussed in Chapter 2, has degraded marginally with respect to the VSL obtained in conventional generator environment as elaborated in Chapter 4. The overall bus voltage profiles obtained for line outage of different line with the condition of load increase at different buses also depict the same pattern. The values of ENVCI under the optimized condition of load increase have followed the patterns obtained with P-V curves. Therefore, it can be said that with realistic modeling of DFIG based WECS in the system, the gain in terms of environment and generation cost is getting somewhat compromised interims of voltage profiles in the system.

With the ever changing policies of real power generation with newer conventional and renewable sources getting augmented, the amount and numbers of available controls in the system are also increasing day by day. By doing a simple optimization of controls within the framework of an OPF may not be sufficient to meet the changing reactive power management of the system to maintain healthy voltages. Therefore, corrective control acting in the system operating from a base of optimized settings of controls may be a good solution in this regard. The subsequent chapter looks into the aspect of designing an intelligent Artificial Neural Network (ANN) based centralized controller that would take some corrective control decision to maintain system voltages during contingent conditions of the system.

APPLICATION OF PROBABILISTIC NEURAL NETWORK FOR VOLTAGE STABILITY ENHANCEMENT IN POWER SYSTEM BASED ON STABILITY INDEX

6.1. Introduction

Modern power systems operate under stressed condition, due to ever increasing demand of load and limited scope of generation and transmission system capacity expansion. Therefore, the task of maintaining the operating system bus voltages within their specified limits has become challenging with limited availability of active and reactive power resources [105]. Moreover, improper coordination between continuous as well as discrete controls has also led to voltage deteriorations [12]. Research works show that the main reasons behind voltage instability are insufficient supply of reactive power and their improper planning and location [72]. Previous chapters have highlighted the need of sensitivity analysis [106, 107] based on different stability indices and the use of optimization techniques [108, 109] for static voltage security improvement. In order to include the effect of external system on the voltage stability analysis of the system, the recently proposed ENVCI [41] has been utilized as a criterion to determine the stability limit. The simplicity and faster computation of this index, has encouraged this study to consider its use.

The benefit of utilization of FACTs devices have also been demonstrated, as the voltage stability margin of power system has improved. The finding further reinforces the outcomes of earlier reported works [110-112]. However, it may not be sufficient to optimally allocate the reactive power resources using conventional or intelligent technique based optimization methods. During the process of optimization, a limited range system operating conditions are taken into consideration expecting the optimum allocation of control settings which would show some robustness during the operational stage of the system. After optimization, the system operating performance is tested for some new operating scenarios. To make the system more robust and adaptive to the changes in the operating conditions the Artificial Neural Network (ANN) and Fuzzy Logic may be beneficial, as they sometimes depict good adaptability to system variations. Moreover, some other studies [113, 114] have also

proposed the use of the theory of fuzzy logic and ANN based remedial control actions that would restore the system from regions of instability. Among various categories and structures of ANN, the Probabilistic Neural Network (PNN) has been a better alternative for problems related to classification [115], and it has been applied in some power system problems [116, 117]. This work proposes to apply PNN, in order to design a suitable discrete corrective control classifier, which shall henceforth be termed as the Voltage Stability Enhancing Neural Network (VSENN). The VSENN would suggest the most suitable control action among several classes of specific control actions, so that a possible unstable condition may be avoided in the system. After suitable training of the VSENN in the test power system considered in this work, the verification of the same is carried out with varieties of stressed simulated conditions.

6.2. Improvement of Power System Voltage Stability under Steady State Condition

The steady state control settings of many available reactive power resources could be optimized to achieve better operating bus voltages throughout the system. Some examples of these variables are as follows

a) Real and reactive power available in the generators
b) Generator P-V bus voltage or AVR settings of generators
c) Values of tap settings of transformers
d) Shunt static capacitive compensation settings
e) Selective percentage of load shedding

Optimal allocation of some of these control settings could achieve better reactive power reserve making the system more efficient to deliver load before it reaches its steady state loadability limit. Further, mere optimization of these variables may not guarantee a stable system operation even after a contingency condition, when the system is already operating very near to the notch point of the P-V Curve. Therefore, during the operational stage, some additional corrective control may be required to operate the system in a secured manner. A properly chosen corrective control action improves the voltage stability margin of the system by an amount ΔP_m compared to the case when no corrective action is undertaken. This is shown in Figure **6.1.**
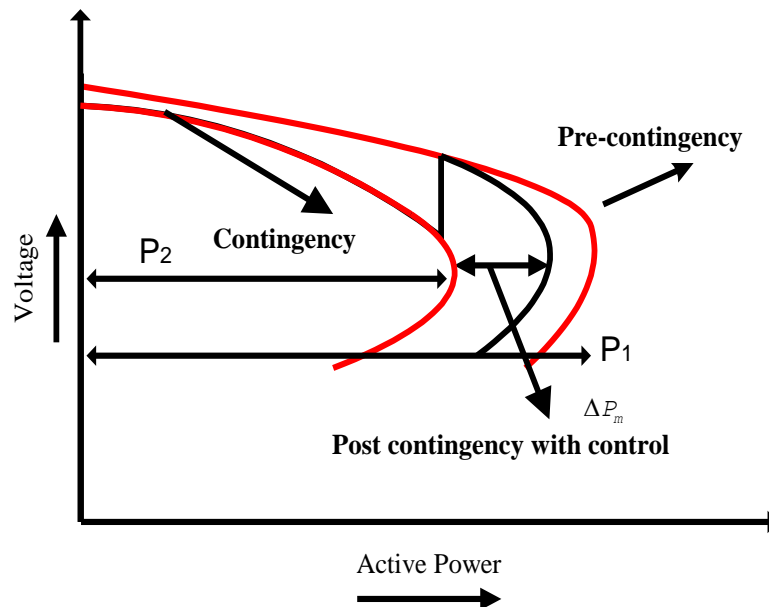
Fig.6.1. Pre-contingency, contingency, and post contingency PV curves.

Here, ΔP_m is increase in the VSM due to the corrective action. The above concept has been the main motivating factor behind the design of a centralized PNN based controller that would improve the system over all stability during the operational stage.

6.3. Enhancement of Voltage Security using PNN Classifier

The primary objective of this work is to design a PNN based classifier, which could identify the most suitable corrective control action necessary to make the system secure even after contingencies or sudden load increase.

The ENVCI is utilized to quantify the extent of voltage instability in the system. The sequence of events adopted to design the planned controller is mentioned as follows:

i) At the outset the set of discrete probable control actions are identified from different types of available settings of reactive power resource similar to the ones mentioned in section 6.2.

ii) In order to simulate stressed operating conditions, at selected weak buses the load is increased gradually in steps with the help of load parameter (λ).

iii) The PNN classifier is trained at these stressed operating conditions. Line outage contingencies are created as individual cases to disturb the system even further to make the system voltage unstable. The most sensitive control action that would stabilize the system was identified at this stage. The information mentioned above for different contingencies is utilized for the training of the classifier.

iv) The trained PNN classifier is tested for some new disturbance for which it was not trained.

6.4. Probabilistic Neural Network: A Brief Overview

The PNN model is one among the supervised learning networks and has the following features distinct from those of other networks in the learning processes [117].

- It is implemented using the probabilistic model, such as Bayesian classifiers.
- A PNN is guaranteed to converge to a Bayesian classifier provided that it is given enough training data.
- No learning processes are required.
- No need to set the initial weights of the network.
- No relationship between learning processes and recalling processes.
- The difference between the inference vector and the target vector are not used to modify the weights of the network.

The PNN approach offers major advantages such as rapid training, easy to add or delete data from training set without lengthy retraining process. The PNN is a category of artificial neural network, which is a structured set of interconnected nonlinear processing elements called neurons. Each connection of the ANN has an associated weight. It can accurately obtain the desired relationship between the input and output data sets, by updating a set of initialized values of weights used between the neurons. The ANN can be efficiently trained with the help of various types of learning processes to achieve the input- output nonlinear mapping. The PNN is a class of radial basis function (RBF) neural network proposed by Specht [115], which follows supervised learning. The other specific benefit PNN models have over SVMs is that their size is fixed. They are parametric models, while SVMs are non-parametric. That is, in an ANN you have a bunch of hidden layers with

sizes h_1 through h_n depending on the number of features, plus bias parameters, and those make up your model. By contrast, an SVM (at least a kernelized one) consists of a set of support vectors, selected from the training set, with a weight for each. In the worst case, the number of support vectors is exactly the number of training samples (though that mainly occurs with small training sets or in degenerate cases) and in general its model size scales linearly. In natural language processing, SVM classifiers with tens of thousands of support vectors, each having hundreds of thousands of features. Also, online training of FF nets is very simple compared to online SVM fitting, and predicting can be quite a bit faster. But for online training of kernel SVMs, specialized algorithms needed.

As depicted in Figure **6.2**, the PNN structure consists of a radial basis layer and a competitive layer. Each set of input-output data are trained and classified by evaluating their distribution values of a probability density function (PDF) as defined in the Equation 6.1 below. The input layer consists of S nodes to accept input feature vector (I). As mentioned in the same, the hth element of the hidden mid layer Hd_h can be evaluated by evaluating the Euclidian distance between the ith input feature I_i and the initialized weight (W_{ih}) connecting I_i to Hd_h.
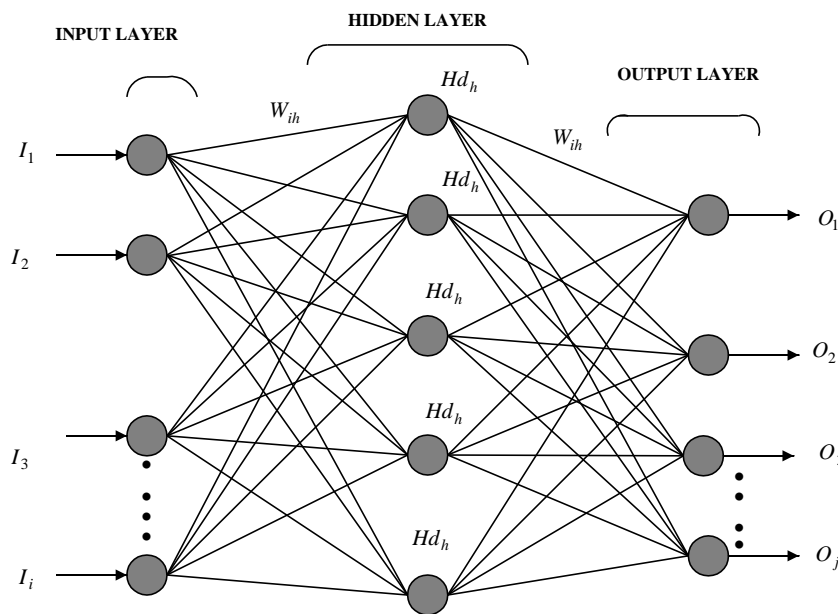
Figure 6.2. PNN Architecture.

$$Hd_h = \exp\left(-\frac{\|W_{ih} - I\|b^2}{\sigma^2}\right) \tag{6.1}$$

where $\|W_{ih} - I\| = \sum_{i=1}^{N_i}(I_i - W_{ih})^2$. Assuming there are N_i numbers of input features in I, b is known as the *bias* which helps adjust the sensitivity of radial basis neuron, and σ is the spread

factor. Similarly, with the help of weights W_{hj} existing between the hth element of the hidden layer and j^{th} element of output layer O_j , the output layer elements can be determined as shown in Equation 6.2.

$$O_j = \frac{1}{N_j} \sum_{j=1}^{N_J} W_{hj} Hd_h \qquad\qquad (6.2)$$

Among other networks for the purpose of classification, PNN offers rapid training with easier data handling. Moreover since the training of algorithm is not iterative in nature, PNN has good potential to classify very fast when more training sets are available. It has the following key features making it a good choice for problems of classification.

i) The implementation of PNN is based on probabilistic model of Bayesian classifiers.

ii) None of the weights requires the process of initialization in the network.

iii) The convergence rate of the Bayesian classifier in PNN is almost certain with sufficient numbers of training data sets.

iv) The learning and recalling processes are independent of each other.

v) The weight modification is not based on the difference between the inference and target vectors.

The next section discusses the detail methodology undertaken for designing the PNN classifier based controller.

6.5. Basic Approach for Designing the PNN Control Classifier: VSENN

The design approach of the VSENN, adopted for successful classification and decision making through PNN are discussed with the following steps.

1. The real powers at some pre-identified weak load buses are increased up to the notch point of the system at the outset. At each point of the PV-curve, the ENVCI values are evaluated so that the steady state stability limit can be checked.

2. Further load increase is stopped near the loadability limiting value and the system is subjected to different contingencies separately. At the limiting points, contingency

conditions are simulated either in the form of another set of load increase or in the form of line outages at different locations.

3. For each of the above disturbances, sensitivities of the change in the value of ENVCI [41] with respect to the corresponding changes in some available control variables are evaluated. These control variables are either increased or decreased from their respective nominal values one by one. For every change in the control action, the corresponding increase or decrease in the values of ENVCI is obtained. Through sensitivity ranking, the most sensitive and effective control action is then determined. For any particular operating condition, the line flows of selected lines and voltage magnitudes of several buses are utilized as the set of input data for the training of VSENN. Similarly, the most sensitive control action which improves (increases) the value of ENVCI is utilized as the output data in the training.

4. It is to be noted that selected numbers of bus voltage and line flow magnitudes totalling N_i numbers of data constitute the input data feature vector I_S for the Sth operating condition. Further, the most sensitive (the highest entry in the sensitivity matrix Ω_S for the Sth operating condition) control action among many available controls, becomes the single dimensional output vector O_S.

5. The VSENN is then trained with the help of large number of input and output data sets, using MATLAB software.

6. After training of the VSENN, it is tested for its ability to take a corrective control action in the event of any other contingency that is not used for the purpose of training. Wide ranges of new contingency cases are simulated and the most sensitive control action was applied, to verify the efficacy of VSENN.

   A flow chart depicting details of training and testing is illustrated in Figure **6.3**. Total of 63 numbers of control variables are considered for taking the control decision. Briefly they are described below.

   i) Values of real power generation of all the 10 generators.
   ii) P-V bus voltage setting of all the 10 generators through their AVR.

iii) Either increase or decrease in tap settings of 12 transformers (12 increased taps + 12 decreased taps = 24)

iv) Real power load shedding in 19 numbers of load buses in the system.

The most sensitive control decision among the 63 (10 + 10 + 24 + 19) number of available discrete control actions as considered above from (i) to (iv), that is the best one and increases the ENVCI value at the Sth operating condition with a particular contingency, is required to be determined. This is achieved by evaluating the sensitivity of each of the control variables towards improving the ENVCI. The most effective one is selected from the sensitivity matrix Ω_S, after its elements are sorted. The methodology is repeated for all the 30 numbers of operating conditions which are generated at different steps of loading in the five weak buses mentioned earlier in Chapter 2.
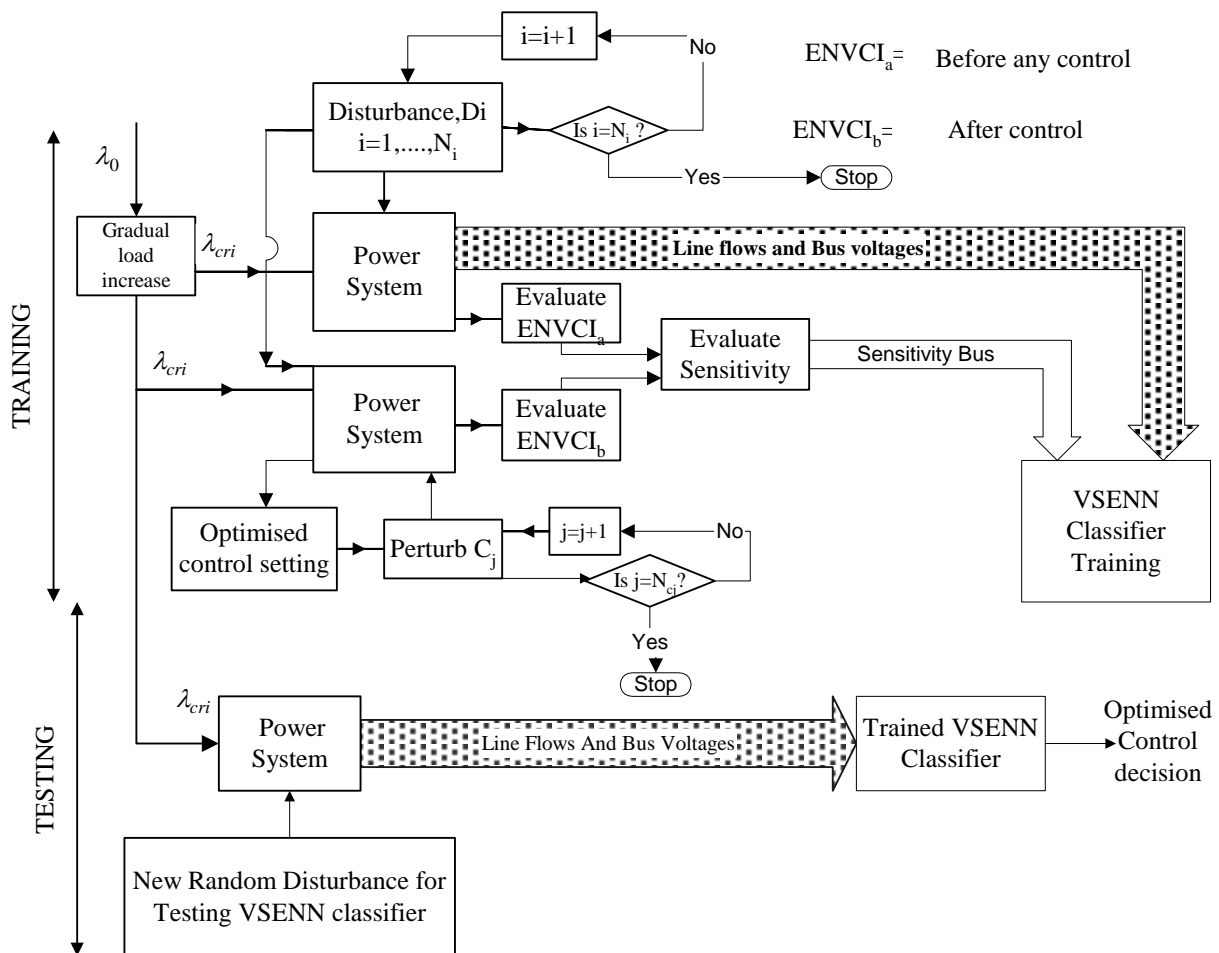
Figure 6.3. Flow chart strategy of VSENN control classifier.

6.6. Simulation Results and Discussions

Considering the same test system as before, the proposed method is simulated using Matlab® 7.0 software in a dual core processor 2.2 GHz, and 4GB RAM. 30 numbers of system operating conditions which are marginally different from data given in Appendix **A**, are considered as the starting point of increasing the load in steps of **2%** within the range of **100%** to **140%** of nominal load. The total load increase being shared by the generators equally. **32** numbers of single line outage (out of the total number of **46** lines) contingencies along with load increase scenarios at **17** different load buses are simulated. The above combination of line outage and load increase is repeated at all the **30** different starting point operating conditions mentioned above. Therefore, in total $32 \times 17 \times 30 = $ **16,320** patterns are generated for the purpose of training. The details of the training statistics are mentioned in Table **6.1**.

Table 6.1. PNN structure parameters and model strategy.

PNN structure	
Number of input	63
Number of output	1
Spread	0.7
Total no of layers	2
Hidden layer	None
Training Data	
Training time	20.0876 s.
Total number of operating scenarios	16320-2564 = 13756
Number of training samples	8000
Testing results	
Testing time	0.8306 s
Total numbers of testing operating scenarios	1142
Total % misses	14/1045

Table 6.2. Maximum loading value in load buses for ENVCI approaches zero.

Serial No	Bus Number	Critical loading / Maximum Loading, λ_{crit}	P_{load} (Real power) at max loading (MW)
1	8	4.36	628
2	20	5.27	522
3	27	6.44	500
4	28	7.24	283
5	29	8.74	206
6	4	9.35	281
7	15	9.87	320
8	7	10.73	233
9	3	11.25	322
10	24	11.33	308
11	21	11.87	274
12	16	13.31	329
13	23	13.79	247
14	25	16.20	224
15	26	19.55	139
16	18	20.28	158
17	12	Above 26	7

It has been observed from the Table **6.2** that among **17** number of load buses, bus numbers **8**, **20**, **27**, **28** and **29** are the five weakest buses, which make the system voltage unstable as the nominal load is increased. For simulation, the real powers in these buses are increased one after the other towards their loadability limit. Very near to the point of instability on the P-V curve, several numbers of contingency conditions are created and ENVCI values are determined at each condition.

A single set of the input data consists of the bus voltages of **29** numbers of load buses and the apparent line power flows of **34** lines out of the total **46** lines, which are not directly fed from any of the 10 generators. Therefore, an input set of 63 data for a particular operating condition is assumed large enough to represent the feature of nonlinearity in the given test system. The output data is a single data, representing the most sensitive control action among several numbers of discrete control actions for a particular operating point. The above selected action improves the ENVCI value after it is being taken. All the output control actions are sequentially numbered; therefore the output data is the control action number that is most sensitive. The ENVCI values obtained with and without the most appropriate control action proposed by VSENN classifier are enumerated in Table **6.3**.

After obtaining the information regarding the most desirable control action required in improving the voltage profile of the system, from the trained VSENN, the same need to be

tested for its ability to stabilize the system under different contingency conditions for which training was not done. For this purpose, 8 numbers of cases (*i.e.*, *Cases* **1** to *Case* **8**) are examined and the voltage profile improvements for each of them, after taking the proposed control action, are illustrated. Moreover, the absolute values of the voltages obtained before and after taking the control actions in all the cases, are also given in Table **6. 4**.

For the sake of better understanding of the performance of PNN controller in taking corrective control action, the voltage limits of power system used in the power flow problem during the process of training testing were relaxed to maximum and minimum values of **1.5** and **0.5** respectively. Within the realms of computation, this approach gives a solution with larger deviations in the magnitudes of bus voltages compared to practical system conditions. However, as can be seen from the simulation and results that this gives a distinct improvement in the bus voltages after application of proper corrective control action.

Table 6.3. Description of control action taken by PNN classifier and the corresponding improvement in ENVCI values for the 8 cases.

Cases	*P* increase from nominal value	*Q* increase from nominal value	Control type	Value of control (% change)		ENVCI with control	ENVCI without control
				Increase	Decrease		
1	20%	54%	1st gen. real power increase	12.5%	-	0.6391	0.211
2	0	0	8th gen. real power increase	15.0%	-	0.2944	0.1865
3	0	10%	Real power load shedding at 25th bus	-	10%	0.5937	0.2768
4	0	10%	Real power gen. increase in 1st gen.	13%	-	0.852	0.318
5	15%	20%	Transformer tap position between lines 12-13	6.61%	-	0.7958	0.0764
6	15%	25%	Real power load shedding 24th bus	-	11%	0. 8585	0.0032
7	2.8%	2.3%	Transformer tap position between lines 29-38	-	7.9%	0.7124	0.1371
8	1%	2%	Real power load shedding 24th bus	21%	-	0.8040	0.6063

Table 6.4. Statistical values of system bus voltages obtained with / without control actions.

Test cases	Average voltage (*p.u.*)		Maximum voltage (*p.u.*)		Minimum voltage (*p.u.*)		Standard deviation in voltage	
	Without control	**With control**	**Without control**	**With control**	**Without control**	**With control**	**Without control**	**With control**
Case 1	1.05	0.98	1.4	1.21	0.87	0.82	0.118	0.08
Case2	0.63	0.94	1.5	1.22	0.5	0.586	0.286	0.11
Case 3	1.23	1.01	1.5	1.35	1.04	0.9	0.107	0.086
Case 4	0.9037	1.01946	1.5	1.05	0.41	0.94	0.41	0.08
Case 5	0.903	0.988	1.1	1.178	0.5	0.932	0.077	0.066
Case 6	0.693	0.972	1.3	1.09	0.5	0.932	0.216	0.063
Case 7	0.6926	0.982	0.98	1.0697	0.5	0.6297	0.136	0.0805
Case 8	1.222759	0.979183	1.5	1.1435	0.5	0.8312	0.421	0.0593

6.6.1. Case 1

In this case real and reactive power in bus number **16** are increased by **20%** and **54%** respectively from their respective nominal values. At this point, the line 15-16 outage contingency is simulated. The control action suggested by the PNN classifier is to increase the real power generation of the 1st generator by **12.5%** from its nominal value of **2.5** *p.u.* The value of ENVCI before changing the control setting was **0.211**, which could be improved to **0.6391**. It may be seen from Figure **6.4** that, the voltage profile of system buses remained close to their respective limiting values, if the proposed control action is not taken.
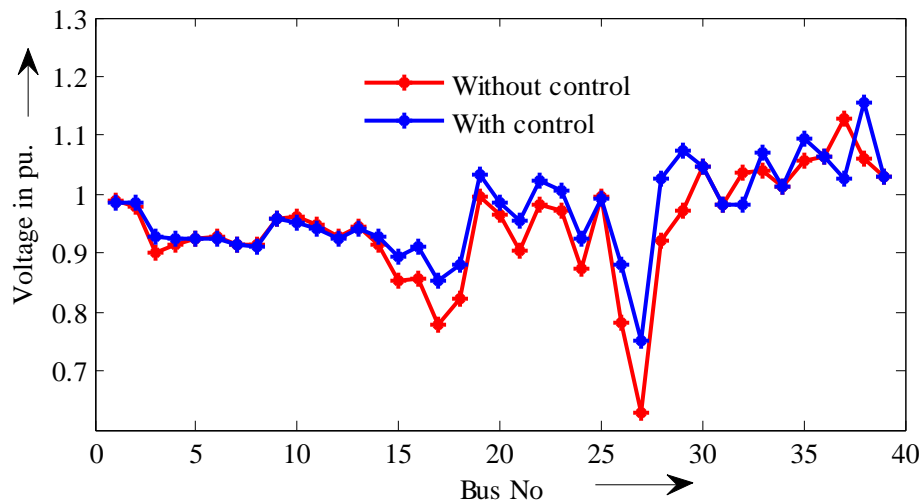
Figure 6.4. System bus voltage profile for case 1.
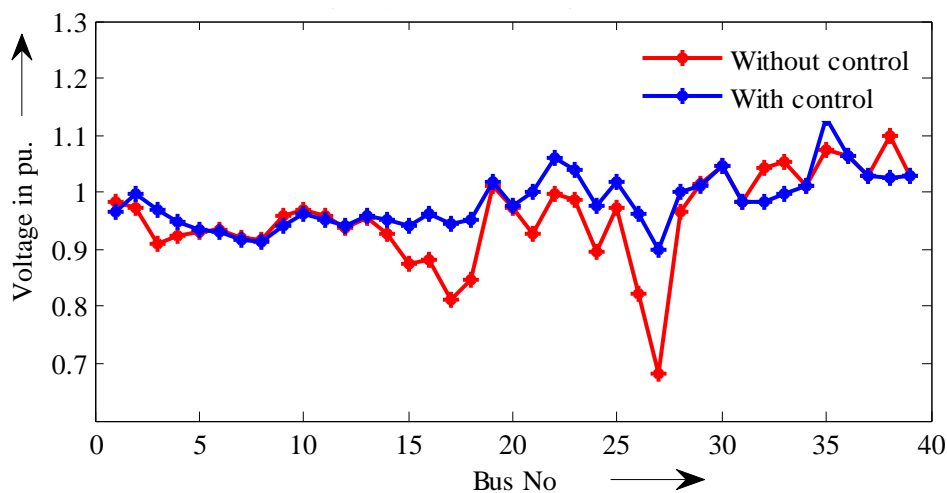
Figure 6.5. System bus voltage profile for case 2.

6.6.2. Case 2

For an line outage **12**-**13** at the nominal loads, the controller classifies to increase the real power generation in the 8th generator by **15.0%** above its nominal value. As a result of which, the value of ENVCI increases from **0.1865** to **0.2944**. Figure **6.5** shows the system bus voltages of bus numbers **26** and **27** are close to their limiting values, and an increase of real power generation resulted in stabilizing the operating voltages effectively.

6.6.3. Case 3

A very critical line connecting buses **2** and **3** is removed, when the reactive power at the load bus number **4** is increased by **10%** from its nominal value. The VSENN has recommended that the most sensitive control action would be to shed the load at bus number **25** by **10%** from its nominal value. After taking this control action, the ENVCI has increased from **0.2768** to **0.5937**. The voltage profiles in this case are depicted in Figure **6.6**, which shows considerable improvement in the voltages.
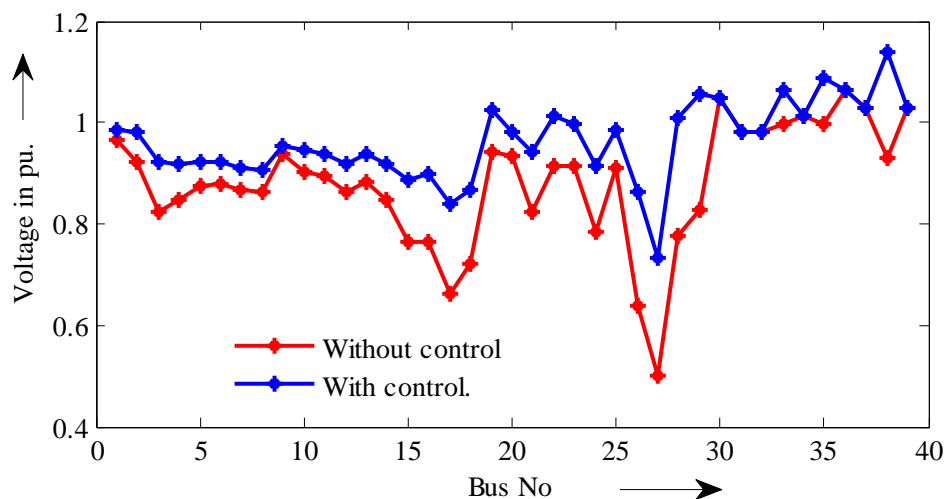
Figure 6.6. System bus voltage profiles for case 3.

6.6.4. Case 4

Similar to *Case 3*, the line connecting bus numbers **2** and **3** is made out along with a **10%** increase in the reactive power at the load bus number **23**. In this condition, the most suitable control action requires the increase in real power generation of 1st generator by **13 %** from its pre contingency value. However, after taking the action the ENVCI becomes **0.852**

increasing from **0.318**. The voltage profile shown in Figure **6.7** justifies the control action as a more flat voltage profile could be achieved.
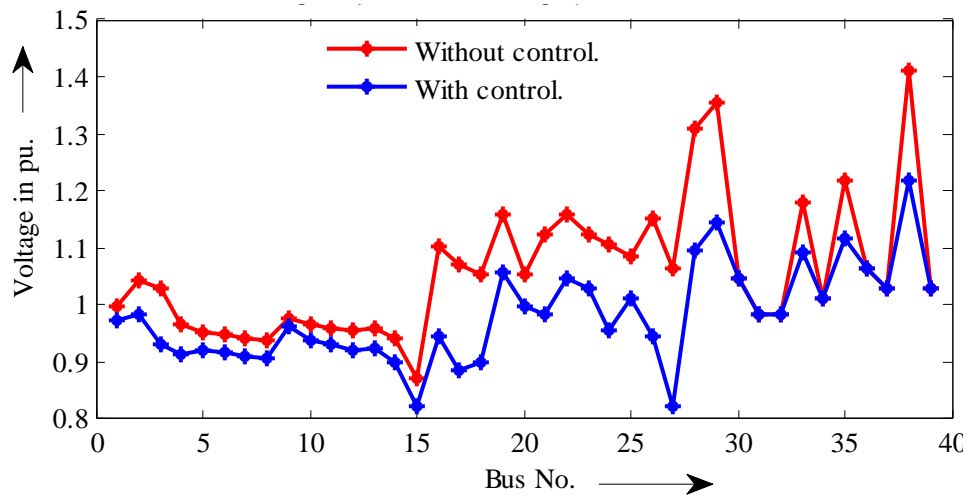
Figure 6.7. System bus voltage profiles for case 4.

6.6.5. Case 5

The line connecting bus numbers **13** and **14** are considered out when the real and reactive powers of loads connected at the **15**[th] bus are increased by **15%** and **20%** respectively. The above line is a critical line, as with its outage most of system bus voltages have reached their maximum or minimum limits. VSENN proposes to increase the tap position of the transformer stationed between buses **12** and **13** by **6.6%** from its original position of **1.0060**. With this control action, the value of ENVCI improved from **0.07643** to **0.7958**, the voltage profiles depicted in Figure **6.8** can be seen to have improved from their lower values obtained without the control action.
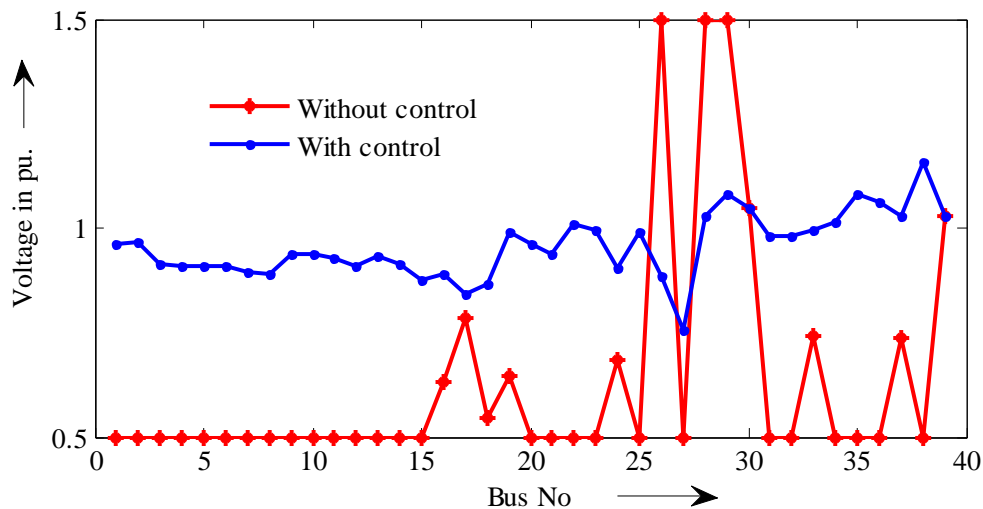
Figure 6.8. System bus voltage profiles for case 5.

6.6.6. Case 6

In this case, the same line **13**-**14** is simulated to be out after increasing the real and reactive powers at the **20**th load bus. VSENN suggests reducing the real power load at the **24**th bus by **11%**, which could improve the ENVCI considerably from **0.0032** to **0.8585**. Figure **6.9** depicts the voltage profiles obtained with the presence and absence of the corrective load shedding at the above mentioned bus.
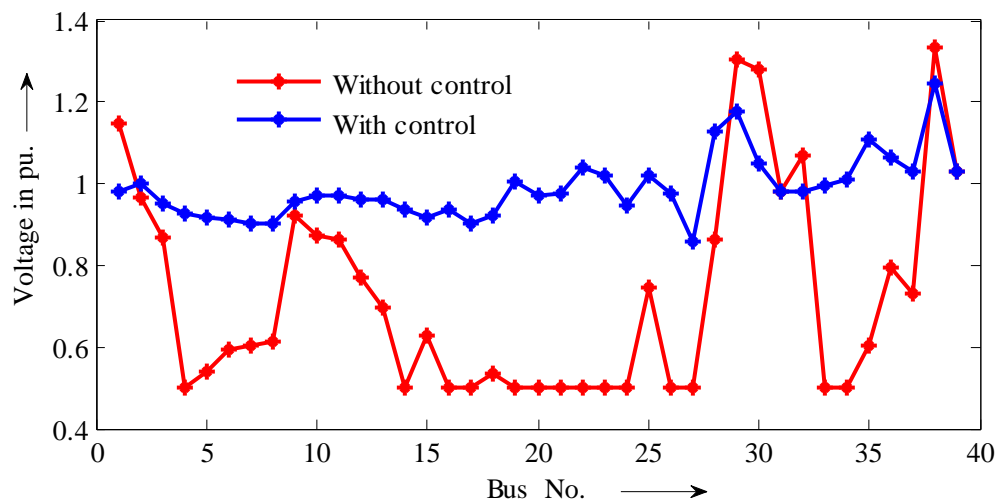
Figure 6.9. System bus voltage profiles for case 6.
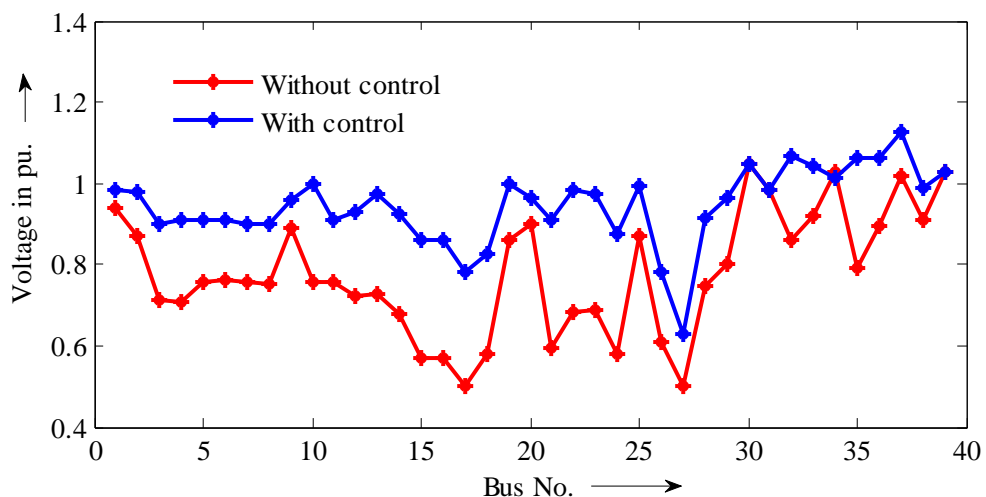
Figure 6.10. System bus voltage profiles for case 7.

6.6.7. Case 7

A line outage of **10**-**11** along with the increase in both real and reactive powers at the **23**rd load bus by **2.8%** and **2.3%** respectively, was simulated. The VSENN proposes to

reduce the tap setting of the transformer between bus no. **29** and **38** by **7.9%** from its nominal value of **1.025**. This action has resulted in an improvement of ENVCI to **0.7124** from **0.1371**. Figure **6.10** clearly justifies the role of control action as the voltages of almost all the buses except some of the generator buses have considerably improved.

6.6.8. Case 8

In this case, the active and reactive powers at the bus number **25** are increased by **1%** and **2%** respectively. At this increased operating point, a line outage of **10**-**13** is carried out. The control action proposed by VSENN is to decrease the real power load of the **24**[th] bus by **21%** from its nominal pre-contingency value. By shedding this key load, the ENVCI improved from **0.6063** to **0.8040**. From the bus voltage profiles depicted in Figure **6.11**, it can be seen that an unstable condition could be restored back to normal condition.
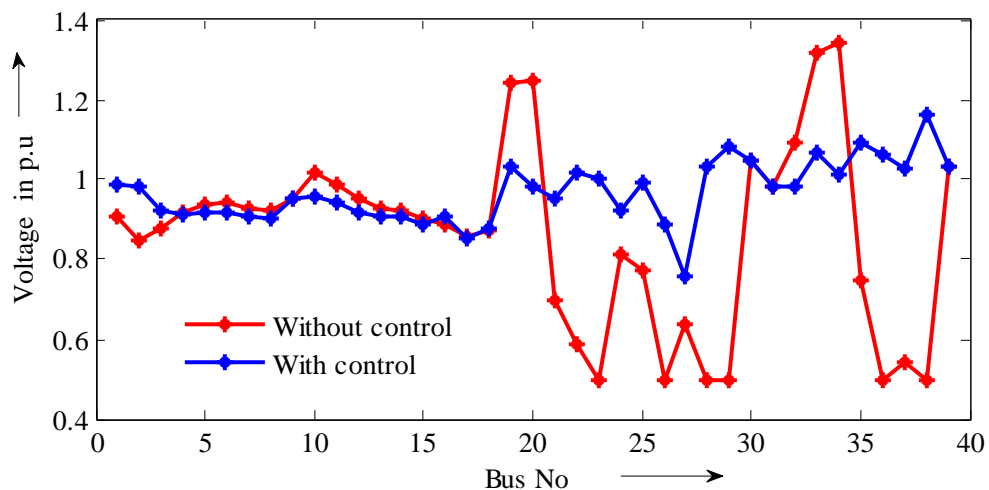
Figure 6.11. System bus voltage profiles for case 8.

Many such similar cases where improvement in voltage profile are studied with different cases of contingencies. In this work only few cases are discussed as above. The graphical representation of maximum, average, and minimum voltage of each bus with and without the controller for all cases given in Figures **6.12**, **6.13**, and **6.14** respectively and the respective values are given in Table **6.4**. Similarly, the standard deviation of bus voltages before and after the recommended control actions in all cases is shown in Figure **6.15**.
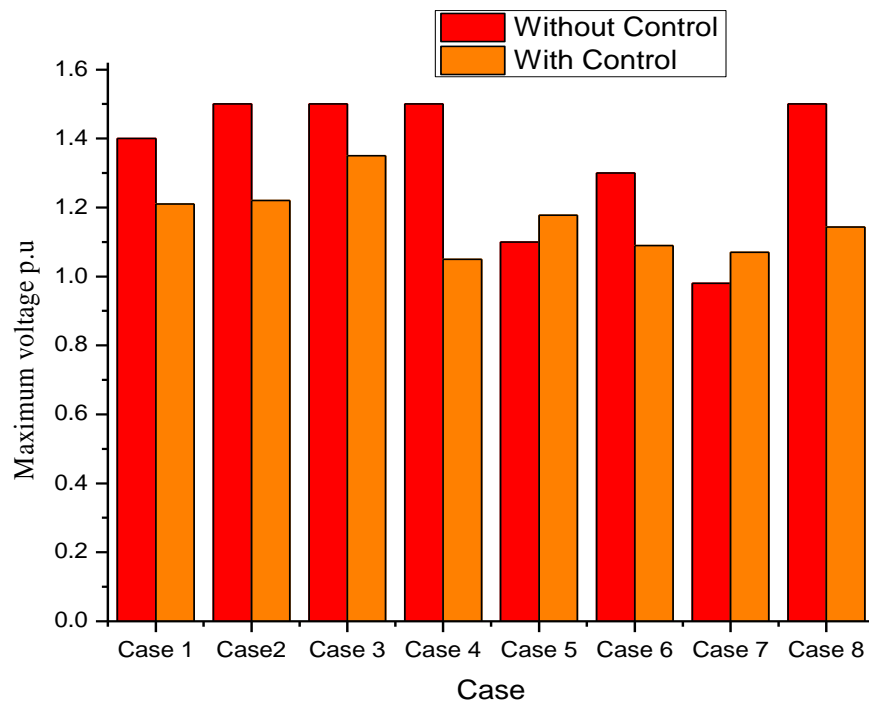
Figure 6.12. The maximum voltage in the system with and without the controller.
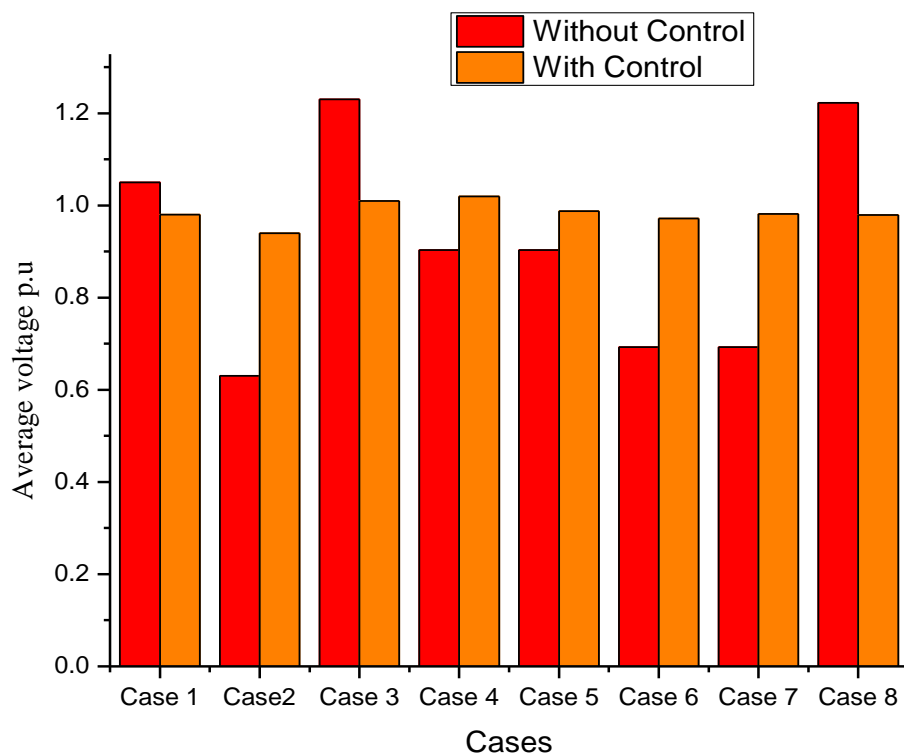
Figure 6.13. The average voltage of the system with and without the controller.
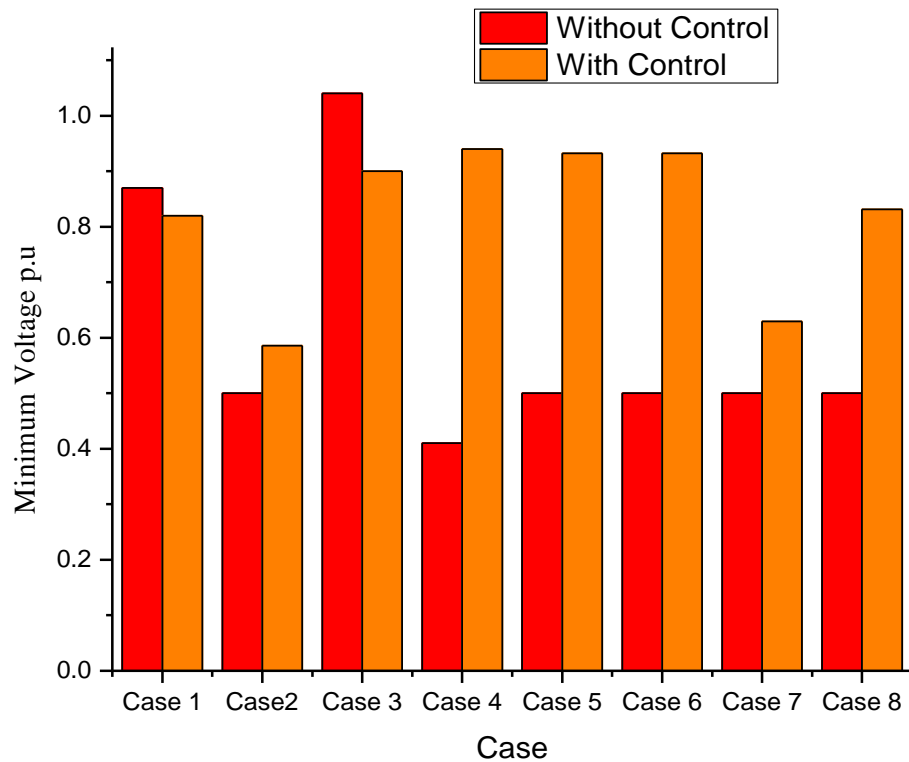
Figure 6.14. The minimum voltage in the system with and without controller.
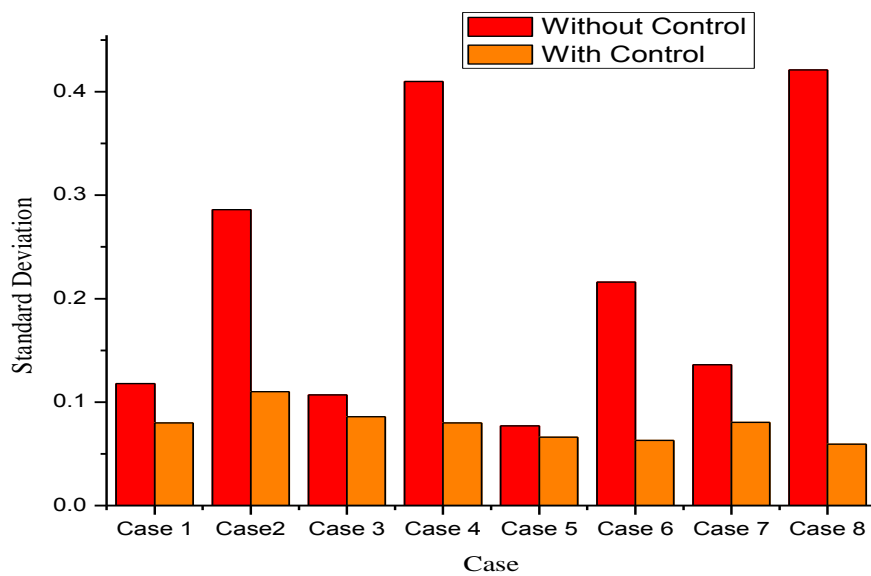
Figure 6.15. The standard deviation in system bus voltage with and without controller.

6.7. Conclusions

This work proposes a PNN classifier termed as VSENN, which suggests the most suitable control action in alleviating a voltage unstable state. Simulation was studied for IEEE 39 bus power system operating at very near to the notch point (operating limit) on its PV curve and simultaneously considering a line outage condition. In order to make VSENN most effective for its application in load dispatch/ control centres to facilitate fast centralized control decisions, a local bus voltage phasor based voltage collapse index, *i.e.,* ENVCI is utilized as in an online manner by obtaining phasor information of bus voltages with the help of PMUs. The proposed classifier is trained by giving selected bus voltages and line flows as input data and the most sensitive control action to improve the ENVCI value as the output. In the end, VSENN is tested for several numbers of contingency cases and the effect of this control action on system bus voltage profiles is verified. Voltage instability state is avoided by taking the control action suggested by VSENN. Moreover, in online applications, several data related to bus voltages, line flows, steady state settings of controls can be estimated through measurements obtained with the help of telemeters and fed to the proposed VSENN classifier as input data, and depending upon the set values of control settings for a particular snapshot of interest, the most suitable incremental corrective control decision may be obtained with the help of the proposed classifier.

CONCLUSIONS AND RECOMMENDATIONS FOR FUTURE RESEARCH

7.1. Conclusions

Increased load demand in modern power systems cannot always be met by augmenting the system with newer capacities in generation and transmission system. Therefore, existing systems are gradually getting overburdened or overloaded, which have led to voltage instability or insecurity in general leading to blackout conditions with improper management of operation. The system operator has always tried to improve upon system operation to make it more and more secure in its operation, even with rising demands. The objective of this work is to achieve a similar objective of improving system VSL and operational corrective control decisions in the event of contingencies.

The 10 generator IEEE 39-bus test system is considered for the study. At the outset, a basic understanding of the system's weakness is realized with the help of voltage stability indices based analysis. To choose a better voltage stability index among many reported indices, the ENVCI was selected as unlike many others it does not neglect the effect of the part of system outside the local network near the point of its evaluation. This may be necessary for the proper design of a centralized corrective control action later on, which chooses the most suitable corrective control action to secure the system in terms of bus voltages during the operational stage of the system. Taking the help of sensitivities of various voltage stability indices including ENVCI and a proposed index WASI to load change, the relative weakness ranking of the system buses are carried out in Chapter 2. Bus no. 8,20, 27,28,29 are the weakest five buses , chosen to be loaded in the subsequent chapter for analysis, so that an accurate worst case load increase condition can be simulated for obtaining best possible compensation.

Increasing load in gradual steps(0.01) at the selected five weakest buses in the previous chapter, the system VSL is aimed to be improved by fixed capacitive compensation at suitable location and amount. Utilizing a modified version of BFOA in Chapter 3, termed as MBFOA, the location and amount of fixed percentage capacitive compensation is optimized to improve the VSL of the system. The load margin is increased to **4.51** times of the nominal load with GA. The optimization with GA for this case gives the two optimal locations and sizes of FC which are at bus no. **28** with compensation of + **45.35%** of Q_{max} (= 90 MVAr) and at bus no. **20** with compensation required to be + **31.57%** of Q_{max} respectively. The load margin increased to 4.55 times of the normal load. The final solution with MBFOA proposes a **42.78 %** of rated FC at bus number **24** and **8.68%** of rated compensation at load bus number **15**. Keeping the location and amounts of compensation obtained with both the methods, separate PV curves are drawn when the load was increased in the weakest bus of the system, *i.e.,* bus number **20**.similarly with DE the compensation amount were 42.84% , 20.25%   and the locations were bus no 25 and bus no 29 respectively. Again with PSO the optimized value of the VAR locations are 27, and 28 and the value of VAR are 42.88%, and 9.78% respectively..

The optimization results were compared with those obtained with GA and found to be better compared to both the GA and without compensation cases. The modifications in the MBFOA is marginally different from the earlier reported. In this the memory of optimum bacteria θ_m^{OP} used in the step of swarming, is retained even after the process of elimination and dispersal.

Exploring some other reactive power control mechanisms available in the system Chapter 4 aims at including the generator bus voltages along with the two location of fixed capacitive compensation, into the domain of optimizing variables. A STATCOM is also placed at the weakest bus in the system and its power flow model is utilized during the process of power flow solution in the optimization. 1st location of compensation Bus no 21, 25.86%, bus no 25.of 14.2%

The mentioned control variable settings are then simultaneously optimized to further improve upon the VSL and reduce system losses, with application of MBFOA. The operation of the system with the optimized settings has not only improved the load margin but also made the system to operate in more voltage secure manner when different types of contingencies were created in the system.

To test the system augmentation with green energy sources based generators, DFIG driven WECS replaces one of the system generator of the same capacity. In the presence of the STATCOM, the control variables considered in the previous chapter are again optimized with MBFOA, considering this time the operating constraints of the power electronics converters of DFIG, in terms of the reactive power capabilities of DFIG. The solution of PV curves in this case explains the need of these constraints, as the VSL is marginally reduced compared to the case when conventional generators case in chapter 4. This is due to the fact of the additional constraints of reactive power capability. Therefore it may be concluded during the process of optimization if this constraint is neglected then the result may be unrealistic in nature. Moreover, the need of additional external reactive power resources is required with increasing penetration of DFIG based wind power in the grid.

The compensation amount at Bus 21 is the optimal location with an amount of 57.67%, and the second location is at bus 25 with 12.37% of the full load rating(20 MVA) of the STATCOM used.

By only optimizing the steady state settings of different types of reactive power control mechanisms it may not be possible to alleviate the insecure voltage conditions during different contingencies in the system. In this condition partial correction in the control settings may alleviate the system condition for some duration before the system enters the state of extremis. However, in the presence of different types of generation capacities in the form of conventional and renewable resources, FACTs and other external compensating devices along with their varieties of controls, it becomes difficult to take centralized corrective control decision that best suits the disturbance. This work gives a background of any such centralized controller with the help of PNN based classification. The designed controller chooses the most suitable corrective control action from the pool of many available controls. The PNN is trained taking many sample

cases of contingency condition with the data of load flows, line flows and bus voltages as inputs and the most suitable control action that improves the value of ENVCI as the output. The load increased in steps of **2%** for a range of **100%** to **140%** of nominal load. The total load increase being shared by the generators equally. **32** numbers of single line outage (out of the total number of **46** lines) contingencies along with load increase scenarios at **17** different load buses are simulated. The above combination of line outage and load increase is repeated at all the **30** different starting point operating conditions mentioned above. Therefore, in total $32 \times 17 \times 30 =$ **16,320** patterns are generated for the purpose of training.

The designed PNN has managed to improve the degraded performance of system bus voltage by taking the most suitable corrective control action in a range of 6%-21%, for contingency cases for which the PNN was not trained.The primary objective of this work is not to prove upon the superiority of MBFOA over many other more recent heuristic techniques rather to work in modified models. With the modifications in the original version of BFOA named as MBFOA with the steady state settings of the mentioned controls. The PNN classifier corrects upon the optimized settings during system operation when contingencies do take place.

7.2. Recommendations for Future Research

The components of the research reported in this thesis have completed some fundamental aspects of having optimized steady state control settings to improve VSL of the system. A larger set of optimizing control variables which regulate the reactive power in the system may be considered in the process of optimization. Some examples of these variables are transformer tap settings, generator real powers, locations and amounts of selective load shedding and other variables of DFIG and STATCOM. Moreover, it has prepared a foundation of designing a centralized controller using more advanced, accurate and consistent ANN structures. The inclusion and testing of other FACTs devices in large test systems may be considered before applying the controller in actual operation in a practical power system.

REFERENCES

[1] AIEE subcommittee on interconnections and stability factors, "First report of power system stability," *AIEE Transactions*., pp. 51-80, 1926.

[2] K. Takahashi and Y. Nomura, "The power system failure on July 23rd 1987 in Tokyo," *CIGRE SC-37 Meeting*, vol. 37, no. 87(JP) 07(E), 1987.

[3] N. Mithulananthan, and S. C. Srivastava, "Investigation of a voltage collapse incident in Sri Lanka power system network," *Proc. of the EMPD 98*, Singapore, IEEE Catalogue No. 98EX137, pp. 47-52, 1998

[4] G. S. Vassell, "Northeast blackout of 1965," *IEEE Power Engineering Review*," pp. 4-8, 1991.

[5] The North American Electrical Reliability Council Steering Group, "Technical Analysis of the August 14, 2003 Blackout What Happened, Why, and What Did We Learn?," Final Report on the August 14, 2003, July J 3, 2004.

[6] U. S.-Canada Power System Outage Task Force, "Blackout in the United States and Canada: causes and recommendations," 2004.

[7] H. Wan, J. D. Mc. Calley, and V. Vittal, "Risk based voltage security assessment," *IEEE Transactions on Power Systems*, vol. 15, no. 4, pp.1247-1254, 2000.

[8] A. A. Gharaveisi, M. Rashidinejad, and A. Mousavi, "Voltage security evaluation based on perturbation method," *EPES,* vol.31, no. 5, pp. 227-235, 2009

[9] L. H. Fink and K. Carlsen, "Operating under stress and strain," *IEEE Spectrum*, vol. 15, no. 3, pp. 48-53, 1978.

[10] National Load Dispatch Centre, "Preliminary report on grid disturbance in NEW grid on 31st July 2012," 2012.

[11] C. W. Taylor, *Power System Voltage Stability*. McGraw- Hill, New York, 1994

[12] P. Kundur, *Power System Stability and Control*, New York, McGraw- Hill, 1994.

[13] IEEE/CIGRE Joint Task Force on Stability Terms and Definitions, "Definition and Classification of Power System Stability," *IEEE Transactions. on Power Systems*, vol. 19, no.3, pp. 1387-1401, 2004.

[14] P. Kundur, "A survey of utility experiences with power plant response during partial load rejections and system disturbances," *IEEE Transactions. Power Apparatus and Systems*, vol. PAS-100, pp. 2471-2475, 1981.

[15] T. V. Cutsem and C. Vournas, "Voltage Stability of Electric Power Systems," Norwell, M. A. Kuwer, 1998.

[16] A. A. Fouad and V. Vittal, *Power System Transient Stability Analysis Using the Transient Energy Function Method*, Englewood Cliffs, NJ: Prentice-Hall, 1991.

[17] CIGRE Task Force 38.02.14 Rep., Analysis and modeling needs of power systems under major frequency disturbances, 1999.

[18] C. W. Taylor, *Power System Voltage Stability*, McGraw- Hill, New York, 1994.

[19] P. Kundur, D. C. Lee, J. P. Bayne, and P. L. Dandeno, "Impact of turbine generator controls on unit performance under system disturbance conditions," *IEEE Transactions. Power Apparatus and Systems*, vol.104, pp. 1262-1267, 1985.

[20] G. K. Morison, B. Gao, and P. Kundur, "Voltage stability analysis using static and dynamic approaches," *IEEE Transactions. Power Systems*, vol. 8, pp. 1159-1171, 1993.

[21] CIGRE Working Group 14.05 Report, Interaction between HVDC convertors and nearby synchronous machines, CIGRE Brochure 119, 1997.

[22] R. Zhang, K. P. Wong, J. Hill, P. A. Lof, and G. Anderson, "Analysis of long-term voltage stability," Proc. 10th *Power Systems Computation Conf*., pp. 1252-1259, 1990.

[23] B. Singh, N. K. Sharma, and A. N. Tiwari. "Prevention of Voltage Instability by Using FACTS Controllers in Power Systems: A Literature Survey," *International Journal of Engineering Science and Technology*, vol. 2, no. 5, pp. 980-992, 2010.

[24] J. M. Ramirez, R. J. Davalos, A. Valenjuela, and I. Coronado, "FACTS based stabilizers co-ordination," *Electrical Power and Energy Systems*, vol. 24, no. 3,pp. 233-243, 2002.

[25] C. Reis and F. P M. Barbosa "A comparison of voltage stability indices," *IEEE-MELECON*, Benalmadena (Malaga), Spain, 2006,

[26] B. H. Chowdhury, and C. W. Taylor, "Voltage stability analysis: V-Q power flow simulation versus dynamic simulation," *IEEE Transactions on Power Systems*, vol. 15, no. 4, pp.1354-1359, 2000.

[27] C. Canizares "Voltage Stability Assessment: Concepts, Practices and Tools," IEEE/PES Power System Stability Subcommittee Special Publication, 2002.

[28] C. Sharma and M. G. Ganness "Determination of power system voltage stability using Modal Analysis," *Power Eng*, Setubal, Portugal, pp.381-387, 2007.

[29] V. Ajjarapu, and C. Christy, "The continuation power flow A tool for steady state voltage stability analysis," *IEEE Transactions on Power Systems*, vol. 7, no. 1. pp. 416-423, 1992.

[30] P.Kessel and H. Glavitsch, "Estimating the voltage stability of a power system," *IEEE Transactions Power Delivery*, PWRD, vol. 1, no. 3, pp.346–54, 1986.

[31] B. Gao, G. K. Morison, and P. Kundur "Voltage stability evaluation using modal analysis," *IEEE Transactions on Power Systems*, vol.7, no. 4, pp.1529-1542, 1992.

[32] M. Moghavvemi, and O.Faruque, "Real-Time Contingency Evaluation and Ranking Technique," *IEEE Proceeding on Generation, Transmission and Distribution*, vol. 145, no. 5, pp 517-124, 1998.

[33] M. Moghavvemi, and F. M. Omar, "Technique for Contingency Monitoring and Voltage Collapse Prediction," *IEEE Proceeding on Generation, Transmission and Distribution*, vol. 145, no. 6, pp. 634-640, 1998.

[34] I. Musirin, and T. K. A. Rahman "Novel fast voltage stability index (FVSI) for voltage stability analysis in power transmission system," *Student Conference on Research and Development Proceedings*, Shah Alam, Malasia, 2002.

[35] M. R. Aghamohammadi, S. Hashemi, and M. S. Ghazizadeh "A novel index for online voltage stability assessment based on correlation characteristic of voltage profiles," *IPEC*, pp.165-170, 2010.

[36] A. Rabiee, M. Vanouni, and M. Parniani, "Optimal reactive power dispatch for improving voltage stability margin using a local voltage stability index," *Energy Conversion and Management,* vol. 59, pp. 66–73, 2012.

[37] I. Smon, G. Verbic, and F. Gubina, "Local voltage-stability index using Tellegen's theorem," *IEEE Transactions. Power System*, vol.21, no. 3, pp. 1267-1275, 2006.

[38] F. Gubina, and B. Strmenik "A simple approach to voltage stability assessment in radial networks," *IEEE Transactions on Power Systems*, vol. 12, no. 3, pp 1121-1128, 1997.

[39] R. Verayiah and I. Z. Abidin "A Study on Static Voltage Collapse Proximity Indicators," *2nd IEEE International Conference on Power and Energy* (PECon 08), 1-3, 2008, Johor Baharu, Malaysia.

[40] H. Young, P. Ching-Tsai and W. W. Lin "Fast calculation of a voltage stability index of power systems," *IEEE Transactions. on Power Systems*, vol.12, no.4, pp. 1555-1560, 1997.

[41] Y. Wang, W. Li, and J. Lu, "A new node voltage stability index based on local voltage phasors," *Electrical Power System Research*, vol.79, pp.265–271, 2009.

[42] G. W. Kim, and K. Y. Lee, "Coordination Control of ULTC Transformer and STATCOM Based on an Artificial Neural Network," *IEEE Transactions On Power Systems*, vol.. 20, no. 2, pp. 580-586, 2005

[43] E. Mesut, F. Baran, and F. Wu, "Optimal capacitor placement on radial distribution systems," *IEEE Transactions on Power Delivery*, vol. 4, no. 1, pp.725-734, 1989.

[44] R. Minguez, F. Milano, Z. Minano, and A. J. Conejo, "Optimal network placement of SVC devices," *IEEE Transactions on Power Systems*, vol. 22, no. 4, pp.1851-1860, 2007.

[45] A. Wiszniewski "New criteria of voltage stability margin for the purpose of load shedding," *IEEE Transactions on Power Delivery*, vol. 22, no. 3, pp. 1367-1371, 2007.

[46] F. Capitanescu, B. Otomega, H. Lefebvre, V. Sermanson, and T. V. Cutsem, "Decentralized tap changer blocking and load shedding against voltage instability: Prospective tests on the RTE system," *Electrical Power and Energy Systems* vol. 31, pp. 570-576, 2009.

[47] H. Raoufi, and K. Mohsenar "Reactive power rescheduling with generator ranking for voltage stability improvement," *Energy Conversion and Management*, vol. 50, pp. 1129-1135, 2009.

[48] J. Qiu and S.M. Shahidehpour "A new approach for minimizing power losses and improving voltage profile," *IEEE Transactions on Power Systems*, vol. PWRS-2, no. 2, pp.287, 1987.

[49] Y. Zhang and J. V. Milanovic, "Global Voltage Sag Mitigation With FACTS-Based Devices," *IEEE Transactions on Power Delivery*, vol. 25, no. 4, 2010.

[50] N. Hingoranni and L. Gyugyi, "*Understanding FACTS-concepts and technology of Flexible AC transmission systems*," Piscataway, NJ: IEEE Press/Wiley, 2000

[51] N. K. Sharma, A. Ghosh, and R. K. Varma, "A novel placement strategy for facts controllers," *IEEE Transactions on Power Delivery*, vol. 18, no. 3, pp. 982-987, 2003.

[52] N. Yorino, E. E. El-Araby, H. Sasaki, and S. Harada "A new formulation for facts allocation for security enhancement against voltage collapse," *IEEE Transactions on Power Systems*, vol. 18, no. 1, pp. 3-10, 2003.

[53] T. Orfanogianni and R. Bacher "Steady-state optimization in power systems with series facts devices," *IEEE Transactions on Power Systems*, vol. 18, no. 1, pp. 19-26, 2003.

[54] R. Minguez, F. Milano, Z. Minano, and A. J. Conejo, "Optimal network placement of SVC devices," *IEEE Transactions on Power Systems*, vol. 22, no. 4, pp. 1851-1860, 2007.

[55] M. M. Farsangi, and H. Mezamabadi-pour, "Placement of SVCs and selection of stabilizing signals in power systems," *IEEE Trans. on Power Systems*, vol. 22, no. 3,pp. 1061-1071 2007.

[56] S. Kannan, S. Jayaram, and M. M. A. Salama, "Real and reactive power coordination for a unified power flow controller," *IEEE Trans on Power Systems*, vol.19, no. 3, pp. 1454-1461, 2004.

[57] S. M. Alamelu and R. P. K. Devi, "Novel optimal placement UPFC based on sensitivity analysis and evolutionary programming," *Journal of Engineering and Applied Sciences*, vol. 3, no. 1, pp. 59-63, 2008.

[58] S. R. Donapati, and M. K. Verma, "An approach for optimal placement of UPFC to enhance voltage stability margin under contingencies," *Fifteenth National Power Systems Conference* (NPSC), IIT Bombay, pp.441-446, 2008.

[59] S. N. Singh, and I. Erlich, "Locating unified power flow controllers for enhancing power system loadability," *International Conference Future Power Systems*, 18 2005, pp 5-5.

[60] S. A. N. Niaki, R. Iravani, and M. Noroozian, "Power-Flow Model and Steady-State Analysis of the Hybrid Flow Controller," *IEEE Transactions on Power Delivery*, vol. 23, no. 4, pp.2330-2338, 2008.

[61] S. Bhowmick, B. Das, and N. Kumar, "An advanced IPFC model to reuse Newton power flow codes," *IEEE Transactions on Power Systems*, vol. 24, no. 2 , pp. 525-532, 2009.

[62] Y. Zhang, and C. Chen, "A novel power injection model of IPFC for power flow analysis inclusive of practical constraints," *IEEE Trans. Power Syst.*, vol. 21, no. 4, pp. 1550-1556, 2006.

[63] M. K. Verma, and S. C. Srivastava, "Optimal placement of svc for static and dynamic voltage security enhancement," *International Journal of Emerging Electric Power Systems*, vol. 2, no. 2, 2005.

[64] K. K. Sen, "STATCOM-static synchronous compensator theory, modeling, and applications," In Proc. *IEEE Power Eng. Soc*. Winter Meeting, vol. 2, pp. 1177-1183, 1999.

[65] G. Y. Yang, G. Hovland, R. Majumder, and Z. Y. Dong "TCSC Allocation based on line flow based equations via mixed-integer programming," *IEEE Transactions on Power Systems*, vol. 22, no. 4, pp. 2262-2269, 2007.

[66] S. Granville, J.C.O. Milo, and A.C.G. Milo. "Application of interior point methods to power flow unsolvability," *IEEE Trans on Power systems*, vol. 11, no. 2 pp. 1096-1103, 1996

[67] R. Fletcher, *The Sequential Quadratic Programming Method*, 2007.

[68] W. Yan, J. Yu, D. C. Yu, and K. Bhattarai, "A new optimal reactive power flow model in rectangular form and its solution by predictor corrector primal dual interior point method," *IEEE Trans. Power Systems*, vol. 21, no. 1, pp. 61-67, 2006 .

[69] D. Devaraj, and J. P. Roselyn "Genetic algorithm based reactive power dispatch for voltage stability improvement," *Int. Journal Electrical Power Energy Syst.*, vol. 32, no. 10 pp. 189-197, 2010.

[70] P. Paterni, S. Vitet, M. Bena, and A. Yokoyama "Optimal location of phase shifters in the French network by genetic algorithm," *IEEE Transactions on Power Systems*, vol. 14, no 1, pp. 37-42, 1999.

[71] R. Sirjani, A. Mohamed, and H. Shareef, "Optimal allocation of shunt Var compensators in power systems using a novel global harmony search algorithm," *Electrical Power and Energy Systems,* vol. 43, pp.562-572, 2012.

[72] Y. Xu, Z Y Dong, K. Meng, Wei Fengyao, R. Zhang, and K. P. Wong "Multi-objective dynamic var planning against short-term voltage instability using a decomposition-based evolutionary algorithm," *IEEE Transactions on Power Systems*, vol. 29, no. 6, pp. 2813-2822, 2014.

[73] B. Mozafari, T.Amraee, and A.M. Ranjbar "An approach for under voltage load shedding using particle swarm optimization," *IEEE ISIE*, pp.9-12, 2006.

[74] C. Huang, and Y. Huang, "Combined differential evolution algorithm and ant system for optimal reactive power dispatch," Proceedings, pp. 1238-1243, 2011, www.elsevier.com/locate/procedia.

[75] S. Gerbex, R. Cherkaoui, and A. J. Germond, "Optimal location of multi-type facts devices in a power system by means of genetic algorithms," *IEEE Transactions on Power Systems*, vol. 16, no. 3, pp. 537-544, 2001.

[76] W. Zhang, and W.L. Yutian "Multi-objective reactive power and voltage control based on fuzzy optimization strategy and fuzzy adaptive particle swarm," *Electrical Power and Energy Systems,* vol. 30, pp. 525–532, 2008.

[77] Y. Wang, F. Li, Q. Wan, and H. Chen "Reactive power planning based on fuzzy clustering, gray code and simulated annealing," *IEEE Transactions on Power Systems*, vol. 26, no. 4, 2011.

[78] A. R. Phadke, M. Fozdar, and K. R. Niazi "A new multi-objective fuzzy-GA formulation for optimal placement and sizing of shunt FACTS controller," *Electrical Power and Energy Systems,* vol. 40, pp. 46-53, 2012.

[79] B. Venkatesh, G. Sadasivam, and M. A. Khan "A new optimal reactive power scheduling method for loss minimization and voltage stability margin maximization using successive multi-objective fuzzy LP technique," *IEEE Transactions on Power Systems*, vol. 15, no. 2, pp. 844-851, 2000.

[80] K. Verma, and K.R. Niazi, "Supervised learning approach to online contingency screening and ranking in power systems," *Electrical Power and Energy Systems*, vol. 38, pp. 97-104, 2012.

[81] A. Chakraborty and S. Halder, *Power System Analysis, Operation and Control*, New Delhi, Third Edition, PHI Publication, 2010.

[82] M. V. Reddy, Y. Pradeep, V. S. K. M. Balijepalli, S. A. Khaparde, and C. V. Dobaria, "Improvement of Voltage Stability Based on Static and Dynamic Criteria," *16th National Power Systems Conference*, 15th-17th, pp. 715-722, 2010.

[83] G. Verbic and F. Gubina, "A New Concept of Voltage-Collapse Protection Based on Local Phasors," *IEEE Transactions. Power Delivery*, vol. 19, no. 2, 2004.

[84] M Nanba, Y Huang, T Kai and S Iwamoto, "Studies on VIPI based control methods for improving voltage stability," *Electrical Power & Energy Systems*, vol. 20, no. 2, pp. 141-146, 1998.

[85] M. Kowsalya, K. K. Ray, and D. P. Kothari, "Loss Optimization for Voltage Stability Enhancement Incorporating UPFC Using Particle Swarm Optimization," *Journal of Electrical Engineering & Technology* vol. 4, pp.492- 498, 2009.

[86] D. E. Goldberg. Genetic algorithms in search, optimization and machine learning. *Addison-Wesley*; 1989.

[87] S. Udgir, S Varshney and L. Srivastava, "Optimal Placement and Sizing of SVC for Voltage Security Enhancement," *International Journal of Computer Applications*, vol. 32, no.6, pp. 44-51, 2011.

[88] S. Das, A. Biswas, S. Dasgupta, and A. Abraham "Bacterial Foraging Optimization Algorithm: Theoretical Foundations, Analysis, and Applications," *Foundations of Computational Intelligence,* vol. 3, Springer, pp. 23-55, 2009.

[89] M. Tripathy, and S. Mishra, "Bacteria Foraging based solution to optimize both real power loss and voltage stability limit," *IEEE Transactions. Power Systems* pp. 240-248, vol. 22, no. 1, 2007.

[90] K. M. Passino, "Biomimicry of bacterial foraging for distributed optimization and control," *IEEE. Control System*, pp. 52-67, 2002.

[91] D. Thukaram, and A. Lomi, "Selection of static VAR compensator location and size for system voltage stability improvement," *Electric Power Systems Research* ,vol.54, 2000 pp. 139-150.

[92] A. S. Yome and N. Mithulananthan, "Comparison of shunt capacitor, SVC and STATCOM in static voltage stability margin enhancement," *Int J Electr Eng Educ*, 2004; vol. 41(2), pp.158-71.

[93] E.Achha, F. E. R. Claudio, A. P. Hugo, *FACTS Modeling And Simulation In Power Network,* John Wiley & Sons Ltd, 2004.

[94] Annual Energy Outlook 2014, US DOE, U.S. Energy Information Administration, Washington, DC, http://www.renewable-energy sources.com

[95] R. A. Jabr, B. C. Pal, "Intermittent wind generation in optimal power flow dispatching,"*IET Gener.Transm.Distrib*; vol. 3, no. 1, pp. 66-74, 2009

[96] N. R. Ullah, K. Bhattacharya, T.Thiringer. "Wind Farm as reactive power ancillary service providers-Technical and economic issues," *IEEE Trans. Energy convs, vol.* 24, no. 3:661-671, 2009.

[97] R. G. Almeida, E. D. Castronuovo, J. P. Lopes, "Optimum generation control in wind parks when carrying out system operator requests,". *IEEE Trans.Power system*, vol. 21, no. 2, pp. 718-725,2006.

[98] T. Ackermann, *Wind power in power system*, John Wiley &Sons. 2005.

[99] J. F. Manwell, J.G. McGowan, Wind Energy Explained, John Wiley &Sons. 2002.

[100] L. H. Hansen, L. Helle, F. Blaabjerg and B. Bak-Jensen, "Conceptual survey of generators and power electronics for wind turbines", Riso National Laboratory, Roskilde, Denmark, Tech. Rep. Riso-R-1205(EN), Dec. 2001.

[101] A. G. Tsikalakis, Y. A. Katsigiannis, P. S. Georgilakis, and N. D. Hatziargyriou, "Determining and exploiting the distribution function of wind power forecasting error for the economic operation of autonomous power system," *IEEE Power Engineering Society General Meeting*, 2006.

[102] M. Singh, E. Muljadi, J. Jonkman, and V. Gevorgian, "*National Renewable Energy Laboratory Simulation for Wind Turbine Generators-With FAST and MATLAB-Simulink Modules*, National Renewable Energy Laboratory, Technical Report NREL/TP-5D00-59195, USA, April 2014

[103] T. Lund, P. Sorensen, and J. Eek, "Reactive Power Capability of a Wind Turbine with Doubly Fed Induction Generator," *Wind Engineering*, vol. 10, pp. 379-394, 2007.

[104] S. Mishra, Y. Mishra, and S. Vigness, "Security constrained economic dispatch considering wind energy conversion systems," *IEEE Power and energy soc. general meeting*, pp. 1-8, 2011.

[105] J. G. Singh, S. N. Singh, and S. C. Srivastava, "An Approach for Optimal Placement of Static VAR Compensators Based on Reactive Power Spot Price*," IEEE Transactions. Power Syst.*, vol.22, no.4, pp. 2021-2029, 2007.

[106] M. T. Al. Hajri, M.A. Abido, "Evaluation of voltage stability indices (VSI) using genetic algorithm," *IEEE Energy Conference and Exhibition*, pp. 268-273, 2010.

[107] P. A. Lof, G. Anderson, and D. J. Hill, "Voltage stability indices of stressed power systems," *IEEE Transactions. PWRS*, vol.8, no.1, pp. 326-335, 1993.

[108] S. Gerbex, R. Cherkaoui, and A. J. Germond, "Optimal Location of Multi-Type FACTS Devices in a Power System by Means of Genetic Algorithms," *IEEE Transactions. on Power Systems*, vol. 16, no. 3, pp. 537-544, 2001.

[109] L. Ippolito, and P. Siano, "Selection of optimal number and location of thyristor-controlled phase shifters using genetic based algorithms," *IEE Proc.-Gener., Transm., Distribut*, vol. 151, no.5, pp.630-637, 2004.

[110] N. Sharma, A. Ghosh, and R. Varma, "A novel placement strategy for FACTS controllers," *IEEE Transactions. Power Delivery*, vol.18, pp. 982-987, 2003.

[111] Y. D. Valle, J. C. Hernandez, G. K. Venayagamoorthy, and R. G Harley, "Optimal STATCOM sizing and placement using particle swarm optimization," *IEEE/PES Transactions Distr Conf Expo*, pp. 1-6, 2006.

[112] C. Vournas, and M Karystianos, "Load tap changers in Emergency and Preventive voltage stability control," *IEEE Transactionsa. Power Systems*, vol. 19, no. 1, pp. 492-498, 2004.

[113] V. Sagar, S. Vankayaia and N. D. Rao, "Artificial Neural Network and their applications to power systems-a bibliographical survey," *Electric Power Systems Research*, vol. 28, pp.67-79, 1993.

[114] V. Mirinda and J. T. Saraiva, "Fuzzy Modelling of Power System Optimal Load Flow," *IEEE Transactions on Power Systems*, vol. 7, no. 2, pp. 843-849, 1992.

[115] D. F. Specht, "*Probabilistic neural networks*," vol. 3, no.1, pp.109-118, 1990.

[116] S. Mishra, C. N. Bhende, and B. K. Panigrahi, "Detection and Classification of Power Quality Disturbances Using S-Transform and Probabilistic Neural Network," *IEEE Transactions on Power Delivery*, vol. 23, no.1, pp. 280-287, 2008.

[117] W. M. Lin, C. H. Lin, and Z. C. Sun, "Adaptive multiple fault detection and alarm processing for loop system with probabilistic network," *IEEE Transactions. Power Delivery.*, vol. 19, no. 1, pp. 64-69, 2004.

[118] D. Thukaram, L. Jenkins and K. Visakha Optimum allocation of reactive power for voltage stability improvement in AC-DC power systems, *IEE Proc.-Gener. Transm. Distrib.*, vol. 153, No. 2, March 2006, pp.237-246, 2006.

[119] S. Naveen, K. Sathish Kumar, K. Rajalakshmi, "Distribution system reconfiguration for loss minimization using modified bacterial foraging optimization algorithm", *Electrical Power and Energy Systems*, vol. 69 pp.90-97, 2015

[120] Y. del Valle, G.K. Venayagamoorthy, S. Mohagheghi,, J. C. Hernandez, and R.G. Harley, "Particle Swarm Optimization: Basic Concepts, Variants and Applications in Power System". *IEEE Transactions on volutionary Computation*, Vol. 12, No. 2, April 2008, pp: 171-195.

[121] R. Stron, K. Price, "Differential evolution – A simple and efficient adaptive scheme for global optimization over continuous spaces", Journal of Global Optimization, vol.11, 1995, pp.341-359.

[122] S. Das and P.N. Suganthan, "Differential Evolution: A Survey of the State-of-the-Art", IEEE transaction Evolution Compt., vol.15, 2011, pp.4-31.

[123] S. Panda, "Differential evolution algorithm for SSSC-based damping controller design considering time delay", J. Franklin Institute, vol.348 (8), 2011, pp.1903-1926.

[124] S. Panda, "Robust coordinated design of multiple and multi-type damping controller using differential evolution algorithm", Electric Power and Energy Systems, vol.33, 2011, pp. 1018-1030.

[125] "PSO Tutorial", available at: http://www.swarmintelligence.org/tutorials.php

APPENDIX-A

IEEE -39 Bus Test System

Bus no.	voltage (p.u.)	angle (δ)	Pgen (p.u.)	Q_{gen} (p.u.)	P_{load} (p.u.)	Q_{load} (p.u.)	G_{shunt} (p.u.)	B_{shunt} p.u.)	bus type	q_{genmax} (p.u)	q_{genmin} (p.u.)	v_{rated} (p.u.)	V_{max} (p.u.)	V_{min} (p.u.)
01	1.0000	0.0000	0.0000	0.00	0.000	0.0000	0.00000	0.00000	3	99	-99	1.0	0	0
02	1.0000	0.0000	0.0000	0.00	0.000	0.0000	0.00000	0.00000	3	99	-99	1.0	0	0
03	1.0000	0.0000	0.0000	0.00	3.220	0.0240	0.00000	0.00000	3	99	-99	1.0	0	0
04	1.0000	0.0000	0.0000	0.00	5.000	0.8400	0.00000	1.00000	3	99	-99	1.0	0	0
05	1.0000	0.0000	0.0000	0.00	0.000	0.0000	0.00000	2.00000	3	99	-99	1.0	0	0
06	1.0000	0.0000	0.0000	0.00	0.000	0.0000	0.00000	0.00000	3	99	-99	1.0	0	0
07	1.0000	0.0000	0.0000	0.00	2.338	0.8400	0.00000	0.00000	3	99	-99	1.0	0	0
08	1.0000	0.0000	0.0000	0.00	5.220	1.7600	0.00000	0.00000	3	99	-99	1.0	0	0
09	1.0000	0.0000	0.0000	0.00	0.000	0.0000	0.00000	0.00000	3	99	-99	1.0	0	0
10	1.0000	0.0000	0.0000	0.00	0.000	0.0000	0.00000	0.00000	3	99	-99	1.0	0	0
11	1.0000	0.0000	0.0000	0.00	0.000	0.0000	0.00000	0.00000	3	99	-99	1.0	0	0
12	1.0000	0.0000	0.0000	0.00	0.075	0.8800	0.00000	0.00000	3	99	-99	1.0	0	0
13	1.0000	0.0000	0.0000	0.00	0.000	0.0000	0.00000	0.00000	3	99	-99	1.0	0	0
14	1.0000	0.0000	0.0000	0.00	0.000	0.0000	0.00000	0.00000	3	99	-99	1.0	0	0
15	1.0000	0.0000	0.0000	0.00	3.2000	1.5300	0.00000	0.00000	3	99	-99	1.0	0	0
16	1.0000	0.0000	0.0000	0.00	3.2940	0.3230	0.00000	0.00000	3	99	-99	1.0	0	0
17	1.0000	0.0000	0.0000	0.00	0.0000	0.0000	0.00000	0.00000	3	99	-99	1.0	0	0
18	1.0000	0.0000	0.0000	0.00	1.5800	0.3000	0.00000	0.00000	3	99	-99	1.0	0	0
19	1.0000	0.0000	0.0000	0.00	0.0000	0.0000	0.00000	0.00000	3	99	-99	1.0	0	0
20	1.0000	0.0000	0.0000	0.00	6.2800	1.0300	0.00000	0.00000	3	99	-99	1.0	0	0
21	1.0000	0.0000	0.0000	0.00	2.7400	1.1500	0.00000	0.00000	3	99	-99	1.0	0	0
22	1.0000	0.0000	0.0000	0.00	0.0000	0.0000	0.00000	0.00000	3	99	-99	1.0	0	0
23	1.0000	0.0000	0.0000	0.00	2.4750	0.8460	0.00000	0.00000	3	99	-99	1.0	0	0
24	1.0000	0.0000	0.0000	0.00	3.0860	-0.9220	0.00000	0.00000	3	99	-99	1.0	0	0
25	1.0000	0.0000	0.0000	1.00	2.2400	0.4720	0.00000	0.00000	3	99	-99	1.0	0	0
26	1.0000	0.0000	0.0000	0.00	1.3900	0.1700	0.00000	0.00000	3	99	-99	1.0	0	0
27	1.0000	0.0000	0.0000	0.00	2.8100	0.7550	0.00000	0.00000	3	99	-99	1.0	0	0
28	1.0000	0.0000	0.0000	0.00	2.0600	0.2720	0.00000	0.00000	3	99	-99	1.0	0	0
29	1.0000	0.0000	0.0000	0.00	2.8350	0.2690	0.00000	0.00000	3	99	-99	1.0	0	0
30	1.0475	0.0000	2.5000	0.00	0.0000	0.0000	0.00000	0.00000	2	8	-5	1.0	0	0
31	0.9820	0.0000	5.7293	0.00	0.0920	0.0460	0.00000	0.00000	2	8	-5	1.0	0	0
32	0.9831	0.0000	6.5000	0.00	0.0000	0.0000	0.00000	0.00000	2	8	-5	1.0	0	0
33	0.9972	0.0000	6.3200	0.00	0.0000	0.0000	0.00000	0.00000	2	8	-5	1.0	0	0
34	1.0123	0.0000	5.0800	0.00	0.0000	0.0000	0.00000	0.00000	2	8	-5	1.0	0	0
35	1.0493	0.0000	6.5000	0.00	0.0000	0.0000	0.00000	0.00000	2	8	-5	1.0	0	0
36	1.0635	0.0000	5.6000	0.00	0.0000	0.0000	0.00000	0.00000	2	8	-5	1.0	0	0
37	1.0278	0.0000	5.4000	0.00	0.0000	0.0000	0.00000	0.00000	2	8	-5	1.0	0	0
38	1.0265	0.0000	8.3000	0.00	0.0000	0.0000	0.00000	0.00000	2	8	-5	1.0	0	0
39	1.0300	0.0000	10.0000	0.00	11.0400	2.5000	0.00000	0.00000	1	15	-10	1.0	0	0

IEEE-39 System Line Data

from bus	to bus	Resistance p.u	reactance p.u	capacitance line (p.u)	tap ratio	tap phase	tap max	tap min	tap size
1	2	0.00350	0.02050	0.69870	0.0000	0	0	0	0
1	2	0.00350	0.04110	0.69870	0.0000	0	0	0	0
1	39	0.00100	0.02500	0.75000	0.0000	0	0	0	0
2	3	0.00130	0.01510	0.25720	0.0000	0	0	0	0
2	25	0.00700	0.00860	0.14600	0.0000	0	0	0	0
2	30	0.00000	0.01810	0.00000	1.0250	0	0	0	0
3	4	0.00130	0.02130	0.22140	0.0000	0	0	0	0
3	18	0.00110	0.01330	0.21380	0.0000	0	0	0	0
4	5	0.00080	0.01280	0.13420	0.0000	0	0	0	0
4	14	0.00080	0.01290	0.13820	0.0000	0	0	0	0
5	8	0.00080	0.01120	0.14760	0.0000	0	0	0	0
6	5	0.00020	0.00260	0.04340	0.0000	0	0	0	0
6	7	0.00060	0.00920	0.11300	0.0000	0	0	0	0
6	11	0.00070	0.00820	0.13890	0.0000	0	0	0	0
7	8	0.00040	0.00460	0.07800	0.0000	0	0	0	0
8	9	0.00230	0.03630	0.38040	0.0000	0	0	0	0
9	39	0.00100	0.02500	1.20000	0.0000	0	0	0	0
10	11	0.00040	0.00430	0.07290	0.0000	0	0	0	0
10	13	0.00040	0.00430	0.07290	0.0000	0	0	0	0
10	32	0.00000	0.02000	0.00000	1.0700	0	0	0	0
12	11	0.00160	0.04350	0.00000	1.0060	0	0	0	0
12	13	0.00160	0.04350	0.00000	1.0060	0	0	0	0
13	14	0.00090	0.01010	0.17230	0.0000	0	0	0	0
14	15	0.00180	0.02170	0.36600	0.0000	0	0	0	0
15	16	0.00090	0.00940	0.17100	0.0000	0	0	0	0
16	17	0.00070	0.00890	0.13420	0.0000	0	0	0	0
16	19	0.00160	0.01950	0.30400	0.0000	0	0	0	0
16	21	0.00080	0.01350	0.25480	0.0000	0	0	0	0
16	24	0.00030	0.00590	0.06800	0.0000	0	0	0	0
17	18	0.00070	0.00820	0.13190	0.0000	0	0	0	0
17	27	0.00130	0.01730	0.32160	0.0000	0	0	0	0
19	33	0.00070	0.01420	0.00000	1.0700	0	0	0	0
19	20	0.00070	0.01380	0.00000	1.0600	0	0	0	0
20	34	0.00090	0.01800	0.00000	1.0090	0	0	0	0
21	22	0.00080	0.01400	0.25650	0.0000	0	0	0	0
22	23	0.00060	0.00960	0.18460	0.0000	0	0	0	0
22	35	0.00000	0.01430	0.00000	1.0250	0	0	0	0
23	24	0.00220	0.03500	0.36100	0.0000	0	0	0	0
23	36	0.00050	0.02720	0.00000	1.0000	0	0	0	0
25	26	0.00320	0.03230	0.51300	0.0000	0	0	0	0
25	37	0.00060	0.02320	0.00000	1.0250	0	0	0	0
26	27	0.00140	0.01470	0.23960	0.0000	0	0	0	0
26	28	0.00430	0.04740	0.78020	0.0000	0	0	0	0
26	29	0.00570	0.06250	1.02900	0.0000	0	0	0	0
28	29	0.00140	0.01510	0.24900	0.0000	0	0	0	0
29	38	0.00080	0.01560	0.00000	1.0250	0	0	0	0
31	6	0.00000	0.02500	0.00000	1.0700	0	0	0	0

BIO-DATA OF THE CANDIDATE

Name: Santi Behera

Date of Birth: 03-07-1972

Address for Communication: Assistant Professor, Electrical Engineering
Qr. 3R-12, Veer Surendra Sai University of Technology, Burla, Sambalpur, Odisha, 768018
E-mail: bsanti.uce@gmail.com

ACADEMIC QUALIFICATIONS:

- Persuing Ph.D in Electrical Engineering, National Institute of Technology, Rourkela.

- M.E (Power System Engineering), VSSUT (Formerly UCE,) Burla, Sambalpur

- B.Tech (Electrical Engineering), College of Engineering and Technology, O.U.A.T, Bhubaneswar.

PUBLICATIONS ARISING FROM THIS WORK

1. Santi Behera, M. Tripathy, and J. K. Satapathy "Optimal Placement and Sizing of SVC for Load Margin Improvement Using BF Algorithm," World Academy of Science, Engineering and Technology, *International Journal of Electrical, Computer, Energetic, Electronic and Communication Engineering*, Vol. 8, No.10, pp. 1653-1658, 2014.

2. Santi Behera, M. Tripathy, and J. K. Satapathy, "A novel approach for voltage secure operation using probabilistic Neural Network in Transmission Network," ELSEVIER, *Journal of Electrical Systems and Information Technology* vol.3. pp. 141-150, 2016.

3. Santi Behera, M. Tripathy, and J. K. Satapathy, "A Novel Approach for Load Margin Improvement with Optimal Location and Size of Static capacitor using BFO Algorithm," In proceedings of IEEE International Conference on Energy, Power and Environment: Towards Sustainable Growth, NIT, Shillong, Meghalaya, June 12-13, 2015, Electronic ISBN: **978-1-4673-6503-1,** IEEE

4. Santi Behera, M. Tripathy, and J. K. Satapathy, "Optimal Reactive Power Planning for Load Margin Increase with Modified BFO Algorithm," International Conference on Electronics, Energy, Environment, Communication, Computer, Control, 17th -20th Dec, 2015, New Delhi, ISBN:2325-9418

5. Santi Behera, M. Tripathy, and J. K. Satapathy, "An Unique Approach for Voltage Stability improvement using Probabilistic Neural Network," IEEE India International Conference on Electronics, Energy, Environment, Communication, Computer, Control, 17th -20th Dec, 2015, New Delhi ISBN:978-1-4673-6504-8.

6. Santi Behera, and M. Tripathy, "Optimal Reactive Power Compensation for Improvement of Steady State Voltage Stability Limit under Stressed System Condition using BF Algorithm," Semcco and Fanco, vol. 7677, pp 388-397, 2012.

7. Santi Behera, and J.M. Behera, "Challenges in financing in small hydro projects in India-Investors Perspectives and possible solution," In the proceedings of International seminar on renewable and sustainable energy, OHPC, Bhubaneswar, pp. 289-299, 2012.